Journal of the Electrochemical Society of India

Indian Institute of Science Campus,
Bengaluru - 560 012, India

Guest Editors

Dr. Pooja Devi

Dr. Sriparna Chatterjee

Vol. No. 73 (1 & 2), Jan-March 2024

CODEN - JESIA 73 [1&2] 2024 ISSN:0013-466X

INSTRUCTIONS TO AUTHORS

GENERAL

Address all manuscripts to the Managing Editor, Electrochemical Society of India,(JECSI) Bengaluru-560012 and send it by email to arunaecsi@gmail.com / ecsiiisc@gmail.com. Submission of an article will be taken to imply that it has not been previously published and is not under consideration for publication elsewhere. And further that if accepted, it will not be published elsewhere. Submit an electronic version of the paper in WORD format along with a pdf version in order not to miss any portion due to transmission faults. Identify the address, affiliation, email address of the author (corresponding author in case of multiple authors). Also, identify the category in which the paper qualifies for publication.

Journal of the Electrochemical Society of India (JECSI) is a multidisciplinary journal in the general area of Electrochemical Science and Technology. Research and review papers of general significance that are written clearly and well organized will be given preference. All submitted papers will be reviewed by three experts to determine suitability. Paper found unsuitable in terms of the overall requirements of the Journal and those not accepted by the reviewers will be returned to the authors. Both solicited and unsolicited papers will be reviewed. Authors will be notified of acceptance, rejection or any need for revision before acceptance for publication. Any illustrations or other material reproduced from other publications must be properly credited. It is the author's responsibility to obtain the necessary permission in such cases.

CATEGORIES OF MANUSCRIPTS

General Articles, not exceeding 5000 words in length, should discuss current trends in research in a field that will be of interest to readers outside the field; interdisciplinary topics; Science policy and administration; Impact of Science and Technology on Society, etc. The paper should include a summary not exceeding 200 words, introductory paragraph(s), brief subheads at appropriate places to point to what follows, Illustrations that will help a general reader and references.

Review Articles, not exceeding 5000 words, are expected to survey and discuss recent developments in a relevant field. They should be well focused and organized. General text book style is not acceptable. Research Articles should report and discuss results of work of a fairly major significance. They should include an Abstract, introductory paragraph(s) and brief subheads indicating materials and methods used, major results and discussion of results, relevant illustrations and references.

Research Communications, not exceeding 2000 words, should contain important findings that are novel and are of fairly broad interest. They should not be broken up under subheads. Correspondences include letters, not exceeding 500 words that are of general interest to Scientist, Engineers and Technologists. Only selected letters will be published. Scientific Correspondence contains technical comments, including those on articles or communications published in JECSI. Appropriate letters will be published.

Book Reviews are reviews of books published in the major areas of Electrochemical Science, Technology and Engineering. Unsolicited reviews will also be considered. Reviews that simply 'list' the contents will not be acceptable for publication. Reviews should have 'context' and convey information about the subject of the book. Historical Comments and Notes inform readers about interesting aspects of personalities or institutions of Science or about watershed events in the history/ development of science. Most are expected to relate to India. Illustrations are welcome with due credit if already published elsewhere.

MANUSCRIPT PREPARATION

The manuscript should be in double line spacing in an area corresponding to A-4 size paper with 25 mm margin all around. Page numbers, including

that for the first page should be given at the bottom centre of the page. The title should be brief, specific and amenable to indexing. Give a maximum of 5 keywords which are carefully chosen and not phrases of several words. Summary and abstract should not have more than 200 words and should convey the main point of the paper, outline the results and conclusions and explain the significance of the work and results.

Text

Papers should begin with an introduction. The text should be intelligible to readers in different disciplines and technical terms should be defined. Tables and figures should be arranged in numerical order and referred to in that order. All symbols and abbreviations must be defined and used only when absolutely necessary. Superscripts and subscripts and ambiguous characters should be clearly indicated. Units of measure should be metric and preferably SI. Methods should, as far as possible, be described briefly in appropriate table and figure legends.

Figures are to be drawn in sizes that are clearly intelligible. Location and orientation of figures is the entire responsibility of the author(s). The actual location of figures and tables may be clearly indicated in the pdf format that accompanies the main word format submission. The same data should not be given in both tables and figures. Photomicrographs and other photographs that require a scale bar or a micron marker should be defined clearly in the caption. Magnifications are not acceptable in place of micron markers. Primary data should be submitted as far as possible as for example actual photograph of an electrophoretic gel rather than an idealized diagram.

References should be numbered in the order in which they appear first through the text and then through table and figure legends. Following examples indicate the different ways of writing the references:

Reference to a journal publication:

[1] J. Name, J.A.J. Name, R.A. Name, Title of article, J. Sci. Commun. Vol.no (year) page number xx–xy. https://doi.org/10.1016/ j.Sc.2010.00372.

Reference to a book:

[3] W. Name, E.B. Name, Title of the book, Edition, Publisher, Place name, year.

Reference to a chapter in an edited book:

[4] G.R. Name, L.B. Name, Chapter title, in: B.S. Name, R.Z. Name (Eds.), Title of book, Publisher, Place name, Year, pp. xxx–yyy.

Acknowledgments should be brief and clear.

Funding: This work was supported by Granting Agency Name [grant numbers xxxx, yyyy];

Cover Photographs. Good photographs (colour or black and white) that pertain to a submitted paper will be considered for use on the cover of an issue.

Proofs and Publication: A final pdf version of the paper may be sent to the author before publication if there are any inaccuracies or doubts of any nature. Such a procedure is redundant in case no major editorial changes are made in the paper.

Publication Ethics and Publication Malpractice Statement

The Journal of Electrochemical Society of India (JECSI) follows the Committee on Publication Ethics (COPE) *Code of Conduct and Best Practice Guidelines for Journal Editors and the Code of Conduct for Journal Publishers*. It is expected that authors, reviewers and editors follow the best-practice guidelines on ethical behaviour.

Responsibilities of Editorial board

Editors evaluate submitted manuscripts only on the basis of their merit such as novelty, originality, importance, and its relevance to the journal's scope. The information or ideas imparted to the editors due to handling the manuscript will be kept confidential and will not be used for their own benefit. The editors will refrain from reviewing a manuscript in which they have conflict of interest and will be handled by other editorial board members. Editors and editorial staff will maintain confidentiality about the submitted manuscripts.

All the manuscripts submitted to the journal will undergo peer-review by at least two reviewers who are experts in that area. Based on the evaluation reports received from the reviewers, copyright permissions and plagiarism will be checked and then the Chief Editor decides on the publication of the manuscript.

The Chief Editor will take actions when ethical concerns are raised with regard to a submitted manuscript or published paper followed by a correction, retraction, expression of concern or relevant other notes will be published in JECSI.

Responsibilities of Authors

The Authors should present detailed and correct account of the work to enable others to reproduce the work. Fraudulent or inaccurate statements are not accepted. If required the authors will be asked to provide the raw data of their study if some suspicious figures are provided in the manuscript. Authors should check their manuscript for originality check using the standard software. Only manuscripts with similarity report <20% will be considered for peer review. The authors should not simultaneously submit the same manuscript to multiple journals and is treated as unethical and such papers will be sent back to the authors and authors will be black listed.

Authors who have made significant contributions to the paper should only be included as authors in the manuscript and the role of each author has to be listed. The other peoples name should be included in the acknowledgement section.

The authors should disclose the conflict of interest that would have influenced the results or their interpretation. Authors should also properly acknowledge the work of others and ensure proper citation of such works in the manuscript. The authors should clearly state in the manuscript if the work involved the use of hazardous chemicals, procedures or equipment.

The authors should co-operate in submitting the revised manuscripts before the deadline and providing befitting replies to the reviewer comments. The authors should inform the Chief Editor when they discover significant errors or inaccuracies in their own published work and publish a corrigendum or retract the paper.

Journal of the Electrochemical Society of India

Vol. No. 73 (1 & 2) Jan-March 2024,

CODEN - JESIA 73 [1&2] 2023 ISSN:0013-466X

Email : ecsiiisc@gmail.com

E-mail : ecsiiisc@gmail.com

Publication Ethics and Publication Malpractice Statement

The Journal of Electrochemical Society of India (JECSI) follows the Committee on Publication Ethics (COPE) *Code of Conduct and Best Practice Guidelines for Journal Editors* and the *Code of Conduct for Journal Publishers*. It is expected that authors, reviewers and editors follow the best-practice guidelines on ethical behaviour.

Responsibilities of Editorial Board

Editors evaluate submitted manuscripts only on the basis of their merit such as novelty, originality, importance, and its relevance to the journal's scope. The information or ideas imparted to the editors due to handling the manuscript will be kept confidential and will not be used for their own benefit. The editors will refrain from reviewing a manuscript in which they have conflict of interest and will be handled by other editorial board members. Editors and editorial staff will maintain confidentiality about the submitted manuscripts.

All the manuscripts submitted to the journal will undergo peer-review by at least two reviewers who are experts in that area. Based on the evaluation reports received from the reviewers, copyright permissions and plagiarism will be checked and then the Chief Editor decides on the publication of the manuscript.

The Chief Editor will take actions when ethical concerns are raised with regard to a submitted manuscript or published paper followed by a correction, retraction, expression of concern or relevant other notes will be published in JECSI.

Responsibilities of Authors

The Authors should present detailed and correct account of the work to enable others to reproduce the work. Fraudulent or inaccurate statements are not accepted. If required the authors will be asked to provide the raw data of their study if some suspicious figures are provided in the manuscript. Authors should check their manuscript for originality check using the standard software. Only manuscripts with similarity report <20% will be considered for peer review. The authors should not simultaneously submit the same manuscript to multiple journals and is treated as unethical and such papers will be sent back to the authors and authors will be black listed.

Authors who have made significant contributions to the paper should only be included as authors in the manuscript and the role of each author has to be listed. The other peoples' name should be included in the acknowledgement section.

The authors should disclose the conflict of interest that would have influenced the results or their interpretation. Authors should also properly acknowledge the work of others and ensure proper citation of such works in the manuscript. The authors should clearly state in the manuscript if the work involved the use of hazardous chemicals, procedures or equipment. The authors should co-operate in submitting the revised manuscripts before the deadline and providing befitting replies to the reviewer comments.

The authors should inform the Chief Editor when they discover significant errors or inaccuracies in their own published work and publish a corrigendum or retract the paper.

Journal of The Electrochemical Society of India

CODEN JESIA, Vol. No. 73 (1&2), Jan-March 2024. ISSN 0013-466X

Patrons of the Society

M/S Ronuk Industries
M/S Titanium Equipment and anode Mfg. Co.,
M/s Reliance Engineers, Bengaluru
M/s Degussa Electroplating Company
M/s B. T. Solders Pvt. Ltd., Mysore
M/s Khoday India Ltd., Bengaluru
M/s Metrohm India Pvt Ltd.
Ms. Mridula Shaw
Dr. C. H. Krishnamurthy Rao
Sri. S. K. Jain
Dr. Franz Simon
Sri. Arvind Toshniwal
Dr. N. Rajalakshmi, Former Head, CFCT, ARCI
Sri. Srihari Khoday

Donor Members

M/s. Mascot Chemical Works, Bengaluru
M/s. Indian Telephone Industries Ltd., Bengaluru
M/s. Kangovi Electronics (P) Ltd., Bengaluru
M/s. Aquair Control Systems, Bengaluru
M/s. Stiver Equipment Pvt. Ltd., Bengaluru
M/s. Hindustan Aeronautics Ltd., Bengaluru
M/s. High Energy Batteries, Madurai
M/s. Electroplating Equipment Co., Bengaluru
M/s. Galvanosols Pvt. Ltd., Bengaluru
M/s. Pyro Technologies, Bengaluru
M/s. Shruthi Enterprises, Bengaluru
M/s. Grauer Weil (India) Ltd., Mumbai
M/s. Zaveri Brothers (P) Ltd., Mumbai
M/s. Standard Batteries, Mumbai
M/s. Geep Industries Syndicate Ltd.
M/s. Larsen and Toubro Ltd., Mysore
M/s. IR Technology Services Pvt. Ltd.
M/s. Brite Platers and Electrical Engineers, Bengaluru
M/s. Vijaya Metal Finishers, Bengaluru
M/s. Vinpla Plating Pvt. Ltd., Bengaluru
M/s. Surface Chem Finishers, Bengaluru

Permanent Sustaining Members

M/s. Tata Chemical
M/s Ashok Charitable Trust, Karaikudi
M/s. Mysore Paper Mills, Bhadravathi
M/s. Tata Iron and Steel Company Ltd., Jamshedpur
M/s. DCM Chemical Works
M/s. Indian Aluminum Company Ltd., Alwaye
M/s. Visveswaraya Iron and Steel Ltd., Bhadravathi

THE ELECTROCHEMICAL SOCIETY OF INDIA

Indian Institute of Science Campus, Bangalore - 560012
Email: ecsiiisc@gmail.com, Website: www.ecsi.in

Analysing Research Trends in Nanomaterials for Green Hydrogen Value Chain: "A Bibliometric approach"

Madhulika Bhati[1], Saurav Kumar[1], Jayita Biswas[1], Nishita[1].*

[1]CSIR- National Institute of Science Communication and Policy Research, New Delhi, India.
**Corresponding author: madhulikabhati@niscpr.res.in*

Abstract:

Nanomaterials can play a significant role in various stages of the hydrogen value chain, from production to storage and utilization. This paper is an overview of how nanomaterials are being explored in different aspects of the hydrogen value chain. The study aims to identify and elucidate emerging trends in catalyst development for hydrogen production. By leveraging the Web of Science's expansive repository, the research will not only reveal the current state of the field but also unveil patterns in research trajectories, highlighting key thematic areas, innovative methodologies, and transformative technologies. The identification of prolific authors, institutions, and leading countries will add a valuable dimension to understanding the global landscape of nanomaterial research in hydrogen catalysts. Overall, this study holds the promise of not only advancing our understanding of the current state of the field but also providing a roadmap for future endeavours, fostering innovation and contributing to the sustainable development of hydrogen technologies.

Keywords: *Titanium; Poly (3,4-ethylenedioxythiophene) (PEDOT); Gallium; Corrosion; Bioactivity; Orthopaedic*

1. Introduction

With the increase in population growth, the demand for energy has also increased in last few years and this is going to increase more in upcoming years. To meet the energy demands, there is a need to increase the use of clean energy and curb the use of conventional fossil-fuel based energy. Taking environmental constraints into consideration, green hydrogen has been considered as a good alternative of fossil – fuel based energy system. Green hydrogen can serve as a long – term and ideal solution for energy related environmental constraints as its heating value is three times more as compared to petroleum and it leads to zero harmful emissions as well [1], [2]. There are a variety of renewable as well as non-renewable methods to produce hydrogen. Non-renewable methods of hydrogen production include natural gas, coal gasification, heavy oil, methane decomposition etc. Renewable methods include water electrolysis, solar photochemical, photobiological water decomposition, biomass – conversion etc. Although these methods are highly efficient and eco-friendly but these are not cost-effective methods. Although hydrogen as a fuel has various advantages but it is a highly flammable gas with the range from 4% to 75% vol in air and can cause an explosion. Since it is colourless and odourless, it is very difficult to discover and configure it in case of leakages [3]. Another challenge is the lack of safe, easy and cost-effective storage method. To address these types of challenges associated with the production and storage of hydrogen, the role of nanomaterials has been increased tremendously. The physico-chemical properties of nanomaterials render its usage in catalysis, complex hydrides, metal organic frameworks etc. There are different types of nanomaterials that are used in hydrogen production and storage such as activated carbon, carbon nanotubes, metal-doped carbon-based nanomaterials, complex hydrides, clathrates, metal-

organic frameworks etc. The size of engineered nanomaterials ranges from 1 – 100 nm and designed in a specific manner to simulate the only properties for specific purpose or application. The storage of hydrogen depends upon two phenomenon i.e. physisorption and chemisorption. MOFs, Zeolites and carbonaceous materials fall in the former category whereas complex hydrides and metal hydrides fall in the later one. The use of nanomaterials has increased tremendously not just in the field of hydrogen production but in other fields also. This has gained a great momentum in water splitting such as photochemical, electrochemical and photoelectrochemical water splitting methods [4], [5].

The materials such as MnO_2 nanosheet is used for photocatalysis, electrocatalysis and electrochemical energy storage whereas TiO_2 is used as a photocatalytic semi-conductor. The TiO_2/ MnO_2 nanocomposites have great photocatalytic activity and can consume solar energy efficiently because of their small energy band gap, negatively charged surface property and large surface area. The scientists are trying to improve photocatalysis by switching to various carbon based nanomaterials [6].

According to the study conducted by researchers, if one introduces the nanomaterials impregnated biomass in SCW (Supercritical Water) gasification, the difficult operating conditions can be reduced and conversion efficiency into product can be enhanced [7]. Other important and prominent magnetic nanocatalysts with or without inherent magnetic properties are Fe_2O_3 and Fe_3O_4 which can be easily separated from the solution and can prove non-hazardous to the environment. According to the materials employed, their properties, efficiencies and applications, nanomaterials have been classified as Zero-Dimensional (0D), One-Dimensional (1D), and Two- Dimensional (2D). Zero-Dimensional (0D) consist of low efficiency materials that are highly corrosive and have high charge-recombination rates. These include carbon quantum dots, CdS and CdSe which are used for H_2 evolution in visible light. One-Dimensional (1D) nanomaterials have superior properties which makes them suitable for photocatalysis process of hydrogen production. These include nanotubes, nanowires, nanorods, and nanofibers. Example of One-Dimensional (1D) nanomaterial is Zn_2GeO_4 that has the highest rate of hydrogen production i.e. 0.6 mmol/h. Two- Dimensional (2D) nanomaterials have higher surface area comparable with that of 0- and 1-D nanomaterials and are in the form of thin films made for hydrogen evolution. Due to the advantageous properties of 2D nanomaterials, researchers explore thin film photocatalysts with novelties such as graphene oxide, g-C_3N_4, and transition metal dichalcogenides (TMDs). The pH range for hydrogen evolution reactions has been studied extensively in 1D, 2D and 3D MOFs (Metal Organic Frameworks) and among which the 2D metal organic frameworks with sheet like morphology have become the highly potential materials [8], [9].

Recently, another class of materials 'halide perovskite materials' has emerged for the photocatalytic applications due to their optical and electronic properties as well as suitable band position, high carrier mobility and great lengths of electron-hole [10]. So, a lot of materials and combinations thereof are used as photo- or electro- or photoelectrocatalysts to produce hydrogen in an efficient and effective manner.

By analysing the literature review, it can be concluded that the use of nanomaterials for hydrogen production is increasing nowadays which will be gaining more momentum in the upcoming years. The overall paper covers the bibliometric analysis using different keywords and operators, co-occurrence based keyword analysis, research trend of countries and institutes and review based analysis. This analysis would help us understand the current status of 'nanomaterials' in the hydrogen value chain.

2. Bibliometric Analysis

Bibliometric analysis is an established technique for assessing the state of the art in a particular field of study. Through the analysis of quantitative data and statistics, the approach can be used to

describe publication trends through time as well as across literature. As a result, information regarding the quantity of papers published by a country, research group, institute, or authors with the highest technological generation may be identified. To analyse the research trend in the use of nanomaterials in Green Hydrogen Production, Bibliometric analysis was done and the result presented in this paper are based on a bibliometric analysis of articles published between 2005 and 2022.

Methodology

Web of Science (WOS) has been chosen as the database for the study of research trend in this area. WOS is one of the most popular and commonly used database which covers various subjects. The search was initiated with the use of string performed in Web of Science which was based on 'topic'. Distinct search queries were developed to retrieve the relevant publications in the time span '2016-2023'. The number of papers retrieved is with respect to the 7 key strings which is given in Table-1. For removing the duplicate as well as ambiguity, manual cleaning of the .csv file extracted from WOS was done. For this authors have gone through the abstract and keywords to remove any ambiguous papers, resulting in 2902 papers, which have been finally screened for further literature analysis for indicators like publication analysis, top countries, and keyword co-occurrence analysis.

Table 1: Keyword Strings Search in Web of Science with total number of counts

Sl. No.	Keywords	Total Papers
1	"Hydrogen Production" and "Nanomaterials"	1076
2	"Hydrogen Evolution" and "Nanomaterials"	1896
3	"Hydrogen generation" and "Nanomaterials"	352
4	"Water splitting" and "Nanomaterials" and "Hydrogen Production"	304
5	"Photocatalysis" and "Nanomaterials" and "Hydrogen Production"	295
6	"Electrocatalyst" and "Nanomaterials" and "Hydrogen Production"	96
7	"Electrolysis" and "Nanomaterials" and "Hydrogen Production"	60
	Paper retrieved after removing duplicates	2902

2.1 Publication analysis

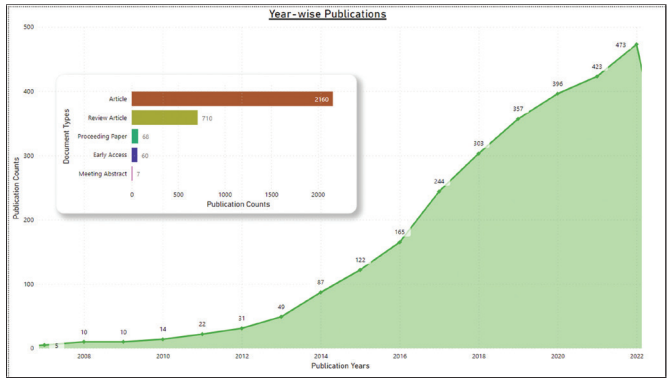

Figure 1: Year-wise publication trends globally

To find the year-wise publication trend and number of publications in different document type, Microsoft Excel and Microsoft Power BI is used. First the analysed data of 2902 papers was downloaded and sorted in excel according to the requirement. After the data was ready, we exported the data in Power BI [33] where we transformed the data in power query, filtered the repeatation and analysed the results till 2022. After creating the line graph it can be clearly seen in Figure 1 that with the year passes the number of publications increases, where the maximum contribution are in Article.

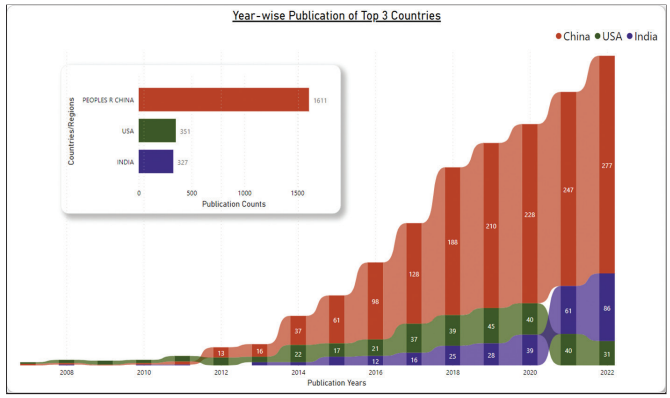

Figure 2: Year-wise publication trends of Top three countries

To analyse the top contributor countries, the same data set was analysed on yearly basis with the filter of top countries, and the result are shown in Figure 2, where China has been stably publishing around 55% of the total publication, USA contributes to around 12% and India shares around 11% of the total publications. The growth in India' publication shows exponentiality after 2020, leaving USA behind.

We also analysed the top Institutes that are countributing within these countries (Figure 3), and in India it shows that IIT and CSIR are the prominent institues contributing around 18.96% and 10% of the publications respectively, apart from this NITs, SRM Chennai and Jain University are a few other institutes and universities which join the top contributors in India. Top institutes of China are Chinese Academy of Sciences contributing around 16% and Jilin University contributes ~6% and in case of China, the contribution for publications are majorly from universities only. The top contribution in USA comes from mainly institutes and universities, the top two are US-DOE, contributing around 12% and University of California, contributing around 11%.

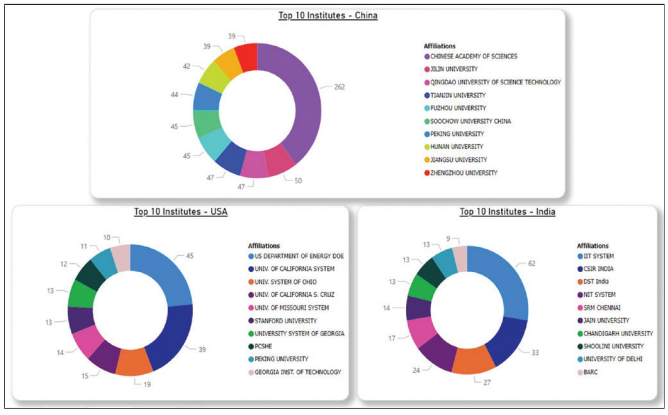

Figure 3: Top 10 institutions of the top three countries

2.2 Keyword Co-occurrence analysis

Keyword analysis plays a crucial role in research by revealing current trends and research topics within a particular field. By examining keyword co-occurrence, researchers can determine the direction of research and the main subjects of a field. In this case, keyword analysis was carried out using data extracted from the 'Web of Science' database [31]. The data was then visualized using 'VOSViewer' software [32] to create a keyword co-occurrence map, which helps identify research focus areas and emerging research trends. We analyzed top 3 countries data. In this network analysis the top cited papers, 10% of total results found i.e. 290 papers are analysed. By extracting the top cited data in text file, we did the network visualisation in VOS Viewer by taking Citation based analysis with unit Country. We took full counting method, where the maximum number of countries per document was 25, and the minimum number of a country was 5. Out of the total 35 countries 14 meet the threshold. From the analysis of top 10% papers of the result that came from the above query in Web of Science. 192 papers of China has 47552 citations, 54 USA papers has 29014 and India has 19 papers having 5878 citations went to 5th position in top 10% citation count where in publication count it was on 3rd position.

The keyword analysis of China (Figure 4) deciphered around 143 items, 11 clusters, 1147 links, and the most dominant group where the study trend is seen are 'Hydrogen', 'photocatalysis', 'evolution reaction', 'nanomaterials', 'hydrogen production' and other smaller clusters.

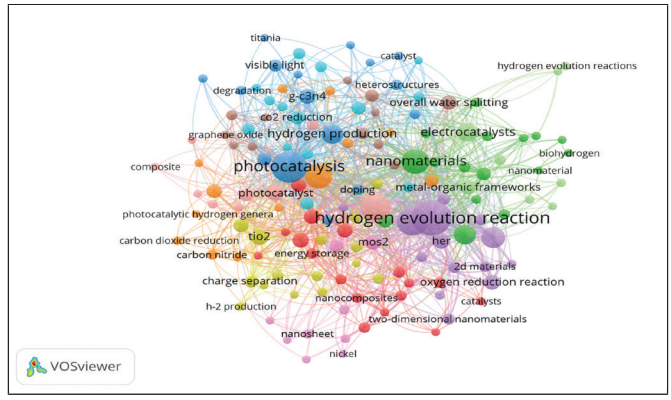

Figure 4: Co-occurrence based Keyword Analysis of China

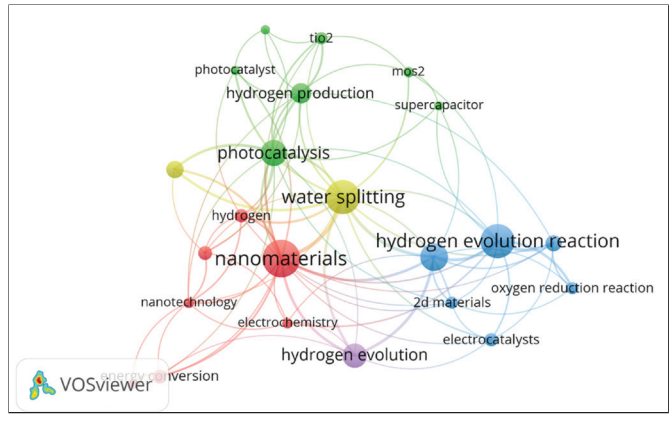

Figure 5: Co-occurrence based Keyword Analysis of USA

The keyword analysis of USA (Figure 5) deciphered around 23 items, 5 clusters, 87 links, and the most dominant group where the study trend is seen are 'nanomaterials', 'Hydrogen', 'photocatalysis',

'water splitting', 'hydrogen evolution', 'hydrogen production' and other smaller clusters.

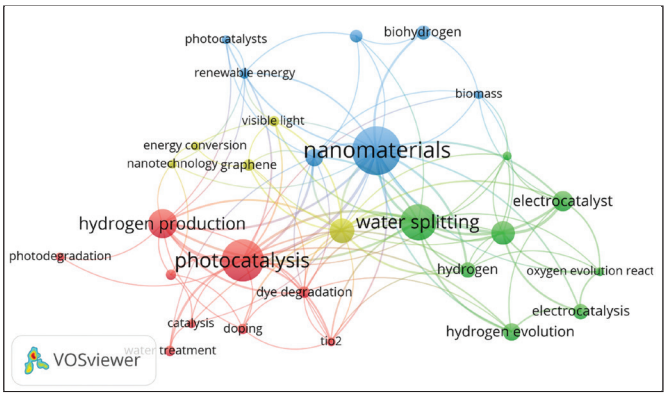

Figure 6: Co-occurrence based Keyword Analysis of India

The keyword analysis of India (Figure 6) deciphered around 29 items, 4 clusters, 111 links, and the most dominant group where the study trend is seen are 'nanomaterials', 'photocatalysis', 'water splitting', 'hydrogen production' 'electrocatalyst', and other smaller clusters.

These finding suggest the most prominent and recent approaches within the top countries scientific community. Keyword analysis provides valuable insights into research focus areas, emerging topics, and new research directions. By understanding the research landscape and areas of interest across different countries, researchers can broaden their research scope and explore new avenues for investigation.

Table 2: Country-wise total publication and citation with total link strength

Sl. No	Country	Documents	Citations	Total Link Strength
1	China	192	47552	511
2	USA	54	29014	307
3	Singapore	32	11431	235
4	Australia	25	8941	125
5	Japan	13	7429	48
6	India	19	5878	58
7	France	8	4717	36
8	South Korea	16	4684	83
9	Czech Republic	7	3480	41
10	England	8	2424	47
11	Saudi Arabia	6	2019	24
12	Germany	6	2004	36
13	Canada	5	1792	23
14	Spain	8	1637	16

In Figure 7, the bar graph is showing documents count and line graph is showing number of citations.

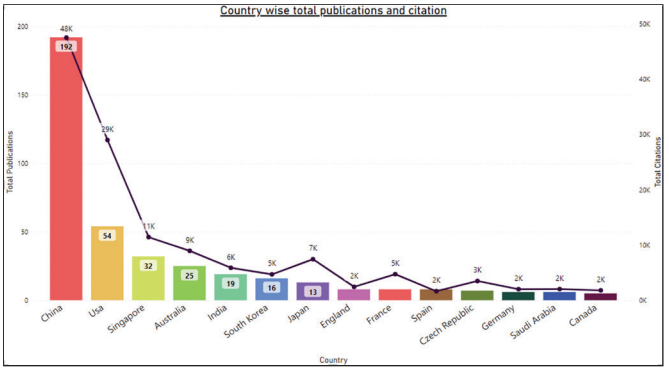

Figure 7: Country-wise total publications and citations

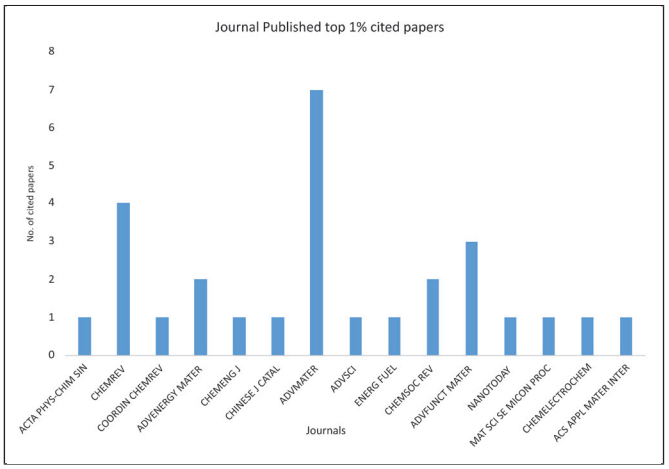

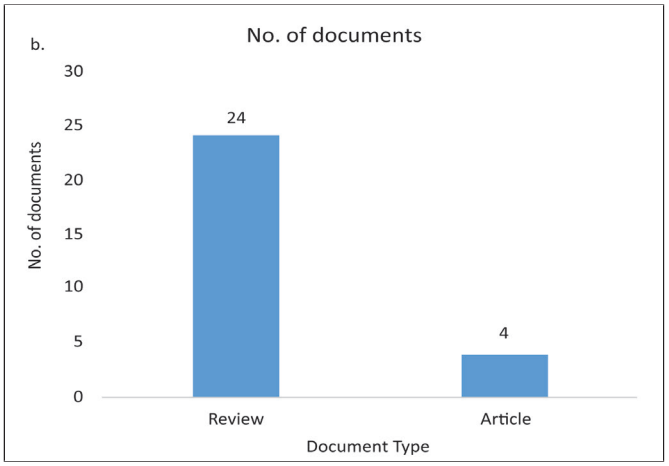

Figure 8 a: No. of Top 1 % cited papers in journals & b: No. of documents (Review and Article)

Figure 8 shows the number of top 1 % cited papers in different journals which clearly indicates the maximum papers in Journal 'Advanced Materials' and mostly the documents are of review type.

2.3 Research Trend analysis based on Top 1 % cited paper

The significance of Metal-Organic Frameworks (MOFs) in forming N- or P-doped graphite-based nanomaterials, enhancing catalysis for water splitting was highlighted [11]. These MOF catalysts, known for their stability and water-resistant properties, particularly excel in photo-degradation of organic pollutants. The controlled thermal transformation of MOFs into Single Atom Catalysts (SACs) adds another layer of complexity, offering potential breakthroughs in catalytic processes [12].

Transitioning to Metal-Nitrogen-doped Carbon (M-N-C) materials, [13] emphasize the importance of tuning metal ion centers and coordination for catalytic reactions, including Oxygen Evolution Reaction (OER), Hydrogen Evolution Reaction (HER), and more. The search for cost-effective and efficient alternatives to commercially used catalysts like Pt/C and IrO2/RuO2 is highlighted by [14].

The exploration of Transition Metal Sulfides (TMS) and Transition Metal Selenides emerges as a vital research focus for improving the performance of electrocatalysts in both HER and OER [15]. The unique properties of TMSs and their conductance, especially in multi-metal selenides, make them a hotspot for further investigation.

Novel approaches, such as sequential electrodeposition techniques for fabricating nanosheets and nanoparticles, showcase promising electrocatalytic properties for Hydrogen Evolution Reaction (HER) and Oxygen Evolution Reaction (OER) [16]. Carbon dots, highlighted by [17], present an intriguing avenue for photocatalysis, though challenges remain in understanding their quantum yields and correlation with formation rates.

Localized Surface Plasmon Resonance (LSPR) emerges as a driving force in photocatalytic reactions, enhancing the activity and selectivity of HER and OER [18]. Structural defects in 2D photocatalysts, as discussed by [19], are identified as critical elements for improving photocatalytic activity, paving the way for future studies on structure-activity relationships.

The review by [20] delves into the progress of co-doping and mono-doping of nitrogen-doped carbon electrocatalysts, emphasizing the need for sustainable, metal-free catalysts. Band gap engineering in two-dimensional nano materials is thoroughly analyzed by [21], exploring materials like 2D MOFs, mxENES, 2D perovskites, and more for advancements in nanotechnology.

Cu-based nanoparticles and their applications in various catalytic processes [22], while [23] focus on semiconductor photocatalysis as a potential solution for environmental degradation and energy demands.

The comprehensive study by [24] proposes strain engineering as a novel route for enhancing the electrocatalytic performances of hydrogen evolution and oxygen evolution reactions, aligning with the growing interest in sustainable hydrogen fuel production.

Effective strategies were unravelled for molecular hydrogen production, concentrating on Transition Metal Phosphides (TMPs) [25]. The challenges in synthesizing TMPs with specific exposed facets are acknowledged, presenting avenues for further research [26].

Transition Metal Nitrides (TMNs) are explored by [27] for electrochemical energy applications, offering insights into nanostructuring as a successful approach to address inherent limitations. Delve into the optimization of catalytic activity through crystalline–amorphous heterojunctions, showcasing the potential for further advancements [28].

In the realm of 2D electrocatalysts, [29] advocate for specific compositions and functionalities, underscoring their significance in clean energy systems. The need for large-scale production of photocatalysts at the industrial level and the optimization of surface areas for increased efficiency are highlighted as future research focuses by [30].

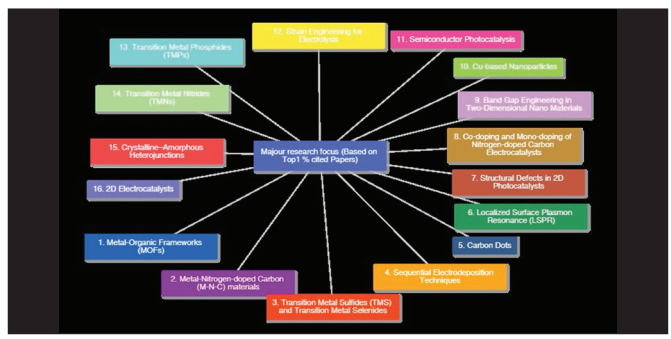

Figure 9: Major research focus (Based on Top1 % cited Papers)

This comprehensive review navigates through a myriad of nanomaterials and their applications in hydrogen production, offering valuable insights into the evolving landscape of this dynamic field. The diverse range of materials discussed, from MOFs to carbon dots and beyond, reflects the multi-faceted approach researchers are adopting to address the challenges in achieving sustainable and efficient hydrogen production.

3. Conclusion

The utilization of nanomaterials in the hydrogen value chain has been a topic of research and development in various countries.

Incorporating nanomaterials across the hydrogen value chain has the potential to enhance efficiency, reduce costs, and address some of the challenges associated with hydrogen production, storage, transportation, and utilization. However, it's important to note that the widespread implementation of these technologies may require further research, development, and consideration of safety and environmental aspects. By leveraging the unique properties of nanomaterials, researchers aim to address challenges, improve efficiency, and optimize various aspects of the hydrogen value chain.

Acknowledgement

The authors express their sincere gratitude to Prof. Ranjana Aggarwal, Director, CSIR-NIScPR and Dr. Ashish Lele, Director CSIR-NCL for giving constant encouragement. We are also thankful to CSIR Head Quarter to provide funding support from CSIR under Hydrogen mission programme.

References

[1] Hassan, Q., Algburi, S., Sameen, A. Z., Salman, H. M., & Jaszczur, M. (2024). Green hydrogen: A pathway to a sustainable energy future. International Journal of Hydrogen Energy, 50, 310–333. https://doi.org/https://doi.org/10.1016/j.ijhydene.2023.08.321

[2] Thapa, B. S., & Thapa, B. (2020). Green Hydrogen as a Future Multi-disciplinary Research at Kathmandu University. Journal of Physics: Conference Series, 1608(1) 012020. https://doi.org/10.1088/1742-6596/1608/1/012020

[3] Zheng, J., Wang, C.-G., Zhou, H., Ye, E., Xu, J., Li, Z., & Loh, X. J. (2021). Current Research Trends and Perspectives on Solid-State Nanomaterials in Hydrogen Storage. Research, 2021. https://doi.org/10.34133/2021/3750689

[4] Epelle, E. I., Desongu, K. S., Obande, W., Adeleke, A. A., Ikubanni, P. P., Okolie, J. A., & Gunes, B. (2022). A comprehensive review of hydrogen production and storage: A focus on the role of nanomaterials. International Journal of Hydrogen Energy, 47(47), 20398–20431. https://doi.org/10.1016/j.ijhydene.2022.04.227

[5] Gupta, A., Baron, G. V., Perreault, P., Lenaerts, S., Ciocarlan, R. G., Cool, P., Mileo, P. G. M., Rogge, S., Van Speybroeck, V., Watson, G., Van Der Voort, P., Houlleberghs, M., Breynaert, E., Martens, J., & Denayer, J. F. M. (2021). Hydrogen Clathrates: Next Generation Hydrogen Storage Materials. Energy Storage Materials, 41, 69–107. https://doi.org/10.1016/j.ensm.2021.05.044

[6] Rasool, M. A., Sattar, R., Anum, A., Al-hussain, S. A., Ahmad, S., Irfan, A., & Zaki, M. E. A. (2023). An Insight into Carbon Nanomaterial-Based Photocatalytic Water Splitting for Green Hydrogen Production. 13(1) - 66. https://doi.org/10.3390/catal13010066

[7] Maleh, H. K., Orooji, Y., Karimi, F., Karaman, C., & Vasseghian, Y. (2023). Integrated approaches for waste to biohydrogen using nanobiomediated towards low carbon bioeconomy. In Advanced Composites and Hybrid Materials. Springer International Publishing. 6 (1) - 29. https://doi.org/10.1007/s42114-022-00597-x

[8] Walake, S., Jadhav, Y., & Kulkarni, A. (2023). Novel spinel nanomaterials for photocatalytic hydrogen evolution reactions: An overview. *Energies*. *16*(12), 4707.https://doi.org/10.3390/en16124707

[9] Paquin, F., Rivnay, J., Salleo, A., Stingelin, N., & Silva, C. (2015). Multi-phase semicrystalline microstructures drive exciton

dissociation in neat plastic semiconductors. J. Mater. Chem. C, 3, 10715–10722. https://doi.org/10.1039/b000000x

[10] Zhang, Z., Zhou, R., Li, D., Jiang, Y., Wang, X., Tang, H., & Xu, J. (2022). Recent progress in Halide perovskite nanocrystals for photocatalytic hydrogen evolution. Nanomaterials(Basel,Switzerland), 13(1),106. https://doi.org/10.3390/nano13010106

[11] Wang, Q., & Astruc, D. (2020). State of the Art and Prospects in Metal-Organic Framework (MOF)-Based and MOF-Derived Nanocatalysis [Review-article]. Chemical Reviews, 120(2), 1438–1511. https://doi.org/10.1021/acs.chemrev.9b00223

[12] Wei, Y. S., Zhang, M., Zou, R., & Xu, Q. (2020). Metal-Organic Framework-Based Catalysts with Single Metal Sites. Chemical Reviews, 120(21), 12089–12174. https://doi.org/10.1021/acs.chemrev.9b00757

[13] Shi, Z., Yang, W., Gu, Y., Liao, T., & Sun, Z. (2020). Metal-Nitrogen-Doped Carbon Materials as Highly Efficient Catalysts: Progress and Rational Design. Advanced Science, 7(15) 202001069. https://doi.org/10.1002/advs.202001069

[14] Sultan, S., Tiwari, J. N., Singh, A. N., Zhumagali, S., Ha, M., Myung, C. W., Thangavel, P., & Kim, K. S. (2019). Single Atoms and Clusters Based Nanomaterials for Hydrogen Evolution, Oxygen Evolution Reactions, and Full Water Splitting. Advanced Energy Materials, 9(22), 1–48. https://doi.org/10.1002/aenm.201900624

[15] Feng, W., Pang, W., Xu, Y., Guo, A., Gao, X., Qiu, X., & Chen, W. (2020). Transition metal selenides for electrocatalytic hydrogen evolution reaction. ChemElectroChem, 7(1), 31–54. https://doi.org/10.1002/celc.201901623

[16] Li, X., Wang, Y., Wang, J., Da, Y., Zhang, J., Li, L., Zhong, C., Deng, Y., Han, X., & Hu, W. (2020). Sequential Electrodeposition of Bifunctional Catalytically Active Structures in MoO^3 / Ni – NiO Composite Electrocatalysts for Selective Hydrogen and Oxygen Evolution. 2003414, 1–10. https://doi.org/10.1002/adma.202003414

[17] Fernando, K. A. S., Sahu, S., Liu, Y., Lewis, W. K., Guliants, E. A., Jafariyan, A., Wang, P., Bunker, C. E., & Sun, Y. P. (2015). Carbon quantum dots and applications in photocatalytic energy conversion. ACS Applied Materials and Interfaces, 7(16), 8363–8376. https://doi.org/10.1021/acsami.5b00448

[18] Li, S., Miao, P., Zhang, Y., Wu, J., Zhang, B., Du, Y., Han, X., Sun, J., & Xu, P. (2021). Recent Advances in Plasmonic Nanostructures for Enhanced Photocatalysis and Electrocatalysis. Advanced Materials, 33(6), 1–19. https://doi.org/10.1002/adma.202000086

[19] Xiong, J., Di, J., Xia, J., Zhu, W., & Li, H. (2018). Surface Defect Engineering in 2D Nanomaterials for Photocatalysis. Advanced Functional Materials, 28(39)1801983. http://dx.doi.org/10.1002/adfm.201801983

[20] Gao, K., Wang, B., Tao, L., Cunning, B. V., Zhang, Z., Wang, S., Ruoff, R. S., & Qu, L. (2019). Efficient metal-free electrocatalysts from N-doped carbon nanomaterials: Mono-doping and co-doping. Advanced Materials (Deerfield Beach, Fla.), 31(13)201805121. https://doi.org/10.1002/adma.201805121

[21] Wang, S., Zhang, J., Li, B., Sun, H., & Wang, S. (2021). Engineered graphitic carbon nitride-based photocatalysts for visible-light-driven water splitting: A review. Energy & Fuels: An American Chemical Society Journal, 35(8), 6504–6526. https://doi.org/10.1021/acs.energyfuels.1c00503

[22] Gawande, M. B., Goswami, A., Felpin, F.-X., Asefa, T., Huang, X., Silva, R., Zou, X., Zboril, R., & Varma, R. S. (2016). Cu and cu-based nanoparticles: Synthesis and applications in catalysis. Chemical Reviews, 116(6), 3722–3811. https://doi.org/10.1021/acs.chemrev.5b00482

[23] Tong, H., Ouyang, S., Bi, Y., Umezawa, N., Oshikiri, M., & Ye, J. (2012). Nano-photocatalytic materials: Possibilities and challenges. Advanced Materials (Deerfield Beach, Fla.), 24(2), 229–251. https://doi.org/10.1002/adma.201102752

[24] You, B., Tang, M. T., Tsai, C., Abild-Pedersen, F., Zheng, X., & Li, H. (2019). Enhancing electrocatalytic water splitting by strain engineering. Advanced Materials (Deerfield Beach, Fla.), 31(17)201807001. https://doi.org/10.1002/adma.201807001

[25] Shi, Y., & Zhang, B. (2016). Recent advances in transition metal phosphide nanomaterials: synthesis and applications in hydrogen evolution reaction. Chemical Society Reviews, 45(6), 1529–1541. https://doi.org/10.1039/c5cs00434a

[26] Pu, Z., Liu, T., Amiinu, I. S., Cheng, R., Wang, P., Zhang, C., Ji, P., Hu, W., Liu, J., & Mu, S. (2020). Transition-metal phosphides: Activity origin, energy-related electrocatalysis applications, and synthetic strategies. Advanced Functional Materials, 30(45)2004009. https://doi.org/10.1002/adfm.202004009

[27] Wang, H., Li, J., Li, K., Lin, Y., Chen, J., Gao, L., Nicolosi, V., Xiao, X., & Lee, J.-M. (2021). Transition metal nitrides for electrochemical energy applications. Chemical Society Reviews, 50(2), 1354–1390. https://doi.org/10.1039/d0cs00415d

[28] Shen, S., Wang, Z., Lin, Z., Song, K., Zhang, Q., Meng, F., Gu, L., & Zhong, W. (2022). Crystalline-amorphous interfaces coupling of CoSe2/CoP with optimized d-band center and boosted electrocatalytic hydrogen evolution. Advanced Materials (Deerfield Beach, Fla.), 34(13)$_2$110631. https://doi.org/10.1002/adma.202110631

[29] Jin, H., Guo, C., Liu, X., Liu, J., Vasileff, A., Jiao, Y., Zheng, Y., & Qiao, S. Z. (2018). Emerging Two-Dimensional Nanomaterials for Electrocatalysis. *Chemical Reviews*, *118*(13), 6337–6408. https://doi.org/10.1021/acs.chemrev.7b00689

[30] Preethi, V., & Kanmani, S. (2013). Photocatalytic hydrogen production. Materials Science in Semiconductor Processing, 16(3), 561–575. https://doi.org/10.1016/j.mssp.2013.02.001

[31] Database 'Web of Science'. https://www.webofscience.com/wos/woscc/basic-search

[32] Van Eck N. J., Waltman L. (2010). Software Survey: VOSViewer, a Computer Program for Bibliometric Mapping, Scientometrics, 84/2: 523–38

[33] Power BI. Microsoft.com. Retrieved from https://www.microsoft.com/en-us/power-platform/products/power-bi

Engineered Nickel Selenide based catalysts for Urea Oxidation Reaction

Sanjeeb Kumar Ojha[1], Kamlesh[1,2], Deepika Tavar[1,2], Manish Mudgal[1,2], Archana Singh[*1,2]

[1]CSIR– Advanced Material and Processes Research Institute (AMPRI), Bhopal, MP, 462026, India
[2]Academy of Scientific & Innovative Research (AcSIR), Ghaziabad, UP, 201002, India.
**archanasingh@ampri.res.in*

Abstract :

The sustainable hydrogen economy has accelerated hydrogen production development, with urea-assisted hydrogen generation being a promising approach due to low voltage requirements and waste water remediation. Over time, significant focus has been placed on enhancing the performance of Ni-based catalysts in the urea oxidation reaction (UOR), a crucial factor in urea assisted hydrogen generation. Nickel selenides in recent years have proved to be a high performing nickel catalyst for UOR. In this review, we have discussed recent advances in nickel selenide-based catalyst for UOR and various strategy adopted for engineering the catalyst properties which resulted in enhancement of their catalytic activity for UOR.

Keywords: *Nickel selenides, Heterostructures, Interface engineering, UOR*

1. Introduction

Depleting fossil fuel and increasing climatic crisis have triggered a race in global energy and environment field to develop a reliable and sustainable energy source which with regard to meeting the global energy demands also generate least to zero carbon emission. With all the renewable energy options present like wind energy, solar energy, hydro energy and so on Hydrogen (H_2) is accepted as a promising sustainable energy candidate for meeting global energy demands because not only it possess high gravimetric energy density which is almost threefold higher than conventional gasoline but also generate lowest or zero carbon emission depending upon the process of production.[1]. Furthermore, hydrogen-based energy technology is recognised as a viable energy storage carrier for the reduction of greenhouse gases CO_2.[2]. Even though hydrogen generation from water electrolysis have various advantages but the sluggish kinetics associated with oxygen evolution reaction (half-cell reaction) results increase in energy input to drive the reaction process hence limiting the energy conversion efficiency of the system.[3]. Additionally, the commercial hydrogen generation through alkaline water-electrolysis relies on the clean or advanced water resources which in term increases the overall investment cost . Hence if anyway, we can use alternate source, such as organic waste water, it will be supported from the standpoint of both sustainable supplies and environmental management. Urea, a significant N-based fuel, is used in agriculture, drug, and adhesive industries. Untreated waste water poses a threat to ground water and air due to harmful products. However, urea is a good hydrogen carrier with a 6.67 wt.% hydrogen content, making it a potential energy carrier in fuel cell technology.[4, 5].

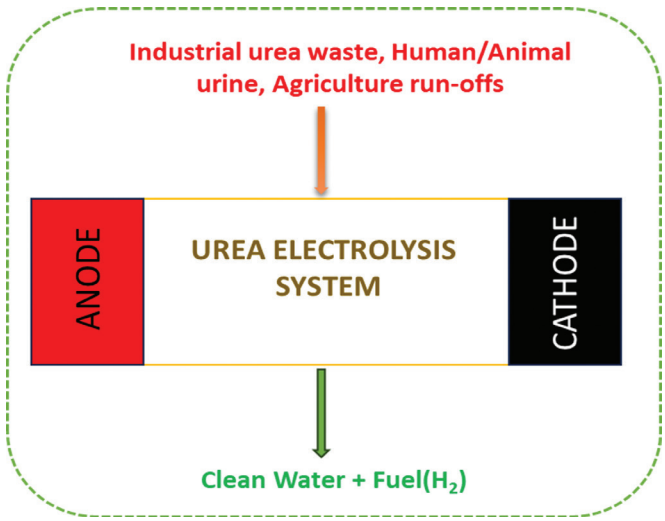

Fig.1. Schematic diagram of urea electrolysis and its applications

From all the available methods for the decomposition of urea, electrooxidation of urea is one of the cost effective and efficient method because along with decomposition of urea to non-toxic byproducts it as also helps generate hydrogen in alkaline medium (Fig.1). Overall urea electrolysis is depicted in the equation below (Fig. 2a):-

Anode:

$CO(NH_2)_2 + 6OH^- \rightarrow N_2 + 5H_2O + CO_2 + 6e^-$ E= - 0.46 V (1)

Cathode:

$6H_2O + 6e^- \rightarrow 3H_2 + 6OH^-$ E= - 0.83 V (2)

Overall:

$CO(NH_2)_2 + 6H2O \rightarrow N_2 + 3H_2 + CO_2$ E = 0.37 V (3)

In comparison to water electrolysis, the theoretical potential required to drive the urea electrolysis process is only 0.37 V, which is significantly lower than the 1.23 V necessary for water electrolysis.[6]. Nevertheless, as can be observed in above equation, the UOR undergoes $6e^-$ transfer process which is responsible for its relatively slower reaction kinetics along with that the byproducts that are produced CO_2,CO_x, etc during UOR make long term stability of catalyst challenging.[7]. Hence to overcome these challenges development of highly efficient catalyst were done and exclude the use of noble materials like ruthenium, platinum, etc since it will further increase the investment cost. The attention is mostly focused towards the nickel-based materials due to low cost and promising catalytic performance.[8-13].

UOR Mechanism

As previously stated, the majority of research into the production of UOR catalysts is centred on nickel and nickel-based compounds. The biocatalytic breakdown of urea in the active sites of urease enzymes, which contain hydroxide bridged Ni^{2+} centres, is thought to have inspired the use of nickel-based catalyst.[14, 15]. Later, it was experimentally discovered that Ni-based catalysts exhibits higher catalytic activity than other researched non-noble metal catalysts. Bottle's group have done extensive study on UOR and its mechanism, employing Raman spectroscopy, in-situ X-ray diffraction (XRD) and Density functional theory (DFT) calculations. Vedharathinam and Botte demonstrated via in-situ Raman spectroscopy that $Ni(OH)_2$ is surface oxidised to NiOOH, which serves as the real oxidation catalyst.[16]. Further, Bottle and group using in-situ XRD investigated Urea electrolysis on $Ni(OH)_2$ and according to their findings $Ni(OH)_2$ is oxidised to NiOOH at a potential between 1.2-1.6 V in 5.0 M KOH. The electrochemically produced NiOOH combines with urea and is reduced to $Ni(OH)_2$, while urea is oxidised to N_2 and CO_2. [17]. With all the findings and electrochemical results, they concluded NiOOH as the electroactive species for UOR and established it as the electro-chemical oxidation mechanism, shown below:-

Electrooxidation: $6Ni(OH)_2 + 6OH^- \rightarrow 6NiOOH + 6H_2O + 6e^-$ (4)

Chemical oxidation: $CO(NH_2)_2 + 6NiOOH + H_2O \rightarrow N_2 + CO_2 + 6Ni(OH)_2$ (5)

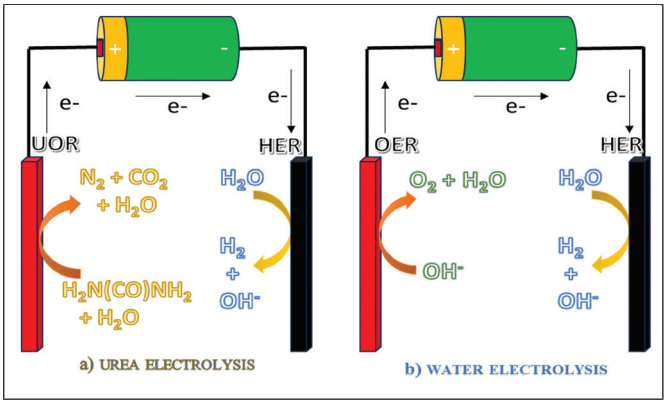

Fig.2 Schematic diagram of urea and water electrolysis

According to the mechanism, in the presence of OH-, $Ni(OH)_2$ was electrooxidized to NiOOH, and then urea molecules were adsorbed onto NiOOH via bridge coordination, in which the nickel atom interacts with the nitrogen and oxygen atoms, and the oxygen atom of nickel oxyhydroxide interacts with the carbon atom of urea. The dissociation of urea on NiOOH is a multistep process that generates a variety of intermediate species. Bottle et al. employed DFT to evaluate the products, catalytic mechanism, and relative rate-determining steps of urea degradation on NiOOH. [18]. The group put forward three possible reaction pathways and calculated the free energy of all the elementary steps. From the study they found out that desorption

of CO_2 is the rate limiting step due to highest Gibbs free energy change (1242.2 kJ mol^{-1}). The reaction pathway of the UOR can be described as follows:

$*CO(NH_2)_2$ → $*CO(NH_2.NH)$ → $*CO(NH_2.N)$ →$*CO(NH.N)$ → $*CO(N_2)$ → *CO(OH) →*COO, and the CO_2 desorption.

Over the years many nickel based catalysts have been designed in order to tackle the challenges associated with UOR and many reviews were published summerising based on various techniques of synthesis, strategy of modifying the catalyst surface for enhancedd adsorbtion and efficent breakdown of urea molecules for the generation of hydrogen. In this review the focus will be on the Nickel Selenide based catalyst which in recent years have drawn considerable attention and a peak in publications based on the same is observed as an electrocalyst for UOR.

2. Why Transition metal chalcogenides (TMCs)?

In brief, transition metal chalocogenides have shown prominent activity for UOR because of certain factors, first due to higher bulk conductivity than traditional nickel oxides and hydroxides which inturns provides a faster path for charge transfer across the electrocatalyst-electrolyte interfaces.[19]. Second, TMCs undergo surface reconstruction by partially exchanging anions with oxide/hydroxide which results in increasing the surface area, hence enhanching the catalytic performance. Third, presence of guest anions (undergo dissolution as oxianions due to formation of thermodynamically favorable metal oxide and hydroxides) causes alteration of the host metal's lattice structure and its electronic structure which according to reported literature is responsible for lower corndination number and longer bond length in transition metal chalocogrnides resulting in weakning of metal-metal bondstrength, enhancing the rate of surface oxidation process like UOR and OER.[20, 21]. Futher moderate abundance and lower cost can be the other factors for the increase in development of chalocogenides based catalyst for UOR (Fig.3).

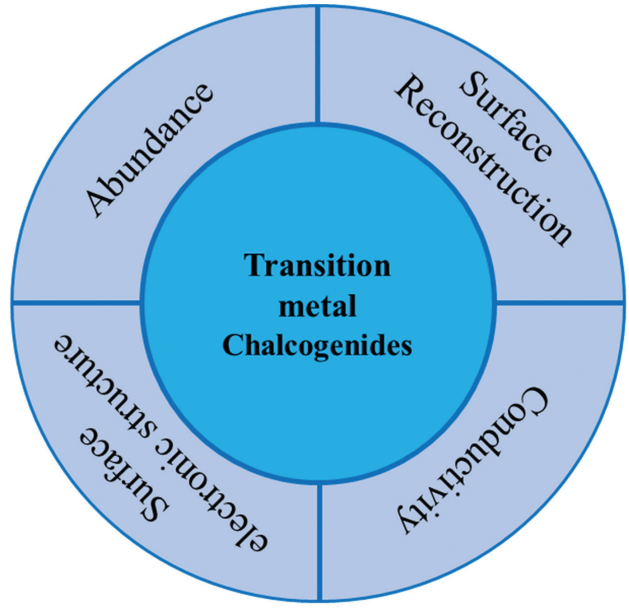

Fig.3. Shematic diagrams representing various factores reposible for implimentation of TMCs based catalyst for UOR

2.1 Nickel selenide and other Transition metal chalcogenides

The bulk conductivity of a catalyst has a substantial impact on its electrocatalytic activity. Increased conductivity is believed to aid in the transfer of charge across interfaces between electrolytes and electrocatalysts. Nickel selenides are semiconductors but oxides of nickel are insulating in nature. Therefore nickel selenides show better catalytic activity compare to its oxide counterpart. Despite tellurides having higher conductivity than selenides, nickel tellurides exhibit lower or comparable activity to nickel selenides. This can be attributed to factors such as the weaker tendency of nickel telluride to undergo surface reconstruction and the poor accessibility of Ni sites buried beneath the large anionic cloud of telluride. Conversely, nickel sulphide exhibits superior surface construction but has a relatively poor conductivity. Hence, nickel selenide was used for various electrocatalytic application like OER, HER, UOR,etc.[19, 22]. In case of UOR nickel based chalcogenides are intensively studied compared to other transition metal chalcogenides since NiOOH was proved to be the catalytic active site for oxidation of urea which was discussed earlier in above section.

3. Nickel Selenides (NiSe)

3.1 Structural and elecronic properties of Nickel selenides

The suitability of a particular nickel chalcogenides for a specfic application is largerly depends upon the stiochiometric ratios and phases of the compound. [23, 24]. The involvement of d electrons in covalent bond formation in TMCs makes their properties dissimilar to their oxide counterparts, which helps in the development of metal-metal interactive bonds. This unique property associated with TMCs is one of the reasons for their enhanced electroactivity towards various application (ie, OER, HER, ORR, CORR, UOR,etc.). Nickel selenide, being one of the TMCs exists in the various polymorphs and its formation is influenced by certain factors, which are: a) multivalent states of nickel from +2 to +4 b) the smaller electronegativity difference between nickel and selenium. There are commonly 4 types of nickel selenides which are NiSe, $NiSe_2$, Ni_3Se_2 and Ni_3Se_4(Fig.4).[25]. The most common nickel selenides are non-stiochiometric in nature.

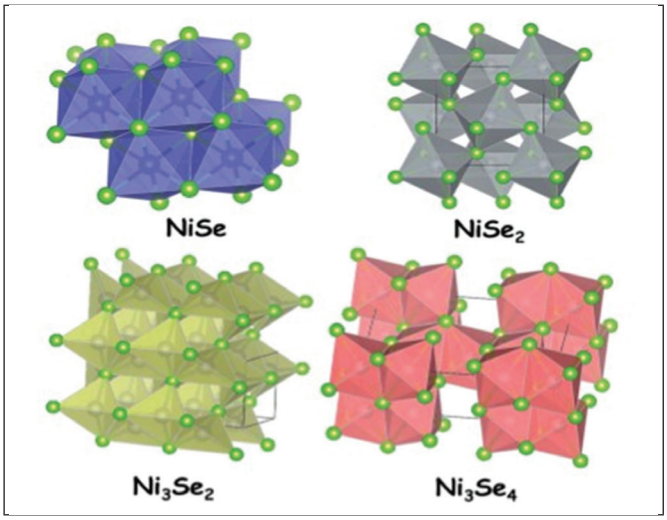

Fig.4. Different crystal structures of Nickel selenides[19](Reproduced from Ref. 19 with permission from the Royal Society of Chemistry)

By controlling the reaction conditions like time , temperature, and pH along with reactant ratio (Ni and Se) the desired nickel selenide can be synthesized, and intrestingly the excess selenium, nickel or both that can't be consumed during reaction can act as a template for obtaining the desired phase of nickel selenides. The impact of various parameters on the formation of different phases of nickel selenide was reported by Zhauang and group. For example, when the ratio of Ni:Se are kept equal at a high temperature (180^0C) for shorter duration of time, resulted in formation of hexagonal NiSe, but on extending the reaction time, the hexagonal NiSe gets transformed into rhombohedral NiSe. Futher, on adjusting the pH (~10) and increasing the percentage of Se resulted in formation of $NiSe_2$ with the cubic cyrstal structure . Lower pH (~10) plays a crucial role here because it results in the formation of both Se (elemental) and Se^{2-} which combine to form Se_2^{2-}, which is required for the formation $NiSe_2$, on incresing the pH to 14 leads to the formation of $Ni_{1-x}Se$ ($0<x\leq0.15$) due to lack of elemental Se. And by increasing nickel concentration (Ni:Se= 3:1) while holding the reaction at 180^0C for a longer period of time, produces pure Ni_3Se_2.[26].

Over the years, many unique synthetic procedures have been developed for the synthesis of nickel selenide phases, and in addition some other phases like monoclinic Ni_3Se_4 and orthorhombic Ni_6Se_5 have also been reported.[27, 28]. In general, nickel selenides synthesized are black in colour and are inslouble in water. The insolubility of nickel selenide acts as a boon for its application as an electrocalyst for urea splitting applications.

3.2 Synthesis strategies

Synthesis of nickel selenides are carried out employing various tehniques such as ele ctrodeposition, hydrothermal/solvothermal, reflux method, microwave irradiation and physical adsorption. In the upcoming section few of the well known, cost-effective and recently reported synthesis procedure is summerized.

3.2.1 Electrodeposition

The electrodeposition technique is one of the most attractive, cost-effective and oldest techniques for the fabrication of desired compounds via cathodic reduction in aqueous or organic solvents.[29]. While the growth of electrodeposited films is influenced by the applied potential, temperature of the reaction condition, time, and mobility of precursor ions, by

manipulating these parameters, films of the desired thickness, morphology, composition, etc. can be synthesized. Zhu and coworkers have synthesized different phases of nickel selenides by varying the applied potential using nickel foam as the cathodic substrate. They have reported that when the deposition is carried out at -0.35 V , -0.46 V and -0.60 V (vs SCE) it results in the formation of cubic $NiSe_2$, hexagonal NiSe and hexagonal Ni_2Se_3, respectively. [30]. Although, electrodeposition via chronoamperometry and CV cycling are very commom, but in recent years, pulse voltage technique have been employed for their synthesis. By adjusting the pulse time and duty cycle Ni-Se of the desired thickness and particle size can be achieved.[31]. Ahn and coworkers reported the use of pulsed voltage deposition to synthesize nickel selenide films with good uniformity and a thickness of 150 nm.[32].

3.2.2 Hydrothermal

Hydrothermal methodology is widely used for the synthesis of compounds of desired morphology, particle shapes, sizes and different phases of desired compound.[33, 34]. Engineering the parameters of the reaction, like time, temperature, solvent volume and type, etc affect the properties of synthesized product. Few advantages associated with hydrothermal method are high crystallinity, phase purity, fast reaction kinetics, etc.[35]. Nickel selenides with different morphology has been reported by changing the selenium precursor, like selenourea ($SeC(NH_2)_2$),selenium dioxide (SeO_2) and potassium slenocyanate (KSeCN) which resulted in production of nickel selenide with wires, spheres and hexagons morphology respectively. [36]. Hydrothermally produced $Ni(OH)_2$ is followed by a hydrothermal anion exchange reaction of nickel hydroxide with chalcogen ions created by using a reducing agent to produce nickel selenide nanosheets. Reduction by $NaBH_4$ causes a rapid exchange of OH- from $Ni(OH)_2$ with Se ions, resulting in the formation of a thin layer of $NiSe_2$. The reaction mention below provides a possible mechanism for anion-exchange reaction.[37].

$$Ni(OH)_2 + 2Se + NaBH_4 \rightarrow NiSe_2 + B(OH)_2^- Na^+ + 2H_2 \quad (1)$$

Advancement in direct selenization of metallic substrate like Ni foil and Ni foam are also observed in recent years. Various techniques other than hydrothermal used for direct selenization of metallic substrate are like thermal deposition[38], Physical vapour deposition[39], chemical vapor deosition[40] and others are employed to obtain desired nickel selenides. The superiority of direct selenization of metallic substrates is envisaged due to the metallic substrate's predominant conductivity and binder-free approach. Tang et. al. synthesized NiSe nanowires on the surface of Ni foam by simple hydrothermal approach in which Ni foam is placed in a solution containing NaHSe as Se source.[41].

3.2.3 Microwave-assisted (MW) synthesis

A rapid growth is observed in MW- assisted synthesis of inorganic nanomaterials since it is considered as one of the fast synthesis practice. It is also postulated that the efficient and controlled heating conditions that can be achieved by microwave irradiation prove to be highly beneficial for the synthesis of nanomaterials and nanostructures, whose growth is highly sensitive towards reaction conditions. Anantharaj and group have reported successful synthesis of Ni_3Se_4 nanoassemblies for the application of water splitting in neutral and alkaline media. In their work, they have fabricated Ni_3Se_4 on the surface of nickel foam (NF) using NaHSe as selenium precursor. The reaction mixture containing NF and NaHSe is irradiated with microwave radiation of power 300 W continuously for 3 minutes for the successful formation of Ni_3Se_4. [42].

4. Engineering Nickel selenides for UOR

In recent years a peak in nickel selenide based catalysts for the application of UOR has been observed, in which various strategies were implemented in order to ehance the structural, electronic and morphological properties of the catalyst for the boost in UOR activity, and those developments are discussed in the upcoming session of the paper.

4.1 Incorporation of Heteroatom

Heteroatom doping is a widely studied area and is being employed to enhance catalyst performance, and it is widely used in the field of UOR to improve catalytic performance by regulating the electronic structure of Ni active sites. Based on this strategy, Yu and coworkers synthesised iron-doped nickel diselenide. Three different Fe doped $NiSe_2$ are produced, which vary with respect to the percentage of iron used for the synthesis. Among the three catalysts with different Fe doping percentages, the one with 1.68 at% iron showed superior activity by achieving a current density of 125.8 mA/cm^2 at a potential of 1.54 V vs. RHE. Iron with a certain concentration can affect Ni valence, as demonstrated in the Fe doped NiO system, where Fe^{3+} ions act as lewis acid, promoting Ni^{4+} formation.[20]. On comparing with $NiSe_2$, in Fe-$NiSe_2$ due to doping of iron resulted in an increase in precentage of high valent Ni^{3+} but also optimized the adsorption capacity of nickel to urea molecules as revealed through DFT analysis. Compared to $NiSe_2$ (-1.12 eV), Fe doped $NiSe_2$ (-1.68 eV) showed a higher adsorption energy of urea molecules on the Ni sites. This enchancement witnessed was caused by the electronic structure regulation induced by doping resulting in increment of electron abundance around Ni atom in Fe-$NiSe_2$. Trimetallic selenide $NiFeCoSe_2$ with superior catalytic activity, owing to the synergy existed between the three metals has been reported for UOR. XPS analysis revealed that, compared to its bimetallic counterpart, the Co 2p XPS spectra showed a shift towards lower binding energy, implying an increase in electron transfer and a stronger interaction between the metals, proving existance of synergy between metals.[43]. Incorporating non-metals like sulphur in nickel selenide (Ni-S-Se/NF) showed a great improvement in the activity for UOR, which can be assigned to the following reasons; a) increase in amorphicity due to sulphur incorporation and higher active site genration, b) Ni-S-Se/NF showed higher hydrophilicity and aerophobicity. Increase in amorphicity of the catalyst compared to its NiSe and NiS counterparts provides Ni-S-Se compound and in-situ generated NiOOH with higher active sites and improvement in hydrophilicity and aerophiolicity of the catalyst aid its long-term performance.[44].

4.2 Nickel selenide integrated Carbon based substarte

Carbon-based materials are cost-effective and environmentally friendly materials, owing to their good conductivity, fast charge transfer, stability, high surface area, & ease of modification have drawn considerable attention of researchers to incorporate various carbon based materials like rGO, CNTs, amorphous carbon with nickel based compounds for the enhancement of catalytic activity.[45]. $Ni_{0.85}Se$ nanocrystals grown on the surface of rGO ($Ni_{0.85}Se$@ rGO) reported to achieve superior catalytic activity in comparison to their non-rGO couterpart. The enhancement is ascribed to the unique cluster structure, which provides higher surface area and exposure to higher catalytic sites and in addition rGO as a carrier improves conductivity and electron transfer rate, thereby boosting UOR activity.[46]. Khalafallah et. al. has synthesised muti-walled CNT supported nickel cobalt selenide composite (Ni-Co-Se/CNT) via one pot hydrothermal method. The synthesised catalyst shows a remarkable activity for UOR (0.29 V vs. Hg/Hgo @10 mA/cm^2). The incorporation of tubular CNTs amended the rate of mass transfer ascribed to their porous network architectures, while presence of Co active sites along with electrochemically active NiOOH layer helped boost the catalytic activity. Morphological analysis revealed the twisted atomic arrangements on the hybrid surface, suggesting disordered selenide formation due to defects. These defects contribute to the enhancement of electroactivity by promoting active edge sites and improving reaction kinetics.[47]. Nitrogen doping in carbon-based substrates enhances composite porosity, surface composition, and interlayer spacing, thereby improving electrochemical performance. Qiuhan and coworkers successfully coupled dual phase nickel selenide ($Ni_{0.85}Se/NiSe_2$) with N-doped carbon through hydrothermal and calcination, revealing higher active sites in the dual phase. Furthermore, interfacial charge transfer existed

from Ni/Se and N/C atoms will generate strong electronic contacts between $Ni_{0.85}Se$, $NiSe_2$, and the NC matrix, allowing charge transfer and electronic modulation, resulting in an increase in catalytic performance. The composite $Ni_{0.85}Se/NiSe_2$@NC demonstrated superior COx poisoning resistance compared to the non-composite counterpart (i.e, $Ni_{0.85}Se/NiSe_2$), attributed to the doped nitrogen element's ability to facilitate COx desorption.[48]. To summerize, combining carbon substrate to nickel selenide revelead to possess advantages of pure nickel selenide. The combination of carbon substrate with nickel selenide demonstrated numerous advantages compared to pure nickel selenide. Top of the list incorporating carbon substrate limits the growth of nickel selenide nanoparticles to prevent agglomeration, which reduces electrical conductivity and the availability of active sites. The direct interaction between carbonaceous platforms and metallic atoms shortens diffusion pathways for electrolyte ions and electrons, enhancing catalytic activity by providing higher electroactive sites and modulating electronic configuration, resulting in superior electrochemical characteristics. CNT with its 3D tubular structure and porous network architecture, improves structural stability and facilitates interaction between the active material and electrolyte ions. This helps prevent connectivity issues, aggregation, and phase separation, ultimately enhancing catalytic performance compared to pure nickel selenide.

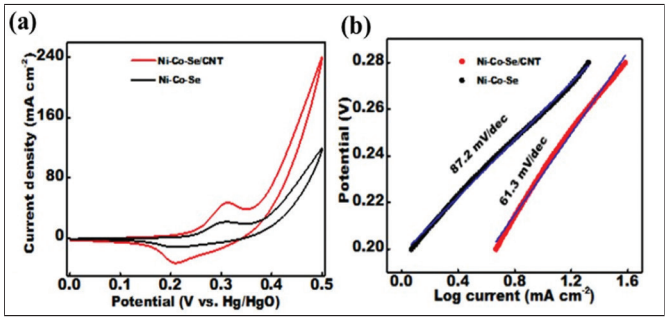

Fig.5. a) CVs of the catalysts recorded at a scan rate of 10 mVs -1 at room temperature in 1 M KOH + 0.5 M urea and b) Tafel plots of Ni-Co-Se and Ni-Co-Se/CNT catalysts in 1 M KOH with 0.5 M urea. [47] (Reproduced from Ref. 47 with permission from the John Wiley and Sons, Inc.)

4.3 Hetrostructuring

Nickel selenides, with their unique electronic configuration and high conductivity, have potential as electrocatalysts for hydrogen production. But their efficacy, is hampered by fewer exposed active areas and poor structural stability. Construction of heterostructures by hybridization of suitable components can substantially improve the percentage of active sites and structural stability , based on that various papers have reported strategies for constructing heterostructures to enhance catalytic performance for UOR, which are discussed in the following section.

4.3.1 Metal oxide-Nickel selenide heterostructures

As for the published literature, NiO shows inferior activity compared to nickel selenide, but when NiO is incorporated with Nickel selenide, the heterostructure generated shows comparably higher activity for UOR (1.33 V vs RHE @10 mA/cm^2). HR-TEM analysis of NiO-$NiSe_2$ edge regions revealed an interface between NiO nanosheets and $NiSe_2$ nanoparticles, generating higher active sites and facilitating faster reactant and electrolyte diffusion. Moreover, the concomitant bonds of Ni-$_O$ and Ni-Se bond induce the high valence state of Ni, which acts as the active site for UOR.[49] Doping CeO_2 onto $Ni_{0.85}Se$ on the surface of N-doped carbon showed superior performance with respect to its non-CeO_2 counterpart since CeO_2-$Ni_{0.85}Se$-NC required a potential of 1.294 V vs RHE to achieve a current density of 10 mA/cm^2 which is about 28 mV lower than $Ni_{0.85}Se$-NC. XPS analysis revealed, CeO_2 incorporation resulted in an alteration of chemical state and electronic structure, as suggested by the Ni 2p spectrum, where a negative shift in peak is observed w.r.t its non-CeO_2 counterpart. Moreover, the Ce 3d spectrum showed increased Ce^{3+} in the catalyst, indicating oxygen vacancies and defect sites, resulting in enhanced catalytic activity due to the generated metal and oxygen defects.[50].

4.3.2 Metal hydroxide-Nickel selenide heterostructures

Chun et.al. produced Se-$Ni(OH)_2$@NiSe/NF via in-situ electroxidation of NiSe/NF, which showed a shift

towards lower potential to achieve a current density of 100 mA/cm^2 i.e. 0.366 V vs. SCE, compared to NiSe/NF nanowires (0.384 V vs. SCE) and $Ni(OH)_2$/NF (0.486 vs. SCE) respectively. The electroxidation of NiSe/NF led to a decrease in crystallinity and the formation of core shell hetrostructure nanowires and abundant nanosheets, as observed through HR-TEM images while a new peak near 857.1 eV is observed ascirbed to NiOOH formation. Generation of core shell heterostructure and higher valent Ni^{3+}(NiOOH) responsible for improved catalytic activity for UOR. [51]. The catalyst core-shell structure consisting of a NiSe core with intrinsic semiconductor properties that facilitate rapid electron transport along the nanowire. The shell, made of Se-$Ni(OH)_2$, offers numerous active catalytic sites and reduces the adsorption/desorption barrier to promote fast reaction kinetics. The synergistic effect of these two features is responsible for the increased activity observed in Se-$Ni(OH)_2$@NiSe/NF compared to NiSe and $Ni(OH)_2$ alone.

4.3.3 Metal sulphide – Nickel selenide heterostructures

Lin and coworkers via electrodeposition, synthesised Heazlewoodite-phased Ni_3Se_2 nanocrystals on a Cu_2S nanowire backbone. The as-generated hierarchical Cu_2S@Ni_3Se_2 exhibits improved catalytic activity for UOR, requiring a potential of 1.338 V vs RHE to obtain a current density of 10 mA/cm^2.The outstanding catalytic activity is attributed to an increase in geometric area achieved due to the vertically grown nanowire morphology of Cu_2S resulting in higher loading and exposure of catalytically active Ni_3Se_2 and a boost in charge transfer between electrode and electrolyte owing to the closely contacted interface between Cu_2S and Ni_3Se_2.[52]. Ultrathin MoS_2 nanosheets composited with NiSe nanowire arrays demonstrated an onset potential of 1.42 V vs RHE for UOR, which is 50 mV lower than its OER counterpart. The positive shift of 0.6 eV for the peak related to Mo^{3+} in Mo 3d of the concerned catalyst w.r.t MoS_2 and similarly, a 0.3 eV positive shift in S $2p_{1/2}$ peak w.r.t MoS_2 S $2p_{1/2}$ peak confirms a strong electronic interaction between NiSe and MoS_2 which is the reason for higher catalytic performance.[53]. The MoS_2 nanosheets can increase the active sites and provide a channel for electrolyte transport and gas release, then the interfacial interaction between NiSe and MoS_2 can promote electron transfer. Hence, NiSe@MoS_2/NF requires lowest onset potential for UOR compared to NiSe@NF and MoS_2@NF.

4.3.4 Metal selenide-Nickel selenide heterostructures

$NiSe_2$/$FeSe_2$ with p-p hetrojunction was developed by Shan and coworkers using a feasible solid-state selenization strategy using Fe-Ni PBA(Prussian blue analogues) as the precursor. Owing to the difference in energy levels between $NiSe_2$ and $FeSe_2$, a built-in electric field is generated at the heterointerface. The built-in electric field creates a space-charge region at the interface, enhancing electron transfer and adsorption of targeted reactants, leading to higher UOR activity.[54]. Xiujuan et al. reported controllable transition engineering from homogeneous $NiSe_2$ nanowrinkles (NWs) to heterogeneous Ni_3Se_4/$NiSe_2$ nanorods (NRs) for the first time by manipulating the selenization temperature, resulting in the development of interfaces. The self-supported nanorod arrays on the 3D nickel foam expose more catalytic sites and allow for unhindered transport of electrolyte ions and released gases. From the DFT study reported in the paper discloses that the redistribution of electrons in the interfacial region resulted in reformation of charge transfer efficiency and electron, which further helped in optimization in the adsorption & desorption of reactive intermediates for the reduction in Gibbs free energy associated with UOR. Owing to enhancements in structural and electronic properties, Ni_3Se_4/$NiSe_2$ NRs only require a potential of 1.296 V vs RHE to achieve a current density of 10 mA/cm^2 which in much lower compared to Ni_3Se_4/$NiSe_2$ NWs (1.339 V vs RHE) and $NiSe_2$ NWs (1.362 V vs RHE).[55] Mixed phased $CuSe_x$@Ni_3Se_2 with interconnected nanoflake morphology resulted in enhancement in UOR activity when compared with individual components owing to its hierarchical heterostructures.[56].

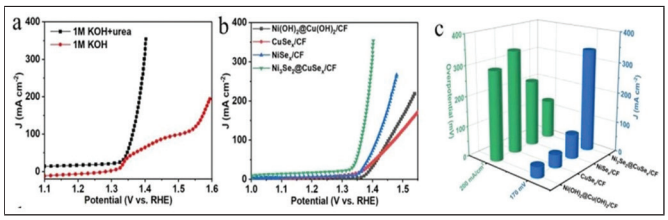

Fig.6. (a) iR-corrected polarization curves of Ni_3Se_2@$CuSe_x$/CF in 1m KOH electrolyte with and without 0.5 m urea. (b) iR-corrected UOR polarization curves and (c) comparison diagram of overpotential at 200 mAcm^2 and current density at 170 mV.[56]. (Reproduced from Ref. 56 with permission from the John Wiley and Sons, Inc.)

4.3.5 Metal Telluride – Nickel selenide heterostructures

Both Te and Se belong to the chalcogen group, and with an increase in atomic number, the elctronegativity decreases; hence Te possess a lower electronegativity than Se. The ionocity and covalent strength of chemical bonds depend on the electronegativity of bonded particles, and as transition metals move from oxygen to Te, ionicity weakens while covelenity strengthens. According to prior research, the stronger the covalent character of the M-X bond, the more favourable the redox reaction at the transition metal center.[57]. The high degree of covalency and higher intrensic metallicity are resposible for the higher conductivity and mass transfer rate of the transition metal tellurides. Ting and coworkers employed interface engineering to integrate both selenide and telluride to take advantage of the benefits of both systems. The HRTEM analysis of Ni0.85Se/NiTe@NF showed nanorod thickening after electrodeposition of nickel selenide onto nickel telluride, justifying the formation of a core shell structure.

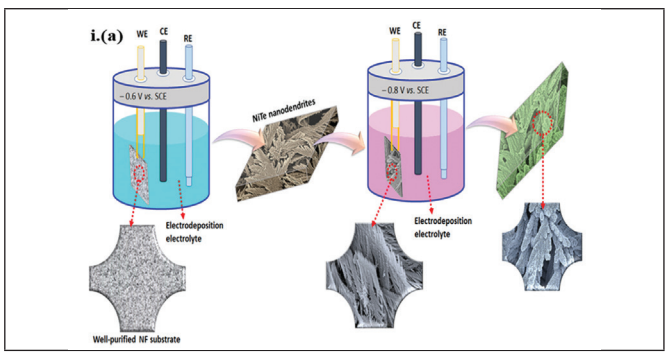

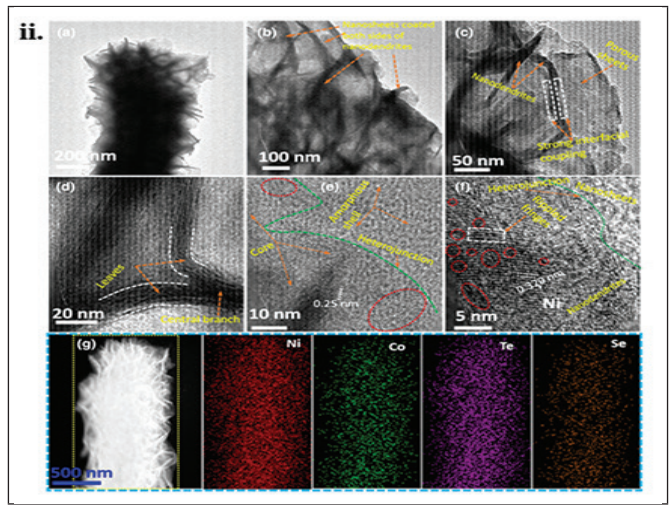

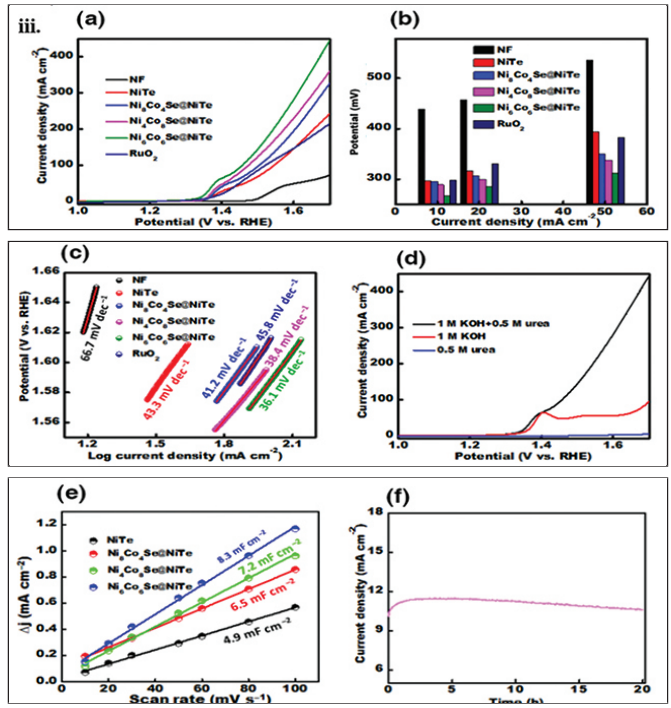

Fig.7. i) schematic diagram of Synthetic strategy ii) HRTEM images of $Ni_xCo_{12-x}Se$@NiTe iii) a. polarization curve of ifferent catalyts, b. comparison graph, c. Tafel plot , d. polarozation plot with and without the presence of urea, e. ECSA and f. stability graph.[58]. (Reproduced from Ref. 58 with permission from the John Wiley & Sons Australia, Ltd)

Further high angle annular dark field-scanning TEM (HAADF-STEM) results showed a uniform distribution of Ni throughout the catalyst surface, while Se and Te were present in the core of the structure. An enhancement in peak area of Ni^{2+} and Ni^{3+} after electrodeposition, while a positive shift

and negative shift in peaks concerned with Te 3d and Se 3d suggested the formation of an interface that favours electron transfer from Te to Se. All this enhancement resulted in achieving superior activity for UOR where it acquired a current density of 200 mA/cm^2 at a potential of just 1.324 mA/cm^2. [59]. Diab et.al. synthesised $Ni_xCo_{12-x}Se$@NiTe via the two stage electrodeposition process shown in (Fig.5.i.a). FESEM images display a greater and uniform coverage of squama-like architectures composed of a 2D $Ni_xCo_{12-x}Se$ nanosheet network on the surface of freestanding NiTe dendritic frameworks, whereas the HR-TEM picture shows interlacing between the 3D arrayed dendrites and the 2D nanosheet network, forming a hierarchical core-shell architecture (Fig.5.ii.a-f) while EDS-mapping reveals the presence of Ni,Co,Te, and Se on the catalyst's surface. Ni_6Co_6Se@NiTe electrode achieves the a current density of 10 mA/cm^2 at a potential of 1.33 V vs RHE while Ni_4Co_8Se@NiTe achieves same current density at 1.35 V vs RHE and Ni_8Co_4Se@NiTe at 1.36 V vs RHE. Similarly, Ni_6Co_6Se@NiTe shows the lowest tafel and highest ECSA due to their unique structure (Fig.5.iiia-f). [58]. In the above discussion we observed various examples of heterostructure engineering where by coupling the advantage of individual components and regulating the redistribution of electrons around metal active centers, resulted in the the optimal adsorption energies of reactive species for rapid reaction kinetics and generation of higher number of active sites compared to its unitary counterparts. Simply put, the Se-Ni(OH)$_2$@NiSe/NF structure combines the conductivity of the NiSe core with the high active sites provided by the Ni(OH)$_2$ shell. The polymetallic $NiSe_2$ and $FeSe_2$ create a p-p heterojunction that facilitates the adsorption of target molecules. By heterostructuring selenides and tellurides of nickel, the system benefits from the advantages of both components. The distinct morphologies and structure achieved through heterostructuring are responsible for the enhanced catalytic performance of heterostructured catalysts compared to their unstructured counterparts.

Table 1. List summerizing catalytic performance of engineered Nickel selenide based catalysts for UOR

S.N.	Catalyst	Electrolyte	Catalytic activity	Tafel	Reference
1.	Fe-$NiSe_2$	1.0 M KOH + 0.33 M urea	1.367 V vs RHE @10 mA/cm^2 1.54 V vs RHE @ 125 mA/cm^2	22.9 mV dec^{-1}	[20]
2.	NiMoSe	1.0 M KOH + 0.33 M urea	1.39 V vs RHE @ 10mA/cm^2	43.3 mV dec^{-1}	[60]
3.	$NiCoFeSe_2$	1.0 M KOH + 0.33 M urea	1.37 V vs RHE @ 50 mA/cm^2 1.44 V vs RHE @ 100 mA/cm^2	149.0 mV dec^{-1}	[43]
4.	MoSe@NiSe & FeSe@NiSe	1.0 M KOH + 0.33 M urea	1.42 V vs RHE @ 100 mA/cm^2 (Both MS@NS & FS@NS)	(48.0 & 57.0) mV dec^{-1}	[61]
5.	$Cu_2S@Ni_3Se_2$	1.0 M KOH + 0.50 M urea	1.338 V vs RHE @ 10 mA/cm^2	76.0 mVdec^{-1}	[52]
6.	$Ni_{0.85}Se$@rGO	1.0 M KOH + 0.50 M urea	1.36 V vs RHE @ 10 mA/cm^2	152.08 mV dec^{-1}	[46]
7.	NiCoSe@CNT	1.0 M KOH + 0.50 M urea	0.29 V vs Hg/HgO	61.3 mV dec^{-1}	[47]
8.	Ni_3Se_2@CuSex/CF	1.0 M KOH + 0.50 M urea	~ 1.35 V vs RHE @ 100 mA/cm^2	45.0 mV dec^{-1}	[56]
9.	$NiSe_2$@NiO	1.0 M KOH + 0.33 M urea	1.33 V vs RHE @10 mA/c^{m}2	38.5 mV dec^{-1}	[49]
10.	$Ni_xCo_{12-x}Se$@NiTe	1.0 M KOH + 0.5 M urea	1.33 V vs RHE @ 10 mA/cm^2	36.1 mV dec^{-1}	[47]
11.	3D-$NiSe_2$@NC	1.0 M KOH + 0.5 M urea	1.32 V vs RHE @ 10 mA/cm^2	---	[62]
12.	Ni-S-Se	1.0 M KOH + 0.50 M urea	1.38 V vs RHE @10 mA/cm^2 1.42 V vs RHE @ 100 mA/cm^2	28.0 mV.dec^{-1}	[44]
13.	$Ni_3Se_4/NiSe_2$	1.0 M KOH + 0.50 M urea	1.296 V vs RHE @ 100 mA/cm^2	44.4 mV dec^{-1}	[55]
14.	Se-Ni(OH)2@ NiSe	1.0 M KOH + 0.33 M urea	0.366 V vs SCE @ 100 mA/cm^2	---	[51]
15.	$NiSe_2$ /$FeSe_2$	1.0 M KOH + 0.5 M urea	~ 1.33 V vs RHE @10 mA/cm^2	32.0 mVdec^{-1}	[54]
16.	$Ni_{0.85}Se/NiSe_2$@NC	1.0 M KOH + 0.33 M urea	252 mA/cm^2 @ 1.6 V vs RHE	64.4 mV dec^{-1}	[48]
17.	$Ni_{0.85}Se/CeO_2$@NC	1.0 M KOH + 0.33 M urea	1.294 V vs RHE @ 10 mA/cm^2	20.09 mV dec^{-1}	[50]
18.	$Ni_{0.85}Se$/NiTe	1.0 M KOH + 0.30 M urea	1.324 V vs RHE @ 200 mA/cm^2	3.66 mV dec^{-1}	[59]

5. Discussion

Catalysts towards urea oxidation reaction are subject to the multi-functionality which includes low overpotential, faster reaction kinetics, long-term stability (superior poising resistance) and high electrocatalytic activity. Unitary catalysts (e.g. NiO, $Ni(OH)_2$, and NiSe,etc.) which exhibit catalytic activity for UOR, may not excel in all the necessary parameters to be considered as a robust catalyst. In the previous sections, we explored how herostructure engineering has been advantageous in enhancing UOR activity. Through heterostructuring we can intergrate two or more components and get benifeted from each of their strength. Transition metal chalcogenides have been widely used in research for applications such as sensors and supercapacitors due to their ability to form diverse and distinct heterostructures, setting them apart from other compounds.[63]. Nickel selenide owing to this property along with its semiconducting nature and higher surface reconstruction ability w.r.t to other chalocogenides is the reason of its intesive use for UOR application. While significant progress has been achieved through heterostructuring, further attention and research are needed to fully utilise its untapped potential. DFT calculations are used to analyse the catalyst mechanism of hetero-structured catalysts, but they do not completely represent the actual working conditions of the catalyst system. Factors like variations in electrolyte, dynamics, and structural changes during catalysis are frequently overlooked. Additionally, a UOR specific mechanistic research is necessary to comprehensively grasp the interplay of heterostructures and their role in the UOR mechanism. Strategical improvements are necessary to fully achieve the potential of both systems. Despite the abundance of reported hetero-structured catalysts, there is still an inadequate understanding of aspects such as crystal planes, chemical bond types, interface position, and spacings between hetero-interfaces that are pertinent to the heterostructure.

6. Conclusion and Outlook

This review discusses about the electrochemical UOR and its cruical role in urea assisted hydrogen generation. Nickel selenides have been endorsed as an efficent materials to promote UOR due to their high abundance, intrinsic electrical conductivity and ability for surface reconstruction. Different strategies that were implemented for enhancement of properties of nickel selenides like incorporation/ doping of heteroatom, constructing heterostructures, synthesizing carbon based composites have been discussed in this review. Apart from these valuable progress there are still some challenges and problems which need to be addressed some of which are; a) UOR mechanism is still debatable and futher studies are required for proper understanding. b) compsites based on 2D materials like rGO, functionalized rGO are needed to be explored, c) Although nickel selenides possess tremendous potential but it also associated with toxicity since higher concentration of Se is harmful for enviroment, therfore proper mangement of waste is required for the success of these catalyst for the application of energy generation.

Acknowledgment

Authors acknowledges the Department of Science and Technology, Govt., India grant no.- SERB/F/4835/2021-22 for the fellowship and for providing financial support to carry out the work.

References

[1] W. Lubitz, W. Tumas, Hydrogen: An Overview, Chemical Reviews, 107 (2007) 3900-3903. doi: https://doi.org/10.1021/cr050200z

[2] K. Oshiro, S. Fujimori, Role of hydrogen-based energy carriers as an alternative option to reduce residual emissions associated with mid-century decarbonization goals, Applied Energy, 313 (2022) 118803. doi: https://doi.org/10.1016/j.apenergy.2022.118803

[3] J. Wang, X. Yue, Y. Yang, S. Sirisomboonchai, P. Wang, X. Ma, A. Abudula, G. Guan, Earth-abundant transition-metal-based bifunctional catalysts for overall electrochemical water splitting: A review, Journal of Alloys and Compounds, 819 (2020) 153346. doi: https://doi.org/10.1016/j.jallcom.2019.153346.

[4] A.N. Rollinson, J. Jones, V. Dupont, M.V. Twigg, Urea as a hydrogen carrier: a perspective on its potential for safe, sustainable and long-term energy supply, Energy & Environmental Science, 4 (2011) 1216-1224. doi: https://doi.org/10.1039/C0EE00705F.

[5] N. Kakati, J. Maiti, K.S. Lee, B. Viswanathan, Y.S. Yoon, Hollow Sodium Nickel Fluoride Nanocubes Deposited MWCNT as An Efficient Electrocatalyst for Urea Oxidation, Electrochimica Acta, 240 (2017) 175-185. doi: https://doi.org/10.1016/j.electacta.2017.04.055.

[6] B.K. Boggs, R.L. King, G.G. Botte, Urea electrolysis: direct hydrogen production from urine, Chem Commun (Camb), (2009) 4859-4861. doi: https://doi.org/10.1039/B905974A.

[7] G. Gnana kumar, A. Farithkhan, A. Manthiram, Direct Urea Fuel Cells: Recent Progress and Critical Challenges of Urea Oxidation Electrocatalysis, Advanced Energy and Sustainability Research, 1 (2020) 2000015. doi: https://doi.org/10.1002/aesr.202000015.

[8] P. Babar, K. Patil, D.M. Lee, V. Karade, K. Gour, S. Pawar, J.H. Kim, Cost-effective and efficient water and urea oxidation catalysis using nickel-iron oxyhydroxide nanosheets synthesized by an ultrafast method, Journal of Colloid and Interface Science, 584 (2021) 760-769. doi: https://doi.org/10.1016/j.jcis.2020.09.108.

[9] G. Liu, C. Huang, Z. Yang, J. Su, W. Zhang, Ultrathin NiMn-LDH nanosheet structured electrocatalyst for enhanced electrocatalytic urea oxidation, Applied Catalysis A: General, 614 (2021) 118049. doi: https://doi.org/10.1016/j.apcata.2021.118049.

[10] X. Li, X. Cui, L. Jiang, Low-temperature and anhydrous preparation of NixFey-LDHs as an efficient electrocatalyst for water and urea electrolysis, Catalysis Communications, 162 (2022) 106390. doi: https://doi.org/10.1016/j.catcom.2021.106390.

[11] Q. Liu, L. Xie, F. Qu, Z. Liu, G. Du, A.M. Asiri, X. Sun, A porous Ni3N nanosheet array as a high-performance non-noble-metal catalyst for urea-assisted electrochemical hydrogen production, Inorganic Chemistry Frontiers, 4 (2017) 1120-1124. doi: https://doi.org/10.1039/C7QI00185A.

[12] S. Anantharaj, S. Noda, Nickel selenides as pre-catalysts for electrochemical oxygen evolution reaction: A review, International Journal of Hydrogen Energy, 45 (2020) 15763-15784. doi: https://doi.org/10.1016/j.ijhydene.2020.04.073.

[13] J. Wang, Z. Zhao, C. Shen, H. Liu, X. Pang, M. Gao, J. Mu, F. Cao, G. Li, Ni/NiO heterostructures encapsulated in oxygen-doped graphene as multifunctional electrocatalysts for the HER, UOR and HMF oxidation reaction, Catalysis Science & Technology, 11 (2021) 2480-2490. doi: https://doi.org/10.1039/ D0CY02333G.

[14] G. Estiu, K.M. Merz, The Hydrolysis of Urea and the Proficiency of Urease, Journal of the American Chemical Society, 126 (2004) 6932-6944. doi: https://doi.org/10.1021/ja049327g.

[15] G. Estiu, K.M. Merz, Enzymatic Catalysis of Urea Decomposition: Elimination or Hydrolysis?, Journal of the American Chemical Society, 126 (2004) 11832-11842. doi: https://doi.org/10.1021/ja047934y.

[16] V. Vedharathinam, G.G. Botte, Direct evidence of the mechanism for the electro-oxidation of urea on Ni(OH)2 catalyst in alkaline medium, Electrochimica Acta, 108 (2013) 660-665. doi: https://doi.org/10.1016/j.electacta.2013.06.137.

[17] D. Wang, G.G. Botte, In Situ X-Ray Diffraction Study of Urea Electrolysis on Nickel Catalysts, ECS Electrochemistry Letters, 3 (2014) H29. doi: https://dx.doi.org/10.1149/2.0031409eel.

[18] D.A. Daramola, D. Singh, G.G. Botte, Dissociation Rates of Urea in the Presence of NiOOH Catalyst: A DFT Analysis, The

Journal of Physical Chemistry A, 114 (2010) 11513-11521. doi: https://doi.org/10.1021/jp105159t.

[19] S. Anantharaj, S. Kundu, S. Noda, Progress in nickel chalcogenide electrocatalyzed hydrogen evolution reaction, Journal of Materials Chemistry A, 8 (2020) 4174-4192. doi: http://dx.doi.org/10.1039/C9TA14037A.

[20] L. Yu, X. Pang, Z. Tian, S. Wang, L. Feng, Fe-doped NiSe2 nanorods for enhanced urea electrolysis of hydrogen generation, Electrochimica Acta, 440 (2023) 141724. doi: https://doi.org/10.1016/j.electacta.2022.141724.

[21] K. Xu, H. Ding, H. Lv, S. Tao, P. Chen, X. Wu, W. Chu, C. Wu, Y. Xie, Understanding Structure-Dependent Catalytic Performance of Nickel Selenides for Electrochemical Water Oxidation, ACS Catalysis, 7 (2017) 310-315. doi: https://doi.org/10.1021/acscatal.6b02884.

[22] O. Mabayoje, A. Shoola, B.R. Wygant, C.B. Mullins, The Role of Anions in Metal Chalcogenide Oxygen Evolution Catalysis: Electrodeposited Thin Films of Nickel Sulfide as "Pre-catalysts", ACS Energy Letters, 1 (2016) 195-201. doi: https://doi.org/10.1021/acsenergylett.6b00084.

[23] N.R. Chodankar, D.P. Dubal, S.-H. Ji, D.-H. Kim, Self-Assembled Nickel Pyrophosphate-Decorated Amorphous Bimetal Hydroxides 2D-on-2D Nanostructure for High-Energy Solid-State Asymmetric Supercapacitor, Small, 15 (2019) 1901145. doi: https://doi.org/10.1002/smll.201901145.

[24] M.A. Khan, W. Hussain, K. Tufail, M. Sulaman, A.R. Ayub, W.A. Khan, H. Li, Relative study of Ni sulfides synthesized from single and multisource precursors for photocatalytic and battery applications, Energy Reports, 7 (2021) 7615-7627. doi: https://doi.org/10.1016/j.egyr.2021.10.122.

[25] N. Moloto, M.J. Moloto, N.J. Coville, S. Sinha Ray, Optical and structural characterization of nickel selenide nanoparticles synthesized by simple methods, Journal of Crystal Growth, 311 (2009) 3924-3932. doi: https://doi.org/10.1016/j.jcrysgro.2009.06.006.

[26] Z. Zhuang, Q. Peng, J. Zhuang, X. Wang, Y. Li, Controlled Hydrothermal Synthesis and Structural Characterization of a Nickel Selenide Series, Chemistry – A European Journal, 12 (2006) 211-217. doi: https://doi.org/10.1016/j.jcrysgro.2009.06.006.

[27] A. Kumar, P.K. Ahluwalia, Electronic structure of transition metal dichalcogenides monolayers 1H-MX2 (M = Mo, W; X = S, Se, Te) from ab-initio theory: new direct band gap semiconductors, The European Physical Journal B, 85 (2012) 186. doi: https://doi.org/10.1140/epjb/e2012-30070-x.

[28] L. Peng, X. Ji, H. Wan, Y. Ruan, K. Xu, C. Chen, L. Miao, J. Jiang, Nickel Sulfide Nanoparticles Synthesized by Microwave-assisted Method as Promising Supercapacitor Electrodes: An Experimental and Computational Study, Electrochimica Acta, 182 (2015) 361-367. doi: https://doi.org/10.1016/j.electacta.2015.09.024.

[29] I. Gurrappa, L. Binder, Electrodeposition of nanostructured coatings and their characterization—A review, Science and Technology of Advanced Materials, 9 (2008) 043001. doi: https://doi.org/10.1088/1468-6996/9/4/043001.

[30] J. Zhu, Y. Ni, Phase-controlled synthesis and the phase-dependent HER and OER performances of nickel selenide nanosheets prepared by an electrochemical deposition route, CrystEngComm, 20 (2018) 3344-3352. doi: http://dx.doi.org/10.1039/C8CE00381E.

[31] S. Esmailzadeh, T. Shahrabi, Y. Yaghoubinezhad, G.B. Darband, An analytical study on nucleation and growth mechanism of nanostructured Ni-Se coating by the chronoamperometry and pulse potential techniques, Journal of Electroanalytical

Chemistry, 881 (2021) 114949. doi: https://doi.org/10.1016/j.jelechem.2020.114949.

[32] Y.-H. Lee, Y.-H. Yun, V. Hong Vinh Quy, S.-H. Kang, H. Kim, E. Vijayakumar, K.-S. Ahn, Preparation of nickel selenide by pulsed-voltage electrodeposition and its application as a highly-efficient electrocatalyst at counter electrodes of quantum-dot sensitized solar cells, Electrochimica Acta, 296 (2019) 364-371. doi: https://doi.org/10.1016/j.electacta.2018.11.076.

[33] M.K. Devaraju, I. Honma, Hydrothermal and Solvothermal Process Towards Development of LiMPO4 (M = Fe, Mn) Nanomaterials for Lithium-Ion Batteries, Advanced Energy Materials, 2 (2012) 284-297. doi: https://doi.org/10.1002/aenm.201100642.

[34] X. Chen, S.S. Mao, Titanium Dioxide Nanomaterials: Synthesis, Properties, Modifications, and Applications, Chemical Reviews, 107 (2007) 2891-2959. doi: https://doi.org/10.1021/cr0500535.

[35] D. Jamwal, S.K. Mehta, Metal Telluride Nanomaterials: Facile Synthesis, Properties and Applications for Third Generation Devices, ChemistrySelect, 4 (2019) 1943-1963. doi: https://doi.org/10.1002/slct.201803680.

[36] S. Kukunuri, M.R. Krishnan, S. Sampath, The effect of structural dimensionality on the electrocatalytic properties of the nickel selenide phase, Physical Chemistry Chemical Physics, 17 (2015) 23448-23459. doi: http://dx.doi.org/10.1039/C5CP03900B.

[37] K.S. Bhat, H.S. Nagaraja, Nickel selenide nanostructures as an electrocatalyst for hydrogen evolution reaction, International Journal of Hydrogen Energy, 43 (2018) 19851-19863. doi: https://doi.org/10.1016/j.ijhydene.2018.09.018.

[38] H. Sun, Z. Liang, K. Shen, M. Luo, J. Hu, H. Huang, Z. Zhu, Z. Li, Z. Jiang, F. Song, Fabrication of NiSe2 by direct selenylation of a nickel surface, Applied Surface Science, 428 (2018) 623-629. doi: https://doi.org/10.1016/j.apsusc.2017.09.201.

[39] F. Yu, H. Yao, B. Wang, K. Zhang, Z. Zhang, L. Xie, J. Hao, B. Mao, H. Shen, W. Shi, Nickel foam derived nitrogen doped nickel sulfide nanowires as an efficient electrocatalyst for the hydrogen evolution reaction, Dalton Transactions, 47 (2018) 9871-9876. doi: http://dx.doi.org/10.1039/C8DT01918E.

[40] S. Song, L. Yu, X. Xiao, Z. Qin, W. Zhang, D. Wang, J. Bao, H. Zhou, Q. Zhang, S. Chen, Z. Ren, Outstanding oxygen evolution reaction performance of nickel iron selenide/stainless steel mat for water electrolysis, Materials Today Physics, 13 (2020) 100216. doi: https://doi.org/10.1016/j.mtphys.2020.100216.

[41] C. Tang, N. Cheng, Z. Pu, W. Xing, X. Sun, NiSe Nanowire Film Supported on Nickel Foam: An Efficient and Stable 3D Bifunctional Electrode for Full Water Splitting, Angewandte Chemie International Edition, 54 (2015) 9351-9355. doi: https://doi.org/10.1002/anie.201503407.

[42] S. Anantharaj, J. Kennedy, S. Kundu, Microwave-Initiated Facile Formation of Ni3Se4 Nanoassemblies for Enhanced and Stable Water Splitting in Neutral and Alkaline Media, ACS Applied Materials & Interfaces, 9 (2017) 8714-8728. doi: https://doi.org/10.1021/acsami.6b15980.

[43] X. Li, P. Babar, K. Patil, S. Kale, E. Jo, X. Chen, Z. Hussain, J.H. Kim, Y.T. Yoo, Bifunctional Ni–Fe–CoSe2 nanosheets electrodeposited on Ni foam for efficient catalysis of the oxidation of water and urea, Materials Chemistry and Physics, 287 (2022) 126310. doi: https://doi.org/10.1016/j.matchemphys.2022.126310.

[44] N. Chen, Y.-X. Du, G. Zhang, W.-T. Lu, F.-F. Cao, Amorphous nickel sulfoselenide for efficient electrochemical urea-assisted hydrogen production in alkaline media, Nano Energy, 81 (2021) 105605. doi: https://doi.org/10.1016/j.nanoen.2020.105605.

[45] T.D. Nguyen, M.T. Nguyen, J.S. Lee, Carbon-Based Materials and Their Applications in Sensing by Electrochemical Voltammetry, Inorganics, 2023. doi: https://doi.org/10.3390/inorganics11020081.

[46] L. Zhao, Y. Chang, M. Jia, J. Jia, Z. Wen, Monodisperse Ni0·85Se nanocrystals on rGO for high-performance urea electrooxidation, Journal of Alloys and Compounds, 852 (2021) 156751. doi: https://doi.org/10.1016/j.jallcom.2020.156751.

[47] D. Khalafallah, C. Ouyang, M. Zhi, Z. Hong, Heterostructured Nickel-Cobalt Selenide Immobilized onto Porous Carbon Frameworks as an Advanced Anode Material for Urea Electrocatalysis, ChemElectroChem, 6 (2019) 5191-5202. doi: https://doi.org/10.1002/celc.201900844.

[48] Q. Cao, W. Huang, J. Shou, X. Sun, K. Wang, Y. Zhao, R. Ding, W. Lin, E. Liu, P. Gao, Coupling Dual-phased nickel selenides with N-doped carbon enables efficient urea electrocatalytic oxidation, Journal of Colloid and Interface Science, 629 (2023) 33-43. doi: https://doi.org/10.1016/j.jcis.2022.08.095.

[49] Z. Liu, C. Zhang, H. Liu, L. Feng, Efficient synergism of NiSe2 nanoparticle/NiO nanosheet for energy-relevant water and urea electrocatalysis, Applied Catalysis B: Environmental, 276 (2020) 119165. doi: https://doi.org/10.1016/j.jcis.2022.08.095.

[50] T. Yue, Y. Shi, Y. Ji, J. Jia, Y. Chang, J. Chen, M. Jia, Interfacial engineering of nickel selenide with CeO2 on N-doped carbon nanosheets for efficient methanol and urea electro-oxidation, Journal of Colloid and Interface Science, 653 (2024) 1369-1378. doi: https://doi.org/10.1016/j.jcis.2023.09.101.

[51] C. Tang, Z.L. Zhao, J. Chen, B. Li, L. Chen, C.M. Li, Se-Ni(OH)2-shelled vertically oriented NiSe nanowires as a superior electrocatalyst toward urea oxidation reaction of fuel cells, Electrochimica Acta, 248 (2017) 243-249. doi: https://doi.org/10.1016/j.electacta.2017.06.159.

[52] L. Lv, Z. Li, H. Wan, C. Wang, Achieving low-energy consumption water-to-hydrogen conversion via urea electrolysis over a bifunctional electrode of hierarchical cuprous sulfide@nickel selenide nanoarrays, Journal of Colloid and Interface Science, 592 (2021) 13-21. doi: https://doi.org/10.1016/j.jcis.2021.02.038.

[53] Y. Li, W. Bao, J. Zhang, T. Ai, D. Wu, H. Wang, C. Yang, L. Feng, Ultrathin MoS2 nanosheets decorated on NiSe nanowire arrays as advanced trifunctional electrocatalyst for overall water splitting and urea electrolysis, Journal of Industrial and Engineering Chemistry, 121 (2023) 510-518. doi: https://doi.org/10.1016/j.jiec.2023.02.006.

[54] S. Ni, H. Qu, Z. Xu, X. Zhu, H. Xing, L. Wang, J. Yu, H. Liu, C. Chen, L. Yang, Interfacial engineering of the NiSe2/FeSe2 p-p heterojunction for promoting oxygen evolution reaction and electrocatalytic urea oxidation, Applied Catalysis B: Environmental, 299 (2021) 120638. doi: https://doi.org/10.1016/j.apcatb.2021.120638.

[55] X. Xu, J. Li, C. Zhang, S. Zhang, G. Su, Z. Shi, H. Wang, M. Huang, Controllable transition engineering from homogeneous NiSe2 nanowrinkles to heterogeneous Ni3Se4/NiSe2 rod-like nanoarrays for promoted urea-rich water oxidation at large current densities, Applied Catalysis B: Environmental, 319 (2022) 121949. doi: https://doi.org/10.1016/j.apcatb.2022.121949.

[56] K. Li, B. Xie, D. Feng, Y. Tong, Ni2Se3−CuSex Heterostructure as a Highly Efficient Bifunctional Electrocatalyst for Urea-Assisted Hydrogen Generation, ChemSusChem, 15 (2022) e202201656. doi: https://doi.org/10.1002/cssc.202201656.

[57] K. Chandra Majhi, P. Karfa, R. Madhuri, Bimetallic transition metal chalcogenide nanowire array: An effective catalyst for overall water splitting, Electrochimica Acta, 318 (2019) 901-912. doi: https://doi.org/10.1016/j.electacta.2019.06.106.

[58] D. Khalafallah, W. Huang, M. Zhi, Z. Hong, Synergistic Tuning of Nickel Cobalt Selenide@Nickel Telluride Core–Shell Heteroarchitectures for Boosting Overall Urea Electrooxidation and Electrochemical Supercapattery, ENERGY & ENVIRONMENTAL MATERIALS, 7 (2024) e12528. doi: https://doi.org/10.1002/eem2.12528.

[59] T. Li, H.C. Fu, X.H. Chen, F. Gu, N.B. Li, H.Q. Luo, Interface engineering of core-shell $Ni_{0.85}Se$/NiTe electrocatalyst for enhanced oxygen evolution and urea oxidation reactions, Journal of Colloid and Interface Science, 618 (2022) 196-205. doi: https://doi.org/10.1016/j.jcis.2022.03.063.

[60] H. Wang, X. Jiao, W. Zeng, Y. Zhang, Y. Jiao, Electrodeposition NiMoSe ternary nanoshperes on nickel foam as bifunctional electrocatalyst for urea electrolysis and hydrogen evolution reaction, International Journal of Hydrogen Energy, 46 (2021) 37792-37801. doi: https://doi.org/10.1016/j.ijhydene.2021.09.050.

[61] B.Z. Desalegn, K. Hern, J. Gil Seo, Synergistically Interfaced Bifunctional Transition Metal Selenides for High-Rate Hydrogen Production Via Urea Electrolysis, ChemCatChem, 14 (2022) e202100969. doi: https://doi.org/10.1002/cctc.202100969.

[62] Y. Shi, H. Li, D. Ao, Y. Chang, A. Xu, M. Jia, J. Jia, 3D nickel diselenide architecture on nitrogen-doped carbon as a highly efficient electrode for the electrooxidation of methanol and urea, Journal of Alloys and Compounds, 885 (2021) 160919. doi: https://doi.org/10.1016/j.jallcom.2021.160919.

[63] K. Chen, J. Deng, Y. Yan, Q. Shi, T. Chang, X. Ding, J. Sun, S. Yang, J.Z. Liu, Diverse electronic and magnetic properties of CrS_2 enabling strain-controlled 2D lateral heterostructure spintronic devices, npj Computational Materials, 7 (2021) 79. doi: https://doi.org/10.1038/s41524-021-00547-z.

Electrocatalytic green ammonia synthesis by nitrate reduction reaction using NiPc–rGO composite

Sourav Paul[1£], Shyamal Murmu[1£], Sourav Bhowmick[1, 2], Supriya Mondal[2*] and Uttam Kumar Ghorai[1*]

[1]Department of Industrial Chemistry & Applied Chemistry, Swami Vivekananda Research Centre, Ramakrishna Mission Vidyamandira, Belur Math, Howrah, 711202, India

[2]Department of Physics, Government General Degree College Chapra, Nadia, West Bengal, 741123, India

*Email: uttam.indchem@vidyamandira.ac.in

*Email: supriyajuphy@gmail.com

£ Equal contribution

Abstract: Converting nitrate, a common water contaminant, into valuable ammonia through electrocatalysis provides a viable substitute for the Haber-Bosch process, with diverse applications and environmental benefits. Although, there are different nitrate reduction routes present, the challenge exists due to the insufficiency of efficient electrocatalysts in controlling the reaction route towards sustainable ammonia synthesis. Herein, we present an active and selective route for reducing nitrate to ammonia on a NiPc_rGO composite catalyst, having a 52% Faradaic efficiency and a rate of ammonia output of 11064 μg h^{-1} mg_{cat}^{-1} at a potential of –0.9 V vs. RHE.

Keywords: *Electrocatalysis; Nitrate reduction; Green Ammonia; Nickel Phthalocyanine.*

1. Introduction:

One of the chemicals with the largest global fabrication output is ammonia, and its market size and value make up 5% of the total value of the chemical industry worldwide. The majority of the ammonia produced is utilized to make chemical fertilizers for use in agriculture. Ammonia serves as a primary component in the production of textiles, pharmaceuticals, explosives, and refrigeration. Ammonia is essential for human life, survival, and growth.[1–3] The Haber-Bosch ammonia synthesis process that is presently used is energy-intensive, and produce a large amount of greenhouse emissions. So, electrochemical nitrogen reduction reaction (NRR) is seen as a very competitive alternative.[4,5] However, the inert character of the N≡N bond, the extremely poor solubility of N_2 molecule in aqueous medium, and the competing hydrogen evolution process (HER) frequently result in restricted FE and a very poor ammonia production rate, rendering inferior electrocatalytic performance.[6–10] From an energy and environmental viewpoint, a sustainable N-containing alternative, nitrate ions (NO_3^-) can be a better alternative than N_2. Due to the following reasons, (a) nitrates are highly soluble in water, (b) have lower bond dissociation energy of 204.0 kJ mol^{-1}, (c) low reaction barrier, electrocatalytic nitrate reduction can occur at the solid–liquid interface. Furthermore, the fact that the nitrogen element in NO_3^- has the greatest oxidation state supports the possibility of a reduction reaction leading to the selective synthesis of NH_4^+. NRR may result in simultaneous intermediate-valence N_2 oxidation and reduction, which reduces the selectivity for NH_4^+.[11–13] Therefore, the process of converting nitrate to ammonia seems to be more facile than NRR. Furthermore, using NO_3^- as a feedstock has the additional benefit of its abundant dispersion in wastewater. Wastewater frequently contains nitrate, which is an adequate reactant for NO_3^- reduction reaction (NO_3RR) pathways.[13–15] Rather than partially reducing NO_3^- to N_2 for purification, the 8-electron exchange process for NO_3RR ($NO_3^- + 9H^+ + 8e^- \rightarrow NH_3 + 3H_2O$) gives the opportunity for the conversion of contaminated NO_3^- into a value-added product. Therefore, the NO_3RR route for ammonia production, offers sustainable nitrogen-cycle employment, has a notable impact on lowering energy consumption

while easing environmental concerns. High FE towards ammonia is strongly sought because the reaction has numerous intermediates and progresses through the transfer of 9 protons and 8 electrons.[16] Although the NO_3RR route is a popular but challenging area of current research, it has several unavoidable drawbacks. Strong competitive side reactions, primarily connected to the 5-electron handover for the partial reduction of NO_3^- ions to N_2 and the hydrogen evolution reaction (HER), may accompany the 8-electron addition reaction for the formation of NH_4^+ from NO_3^- .[17,18] Furthermore, it is widely acknowledged that the main factors affecting the rate of yield and selectivity of ammonia are the development of new catalytic materials, accurate control of the reaction's variables, and thorough study of the reaction's mechanism. For a comprehensive catalysis system to successfully support catalytic performance, a logical design is therefore required.

In response to these challenges, scientists have invented various catalysts, like defect site engineering in heterostructure interface (CuPc-CeO_2),[19] 2D iron-cyano catalyst with hydrophilic surface,[18] transition metal (TM) complexes where TM centre functions as the primary site for electrochemical reduction reactions, while the organic cyclic ring prevents the occurrence of competing hydrogen evolution reactions (HER).[3,5] Therefore drawing inspiration from the various strategies we investigated on the aspect of inhibiting HER by introducing a non-metallic constituent, and promoting NO_3RR via the TM centre. Herein, we showed a general strategy to synergistically combine the unique properties of two–dimensional materials (rGO) and transition metal phthalocyanine; to capitalize on the strong interfacial interplay between the rGO surface and NiPc, which leads to facile charge transfer, efficient proton coupled electron transfer which is vital for reduction processes.[20–24] As far as we know, the NiPc_rGO catalyst has not been investigated as an effective electrocatalyst for electrochemical NO_3RR to ammonia before. The NiPc_rGO catalytic system displayed remarkable electrochemical durability and structural stability, and it obtained an excellent ammonia yield rate of 11064 $\mu g\ h^{-1}\ mg_{cat}^{-1}$ and FE of 52% at a potential of –0.9 V (vs. RHE).

2. Experimental details:

2.1 Materials

Phthalonitrile (Sigma Aldrich), nickel (II) acetate (Merck), ethylene glycol (Merck), ammonium heptamolybdate tetrahydrate (Merck), hydrazine hydrate (Sigma Aldrich), sodium hypochlorite solution (Merck), sodium nitroprusside dihydrate (Loba Chemie) sodium hydroxide (Merck), salicylic acid (Merck) and trisodium citrate were used without any additional purification.

2.2 Catalyst synthesis

A recent demonstration has highlighted the facile synthesis of nickel phthalocyanine via a solvothermal route. This method utilizes metal salts like nickel acetate and an organic precursor, phthalonitrile, in an ethylene glycol solvent medium, enabling the preparation of transition metal-based electrocatalysts.[5] Graphene oxide (GO) was prepared via a modified Hummers' method. The obtained GO dispersed in DMF, was treated with a solution of hydrazine hydrate in ammoniacal solution at 90 °C to reduce it to reduced graphene oxide (rGO).[24] NiPc and rGO were mixed in equal parts and suspended in isopropyl alcohol. The NiPc–rGO catalyst was created by centrifuging the material that was left over after the solution was mixed for a few hours and repeatedly washing it with deionized water.[24]

2.3 Instrumentation

Using a Bruker D-8 advanced Eco X-ray powder diffractometer (voltage 40 kV, current 25 mA, λ=0.15404 nm radiation of Cu-K_α), the phase purity of the synthesised NiPc–rGO catalyst was examined using XRD characterisation technique. The IRAffinity-1S FTIR spectrometer (Shimadzu) was used to examine the chemical bonds in the synthesised NiPc–rGO system. The Shimadzu UV-3600 Plus spectrophotometer was used to analyse the absorbance spectroscopy data.

2.4 Electrochemical nitrate reduction

An electrochemical workstation (Model No. CHI760E) along with a three-electrode arrangement in an H-type cell divided by a proton-exchangeable

Nafion 117 membrane was used to analyse the electrochemical experiments in ambient circumstances. Pt foil and Ag/AgCl (3.5 M saturated KCl) were taken as the counter and reference electrodes, respectively. All electrochemical tests were executed at standard temperature and pressure. For the nitrate reduction reaction, 0.1 M $NaNO_3$ and 0.1 M Na_2SO_4 was considered as electrolytes.

The following relation was used to shift all applied potentials from Ag/AgCl to the standard hydrogen electrode: E (vs. RHE) = E (vs. Ag/AgCl) + (0.059 V × pH) + 0.198 V.

2.5 Product Analysis

Quantification of ammonia: The indophenol blue spectrochemical method was applied to quantitatively measure the ammonia concentration using UV-visible spectroscopy. First, 2 ml of the 100 times diluted electrolyte collected after chronoamperometry was mixed with 1 ml of the oxidizer solution made with a 0.05 M sodium hypochlorite solution. Next, 0.2 ml of catalyst was added using a 3.34 mM sodium nitroprusside dihydrate solution. Next, 2 ml of a colourant solution was added. This solution was created by adding 1 M sodium hydroxide solution to 5 weight percent salicylic acid solution and 5 weight percent trisodium citrate. After two hours of incubation at room temperature, the solution's absorbance was assessed. The maximum absorbance in the UV-vis data was observed at 655 nm, suggesting that indophenol blue had formed. A calibration series was created by plotting an ammonium sulphate solution with different concentrations ranging from 1.0, 0.8, 0.6, 0.4, 0.2, and 0.0 (µg/ml)} in 0.1 M Na_2SO_4 and 0.1 M $NaNO_3$ solution. The plot of absorbance vs. concentration was then created using UV–vis data **(Figure 1a)**. The absorbance and concentration have a linear relationship (y = 0.2442x + 0.03987; R^2 = 0.997) in **Figure 1b**.

Quantitative estimation of hydrazine: For hydrazine quantitation, the Watt and Chrisp method was used.[25] Typically, 300 ml of absolute ethanol, 5.99 g of para (dimethylamino) benzaldehyde, and 30 ml of concentrated HCl were combined to create a coloured solution. 4 ml of the coloured solution and 1 ml of the analyte solution were then added. After incubating for around 15 minutes, the mixture's UV-vis absorbance spectrum data were acquired, with the highest absorption at 455 nm. The following steps were used in the preparation of the calibration solution series: Initially, hydrazine-monohydrate standard solutions were made with concentrations ranging from 0.0, 0.2, 0.4, 0.6, 0.8, and 1.0 (µg/mL) (**Figure 1c**). Then, after addition of the prepared coloured solution to the calibrated hydrazine monohydrate solution(s) it was nurtured in the dark for around 15 minutes at RT. The maximum absorbance in the UV-vis spectral data was observed at 455 nm. When absorbance and hydrazine-monohydrate concentrations were plotted against one another, a straight line (y = 0.20614x + 0.0087; R^2 = 0.996) was produced (**Figure 1d**).

Equation for the rate of ammonia yield and Faradaic efficiency determination

It is necessary to quantify the ammonia generated during electrocatalysis; the following equations were utilised to perform the calculation:

$$R_{NH_3} = \frac{(C_{NH_3} \times V)}{(m_{cat} \times t)} \quad \ldots\ldots\ldots\ldots\ldots\ldots\ldots (1)$$

Where C_{NH_3} is the ammonia concentration. The electrolyte volume is denoted by V, the catalyst mass placed on carbon paper is represented by m_{cat}, and the reaction duration is denoted by t.

$$FE (\%) = \frac{(8 \times V \times C_{NH_3} \times F)}{(17 \times Q)} \times 100\% \ldots\ldots\ldots\ldots\ldots\ldots (2)$$

Here, F stands for Faraday constant, C_{NH_3} is the ammonia concentration, V refers to the electrolyte volume used for each reaction, and Q refers to the total charge on the electrode surface.

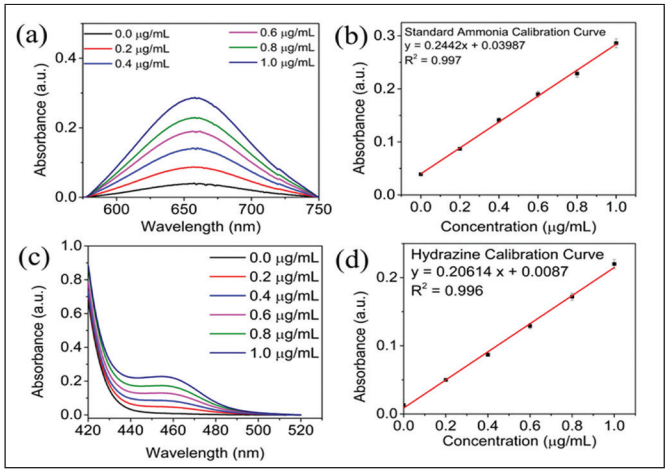

Figure 1. Ammonia's UV-vis calibration curve utilising standards of ammonium sulphate solutions at known concentrations: (a) the indophenol assays' UV-vis curves containing NH_4^+ ions after two hours of incubation and (b) calibration curve used for ammonia estimation by NH_4^+ ions of different concentrations. UV-vis calibration curve of N_2H_4 of known concentration as standards (c) UV-vis absorption spectra at different concentrations of standard hydrazine during a 15-minute incubation period in ambient circumstances (d) The standard calibration curve for hydrazine content determination.

3. Results and Discussion

3.1 Characterization of catalyst: The produced NiPc_rGO electrocatalyst was investigated by XRD, and **Figure 2** illustrates the XRD spectrum of NiPc system, and also the rGO component.

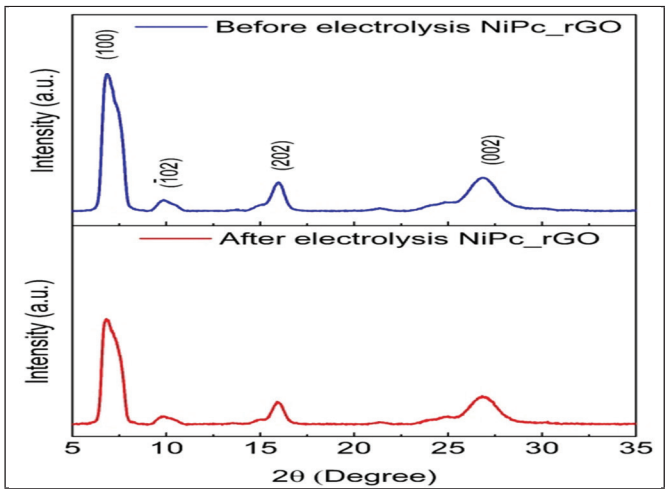

Figure 2. XRD pattern of NiPc–rGO catalytic system

Figure 2 corresponds to the NiPc and rGO in accordance to their reported diffraction peaks, with major reflections around 6.7°, 9.6° and 15.8° corresponding to the reflections from the (100), ($\bar{1}$02) and (202) planes of NiPc respectively, and the broad diffraction peak at ~26° indicates the presence of (002) plane of reduced graphene oxide.[24] Furthermore, to assess the stability of the catalyst, the XRD study was carried out after electrochemical NO_3RR process; **Figure 2** also reveals the XRD pattern after NO_3RR process, which showed no such significant change in the diffraction peaks which demonstrates structural durability of NiPc_rGO catalyst. "The bending of in-plane benzene is represented by the peak at 1118 cm-1 in the FTIR spectra (Figure 3), whereas the Ni–N bond seen in NiPc is associated with the peak at 1165 cm-1." The C-N-C bridges are associated with the primary peak at 1335 cm^{-1}, whereas the stretching of C-C bonds in pyrrole are correlated with the peak at 1428 cm^{-1}.[5] The positive interaction between the π–π stacking interactions and the NiPc's non-covalent interaction with the rGO reduces the strength of the peaks.

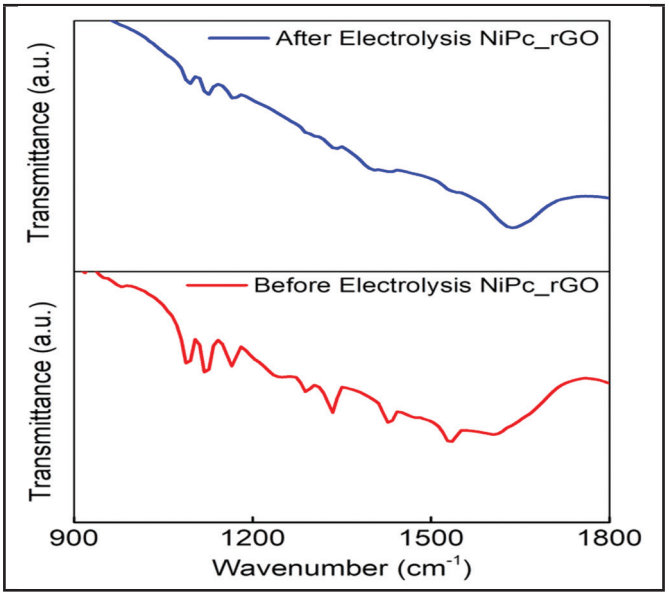

Figure 3. FTIR spectra of NiPc–rGO catalytic system

3.2 Performance of the electrochemical nitrate reduction process

In an H-cell, electrocatalytic nitrate reduction was performed. NiPc–rGO (0.2 mg catalyst) was

coated over carbon paper (1× 1 cm^2) to serve as the working electrode. First, we employed linear sweep voltammetry in Na_2SO_4 electrolyte with and without $NaNO_3$ to examine the nitrate reduction activity of NiPc–rGO (**Figure 4a**). The obvious rise in current density at the same potential suggests that nitrate ion reduction by the NiPc–rGO may be effective. In order to assess the product selectivity, chronoamperometry (CA) studies were performed in 0.1 M Na_2SO_4/0.1 M $NaNO_3$ electrolyte at specified potentials each time for an hour, with generated NH_3 products quantified by spectrophotometry.

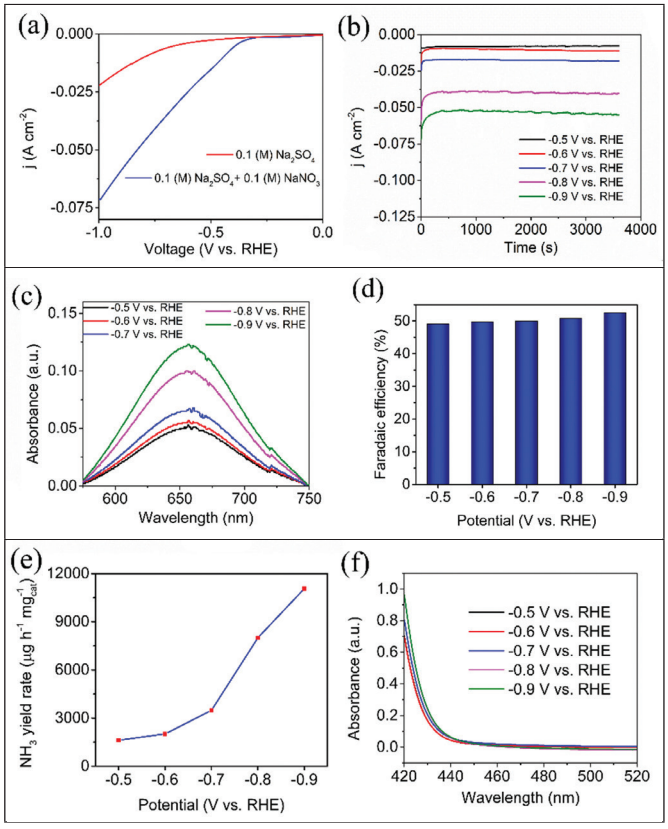

Figure 4. Electrochemical nitrate reduction activity. (a) LSV curves of the NiPc_rGO in 0.1 M Na_2SO_4 electrolyte and 0.1 M Na_2SO_4/0.1 M $NaNO_3$ mixed electrolyte. (b) Current density and reaction time at different potentials of NiPc–rGO (c) UV-visible absorption spectra of the electrolytes at different potentials after 3600 sec NO_3RR electrolysis. (d) NH_3 FE of NiPc_rGO at each given potential. (e) NH_3 yield rate at various potentials using NiPc–rGO catalyst. (f) UV–vis spectra of electrolytes for detecting N_2H_4.

The CA study (**Figure 4b**) showed insignificant fluctuations of current density with respect to time implying that stable current is maintained by the catalyst which aids in the process of efficient nitrate reduction reaction, via constant supply of electrons to the nitrate ions uniformly which facilitates the process of nitrate reduction. **Figure 4c** illustrates the UV-visible spectra with a maximum absorption at 655 nm verifying the electrochemical nitrate reduction at various potentials ranging from –0.5 V to –0.9 V. The rate of NH_3 generation and FE of generated NH_3 were quantitatively measured using the indophenol blue technique. As seen in **Figure 4c**, our NiPc–rGO catalyst exhibits great selectivity and a better yield rate for electrocatalytic NO_3^- to NH_3 conversion. The NH_3 product can be easily identified in **Figure 4d,** with a FE of 50%, corresponding to a yield rate of 3478 μg h^{-1} mg_{cat}^{-1} (**Figure 4e**) at the reaction carried out at –0.70 V vs. RHE with an average current density of 0.018 A cm^{-2}). The yield rate is 11064 μg h^{-1} mg_{cat}^{-1} as the NH_3 selectivity steadily rises to a 52% at –0.9 V with an average current density of 0.055 A cm^{-2}. **Figure 4f** verifies the excellent selectivity of the catalyst for converting NO_3^- to NH_3, revealing that no such absorbance is present at 455 nm in the UV-vis spectrum, indicating that hydrazine (N_2H_4) is not formed during the NO_3RR process. It also shows that ammonia formation is preferred over hydrazine formation with negligible amounts of the latter occurring. Due to the radically different kinetical energy barriers to overcome,[26] the rate of yield and FE of NO_3^- to NH_3 conversion on NiPc_rGO are orders of magnitude larger than the reported N_2 to NH_3 conversions.

3.3 Control Experiment

The NiPc–rGO and NiPc catalyst system's cyclic voltammetry (CV) curves, shown in Figures 5a and 5b, respectively, were examined to find the current density at different sweep speeds (20, 40, 60, 80, and 100 mV s^{-1}) within the potential range of –0.5V to 0.5V vs. RHE. The electrochemical double layer capacitance (C_{dl}) was then computed using the data that was taken out of the CV plots. To find the electrochemical surface area (ECSA) of NiPc–rGO and NiPc, the C_{dl} was measured.[27,28] The

C_{dl} value for NiPc–rGO (1.25 mF cm^{-2}) significantly exceeds that of the NiPc (1.06 mF cm^{-2}), as **Figure 5c** illustrates. This result suggests that NiPc–rGO exhibits a greater number of active sites compared to pristine NiPc, thereby indicating its enhanced NO_3RR activity relative to NiPc. Additionally, the charge transfer resistance (R_{ct}) during NO_3RR operation was investigated using electrochemical impedance spectroscopy (EIS). **Figure 5d** presents the EIS findings for the NiPc–rGO system, indicating a much smaller semicircle compared to NiPc. This suggests that NiPc–rGO, exhibits lower charge transfer resistance and reduced electron transfer impedance.[29,30] Additionally, we assessed the ammonia yield through the NO_3RR process at the potential of -0.9 V vs. RHE using three distinct control systems aside from NiPc–rGO. As depicted in **Figure 5e,** the maximum NH_3 yield of 11064 μg h^{-1} mg_{cat}^{-1} was observed for NiPc–rGO, while for other control systems such as NiPc, rGO, and carbon paper, the NH_3 yield was measured at 6374, 1985, and 212 μg h^{-1} mg_{cat}^{-1}, respectively. To assess the durability of the electrocatalyst, a prolonged chronoamperometry test was performed at −0.9 V for 5 hours for 5 cycles. As depicted in **Figure 5f,** minimal fluctuation in current density was observed, pointing that the composite catalyst exhibited stable electrocatalytic activity without significant variations in the current density throughout the electrochemical reaction.

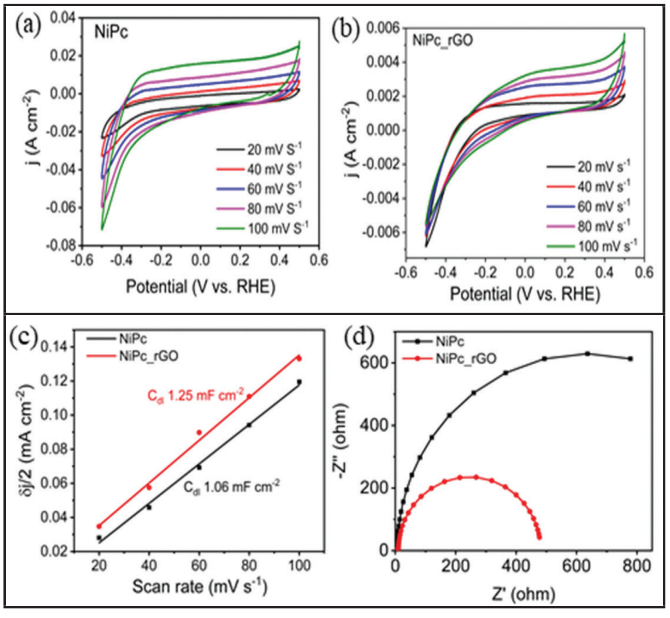

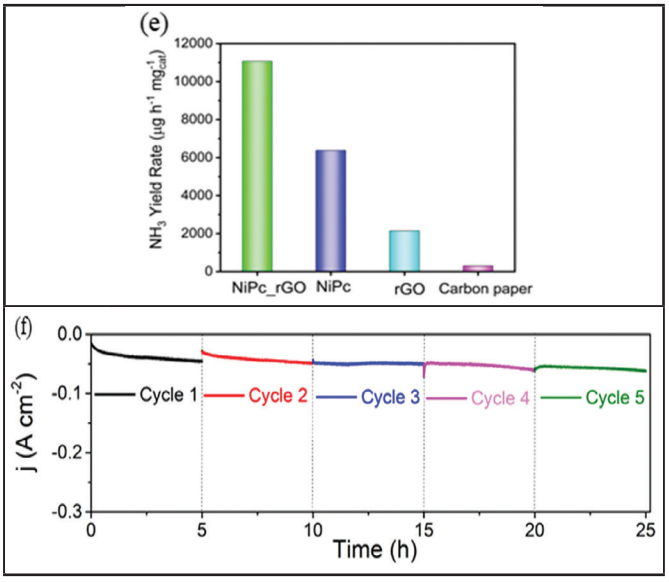

Figure 5. Control experiment. (a) Cyclic voltametric plot of NiPc, (b) Cyclic voltametric plot of NiPc–rGO at varying sweep rates, (c) Plot of the variance in current density (δj/2) against scan rate for determining the C_{dl} values, (d) EIS spectra for NiPc, and NiPc–rGO, (e) The bar diagram illustrates the control experiments at –0.9V vs RHE for rGO, carbon paper, NiPc, and NiPc–rGO, (f) 5 time recycling electrochemical tests for 5 h long term chronoamperometry curves of NiPc–rGO.

4. Conclusions: Nitrate pollution could be reduced using electrochemical nitrate reduction to ammonia synthesis under ambient conditions. Effective catalysts are needed because of the nitrate-to-ammonia reaction's slow kinetics. Our synthesized composite NiPc_rGO catalyst demonstrated a high degree of selectivity and stability, resulting in an ammonia yield rate of 11064 μg h^{-1} mg_{cat}^{-1} and a FE of 52% at –0.9 V vs. RHE. This work provides a fresh approach to the tactical planning of an electrocatalytic nitrate reduction to ammonia system based on transition metal phthalocyanine supported by conducting carbon support in an ambient environment.

Acknowledgements:

SM acknowledges SERB, Govt. of India, for providing the financial support (EEQ/2022/001082). SM wishes to thank Dr. Subhasis Panda, Principal, Government General Degree College Chapra, for his endless and enthusiastic support towards this project.

References:

[1] A. Good, Toward nitrogen-fixing plants, Science, 359 (2018), 869-870. https://www.science.org/doi/10.1126/science.aas8737.

[2] J. Lim, C.A. Fernandez, S.W. Lee, M.C. Hatzell, Ammonia and Nitric Acid Demands for Fertilizer Use in 2050, ACS Energy Lett., 6 (2021), 3676−3685. https://doi.org/10.1021/acsenergylett.1c01614.

[3] U.K. Ghorai, S. Paul, B. Ghorai, A. Adalder, S. Kapse, R. Thapa, A. Nagendra, A. Gain, Scalable Production of Cobalt Phthalocyanine Nanotubes: Efficient and Robust Hollow Electrocatalyst for Ammonia Synthesis at Room Temperature, ACS Nano, 15 (2021), 5230-5239. https://doi.org/10.1021/acsnano.0c10596.

[4] C. Tang, S.Z. Qiao, How to explore ambient electrocatalytic nitrogen reduction reliably and insightfully, Chem. Soc. Rev., 48 (2019), 3166−3180. https://doi.org/10.1039/C9CS00280D.

[5] S. Murmu, S. Paul, S. Kapse, R. Thapa, S. Chattopadhyay, A. Nagendra, S.N. Jha, D. Bhattacharyya, U.K. Ghorai, Unveiling the genesis of the high catalytic activity in nickel phthalocyanine for electrochemical ammonia synthesis J. Mater. Chem. A, 9 (2021), 14477-14484. https://doi.org/10.1039/D1TA00766A.

[6] N. Zhang, L. Li, J. Wang, Z. Hu, Q. Shao, X. Xiao, X. Huang, Surface-Regulated Rhodium–Antimony Nanorods for Nitrogen Fixation, Angew. Chem., Int. Ed., 59 (2020), 8066. https://doi.org/10.1002/anie.201915747.

[7] S. Paul, S. Sarkar, A. Adalder, A. Banerjee, U. K. Ghorai, Dual metal site-mediated efficient C–N coupling toward electrochemical urea synthesis, J. Mater. Chem. A, 11 (2023), 13249-13254. https://doi.org/10.1039/D3TA01011B.

[8] Z. Geng, Y. Liu, X. Kong, P. Li, K. Li, Z. Liu, J. Du, M. Shu, R. Si, J. Zeng, Achieving a Record-High Yield Rate of 120.9 μg_{NH3} mg_{cat}^{-1} h^{-1} NH_3 for N_2 Electrochemical Reduction over Ru Single-Atom Catalysts, Adv. Mater., 30 (2018), 1803498. https://doi.org/10.1002/adma.201803498.

[9] Y. J. Jang, A. E. Lindberg, M. A. Lumley, K.-S. Choi, Photoelectrochemical Nitrogen Reduction to Ammonia on Cupric and Cuprous Oxide Photocathodes, ACS Energy Lett., 5 (2020), 1834–1839. https://doi.org/10.1021/acsenergylett.0c00711.

[10] J. Mukherjee, A. Adalder, N. Mukherjee, U. K. Ghorai, Solvothermal synthesis of α–CuPc nanostructures for electrochemical nitrogen fixation under ambient conditions, Catal. Today, 423 (2023), 113905. https://doi.org/10.1016/j.cattod.2022.09.011.

[11] L. Li, C. Tang, X. Cui, Y. Zheng, X. Wang, H. Xu, S. Zhang, T. Shao, K. Davey, S.Z. Qiao, Efficient Nitrogen Fixation to Ammonia through Integration of Plasma Oxidation with Electrocatalytic Reduction, Angew. Chem. Int. Ed., 60 (2021), 14131–14137. https://doi.org/10.1002/anie.202104394.

[12] H. Hirakawa, M. Hashimoto, Y. Shiraishi, T. Hirai, Selective Nitrate-to-Ammonia Transformation on Surface Defects of Titanium Dioxide Photocatalysts, ACS Catal., 7 (2017), 3713–3720. https://doi.org/10.1021/acscatal.7b00611.

[13] S. Paul, S. Sarkar, A. Adalder, S. Kapse, R. Thapa, U. K. Ghorai, Strengthening the Metal Center of Co–N_4 Active Sites in a 1D–2D Heterostructure for Nitrate and Nitrogen Reduction Reaction to Ammonia, ACS Sustainable Chem. Eng., 11 (2023), 6191-6200. https://doi.org/10.1021/acssuschemeng.2c07114.

[14] L. Zhou, Y. Jiang, Y. Wan, X. Liu, H. Zhou, W. Li, N. Li, Xin Wang, Electron Flow Shifts from Anode Respiration to Nitrate Reduction During Electroactive Biofilm Thickening, Environ. Sci. Technol., 54 (2020), 9593–9600. https://doi.org/10.1021/acs.est.0c01343.

[15] N. C. Kani, J. A. Gauthier, A. Prajapati, J. Edgington, I. Bordawekar, W. Shields, M. Shields, L. C. Seitz, A. R. Singh, M.R. Singh, Solar-driven electrochemical synthesis of ammonia using nitrate with 11% solar-to-fuel efficiency at ambient conditions, Energy Environ. Sci., 14 (2021), 6349–6359. https://doi.org/10.1039/D1EE01879E.

[16] J.-X. Liu, D. Richards, N. Singh, B. R. Goldsmith, Activity and Selectivity Trends in Electrocatalytic Nitrate Reduction on Transition Metals, ACS Catal., 9 (2019), 7052. https://doi.org/10.1021/acscatal.9b02179.

[17] Y. Wang, W. Zhou, R. Jia, Y. Yu, B. Zhang, Unveiling the Activity Origin of a Copper-based Electrocatalyst for Selective Nitrate Reduction to Ammonia, Angew. Chem. Int. Ed., 59 (2020), 5350–5354. https://doi.org/10.1002/anie.201915992.

[18] P. Li, Z. Jin, Z., Fang, G. Yu, A single-site iron catalyst with preoccupied active centers that achieves selective ammonia electrosynthesis from nitrate, Energy Environ. Sci., 14 (2021), 3522–3531. https://doi.org/10.1039/D1EE00545F.

[19] X. Li, W. Fan, Y. Bai, Y. Liu, F. Wang, H. Bai, W. Shi, Photoelectrochemical reduction of nitrate to ammonia over CuPc/CeO_2 heterostructure: Understanding the synergistic effect between oxygen vacancies and Ce sites, Chem. Eng. J., 433 (2022), 133225. https://doi.org/10.1016/j.cej.2021.133225.

[20] W. Liao, L. Qi, Y. Wang, J. Qin, G. Liu, S. Liang, H. He, L. Jiang, Interfacial Engineering Promoting Electrosynthesis of Ammonia over Mo/Phosphotungstic Acid with High Performance, Adv. Funct. Mater., 31(2021), 2009151. https://doi.org/10.1002/adfm.202009151.

[21] Q. Li, Y. Zhang, X. Wang, Y. Yang, Dual Interface-Engineered Tin Heterostructure for Enhanced Ambient Ammonia Electrosynthesis, ACS Appl. Mater. Interfaces, 13 (2021), 15270–15278. https://doi.org/10.1021/acsami.1c01160.

[22] J. Yin, Z. Gao, F. Wei, C. Liu, J. Gong, J. Li, W. Li, L. Xiao, G. Wang, J. Lu, L. Zhuang, Customizable CO_2 Electroreduction to C_1 or C_{2+} Products through Cu_y/CeO_2 Interface Engineering, ACS Catal., 12 (2022), 1004–1011. https://doi.org/10.1021/acscatal.1c04714.

[23] H. Ma, Z. Chen, Z. Wang, C. V. Singh, Q. Jiang, Interface Engineering of Co/CoMoN/NF Heterostructures for High-Performance Electrochemical Overall Water Splitting, Adv. Sci., 9 (2022), 2105313. https://doi.org/10.1002/advs.202105313.

[24] S. Murmu, S. Paul, A. Santra, M. Robert, U. K. Ghorai, Graphene wrapped nickel phthalocyanine nanohybrid: Efficient electrocatalyst for nitrogen reduction reaction, Catal. Today, 423 (2023), 113938. https://doi.org/10.1016/j.cattod.2022.10.020.

[25] G. W. Watt, J. D. Chrisp, Spectrophotometric Method for Determination of Hydrazine, Anal. Chem., 24 (1952), 12, 2006–2008. https://doi.org/10.1021/ac60072a044.

[26] G. F. Chen, Y. Yuan, H. Jiang, S.Y. Ren, L.X. Ding, L. Ma, T. Wu, J. Lu, H. Wang, Electrochemical reduction of nitrate to ammonia via direct eight-electron transfer using a copper–molecular solid catalyst, Nat Energy, 5 (2020), 605–613. https://doi.org/10.1038/s41560-020-0654-1.

[27] A. Adalder, S. Paul, N. Barman, A. Bera, S. Sarkar, N. Mukherjee, R. Thapa, U. K. Ghorai, Controlling the Metal–Ligand Coordination Environment of Manganese Phthalocyanine in 1D–2D Heterostructure for Enhancing Nitrate Reduction to Ammonia, ACS Catal., 13 (2023), 13516–13527. https://doi.org/10.1021/acscatal.3c02747.

[28] S. Sarkar, A. Adalder, S. Paul, S. Kapse, R. Thapa, U. K. Ghorai, Iron phthalocyanine hollow architecture enabled ammonia production via nitrate reduction to achieve 100 % Faradaic efficiency, Appl. Catal. B: Environ., 343 (2024), 123580. https://doi.org/10.1016/j.apcatb.2023.123580.

[29] N. Mukherjee, A. Adalder, N. Barman, R. Thapa, R. Urkude, B. Ghosh, U. K. Ghorai, $Fe(TCNQ)_2$ nanorod arrays: an efficient electrocatalyst for electrochemical ammonia synthesis via the nitrate reduction reaction, J. Mater. Chem. A, 12 (2024), 3352-3361.

https://doi.org/10.1039/D3TA05300H.

[30] G. Zhu, X. Xie, X. Li, Y. Liu, X. Shen, K. Xu, S. Chen, Nanocomposites Based on $CoSe_2$-Decorated $FeSe_2$ Nanoparticles Supported on Reduced Graphene Oxide as High-Performance Electrocatalysts toward Oxygen Evolution Reaction, ACS Appl. Mater. Interfaces, 10 (2018), 19258–19270. https://doi.org/10.1021/acsami.8b04024.

Anchoring 2D Metal-Organic Frameworks (MOFs) for Electrochemical Energy Storage: Recent Advances, Challenges and Key Applications

Rahul Mitra [1, 3, #], Swagatika Mohanty [2, 3, #], Unnikrishnan Manju [1, 3, *]

[1] Materials Chemistry Department, CSIR-Institute of Minerals and Materials Technology, Bhubaneswar - 751 013, India

[2] Central Characterization Department, CSIR-Institute of Minerals and Materials Technology, Bhubaneswar - 751 013, India

[3] Academy of Scientific and Innovative Research (AcSIR), Ghaziabad - 201 002, India

**Corresponding author: manju@immt.res.in, orcid.org/0000-0001-9842-6648*

Abstract

Two-dimensional (2D) materials have received a lot of interest in recent years due to their distinctive properties and staggering potential in energy storage systems. Due to its propensity to support electrochemically active sites that increase the capacity for charge storage, 2D metal-organic frameworks (MOFs) have risen in prominence. It alludes to a novel family of 2D materials that can provide distinct open channels and regular active sites. However, a limited number of articles have revealed how 2D MOFs offer attributes that can improve the functionality of energy storage devices. In this study, we have outlined the structure and state-of-the-art synthesis strategies of 2D MOFs and their use as energy storage devices in supercapacitors and batteries. Finally, key challenges and limitations are addressed while the future view offers a comprehensive idea and a fresh perspective for potential future research possibilities to use this family of materials in energy storage applications. These 2D-MOFs are excellent for energy applications owing to their exceptional qualities, including swift charge and discharge, phenomenal power density, and longer life cycles.

Keywords: *2D materials, Metal-organic frameworks, Batteries, Supercapacitors, Electrochemical Storage*

1. Introduction

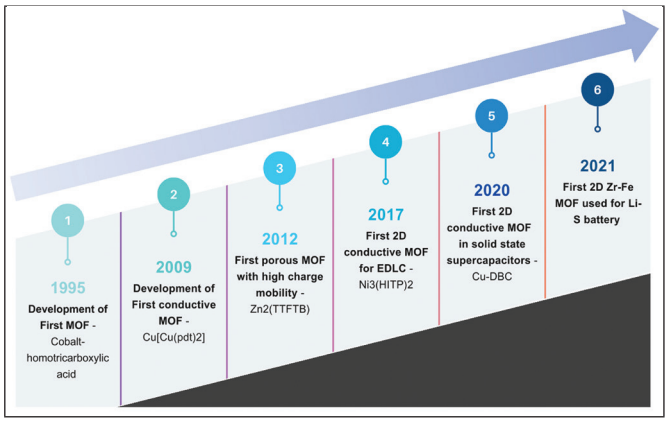

Fig. 1 Schematic representation of major milestones in the development of MOFs. [1–10]

Metal-organic frameworks (MOFs) have attracted increasing attention due to their porous structure, thermal stability, adaptable surface chemistry, robust configuration, and high surface area [11–13]. These materials are formed by the interconnection of metal ions and organic ligands through coordination bonds. The flexible nature of MOF structures allows for regulation by modifying the type of metal cation and organic linkers. The synthesis process also plays a crucial role in determining the morphology and structure of MOFs [14]. Since the synthesis of the first metal-organic framework material, layered cobalt-homophonic acid, in 1995, more than 20,000 MOFs have been reported as of 2022, with the major

milestones depicted in Fig. 1 [1–10]. These materials have found widespread applications in catalysis, sensing, separation, and energy storage systems, that have led to numerous contributions in the scientific fields in terms of publications from across the world and its year-on-year growth, as compiled from Web of Science in Figs. 2(a-c) [2,15,16]. However, traditional 3D MOFs synthesized in the past have inherent limitations that hinder their extensive use in electrochemical energy storage. These drawbacks include sensitivity to moisture, reduced capacity in humid conditions, poor electrical conductivity leading to subpar rate performance, and narrow micropores that limit rapid ion diffusion, affecting their ion storage capabilities [17,18]. Moreover, the incomplete exposure of active sites in the common 3D MOF morphologies, characterized by a 3D frame, restricts contact with diffusing ions, thereby impairing electrochemical performance.

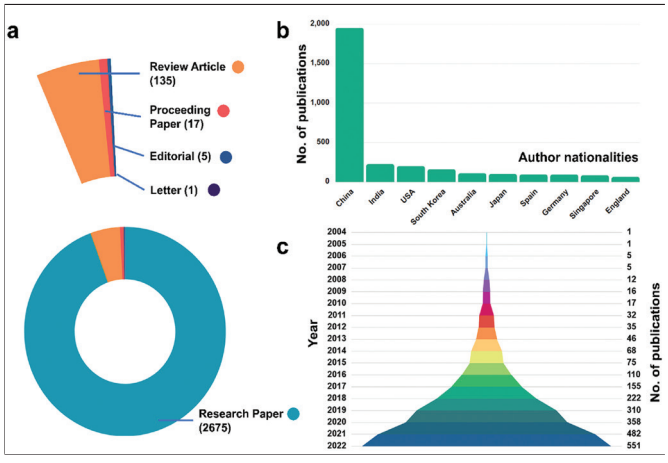

Fig. 2 (a) Pie chart showing the distribution of research article types in the field of 2D MOFs. (b) Number of publications vs Associated author nationalities and (c) Year-wise distribution of publications in the field showing an ever-increasing trend in the last 20 years.

Due to these shortcomings, 3D MOFs have seldom been directly employed as energy storage materials. Fortunately, the porous skeleton structure and pore size of MOFs are adjustable, offering opportunities to enhance their electrochemical performance as electrode materials for energy storage devices. This can be achieved by improving MOF conductivity and optimizing their structural characteristics.

In the current landscape of energy storage technologies, both supercapacitors and batteries play pivotal roles, each with distinct advantages and challenges. Supercapacitors excel in high-power applications due to their rapid charge and discharge rates but face limitations in energy density [19–21]. On the other hand, batteries provide higher energy density but often have slower kinetics and may suffer from issues related to cycle life and safety [22–26]. Achieving optimal properties such as high specific capacitance, extended cycle life, and enhanced energy density remains a central focus for both supercapacitors and batteries. In this context, MOFs exceedingly emerge as a compelling avenue for investigation. MOFs exhibit unique structural features, including high surface area, tunable porosities, and versatile chemical compositions, making them promising candidates for addressing the challenges in both supercapacitors and batteries. The tunable nature of MOFs allows for the design of materials with tailored redox potentials, facilitating improved energy storage capabilities in supercapacitors. Additionally, the porous nature of MOFs provides opportunities for efficient ion transport and storage, enhancing the performance of batteries. The integration of MOFs into these energy storage devices holds potential for advancing the efficiency and sustainability of emerging technologies, offering a bridge between the traditionally separate domains of supercapacitors and batteries. The investigation of MOFs in this context is driven by the prospect of harnessing their unique properties to overcome existing limitations, ultimately contributing to the development of next-generation energy storage systems that balance power and energy density while promoting sustainability in the face of increasing global energy demands.

In this review, we have extensively summarized a range of preparation techniques for two-dimensional metal-organic frameworks (2D MOFs). These methods encompass both top-down approaches and bottom-up strategies, providing a foundational understanding for the precise fabrication of 2D MOFs within advanced energy storage systems.

Furthermore, we have conducted a systematic analysis of the recent research progress concerning the utilization of 2D MOFs in energy storage applications, with a particular focus on their roles in supercapacitors and various battery configurations. Finally, we have highlighted the current limitations in existing research efforts and proposed future directions for the development of 2D MOFs in the field of energy storage, with the aim of advancing energy storage systems to their full potential. The complete overview is represented as a bubble chart in Fig. 3.

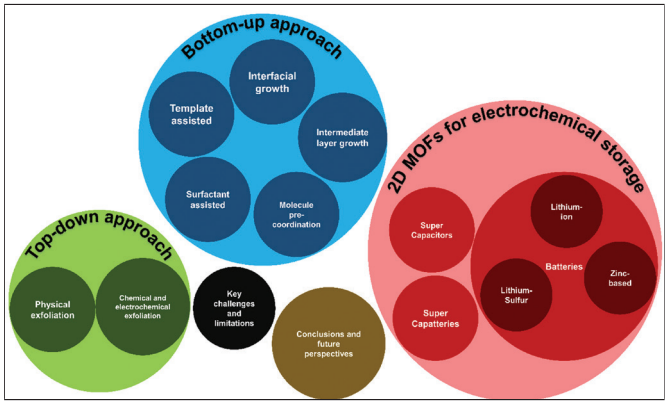

Fig. 3 Bubble chart illustrating the sections and classifications in the review.

2. Synthesis strategies of 2D MOFs

2.1 Top-down approach

2.1.1 Physical exfoliation method

The exfoliation of 2D MOF nanosheets from their layered bulk MOF into single- or few-layers is crucial for realizing the full potential of these MOF nanosheets since structural degradation and morphological damage have made it difficult to produce high-quality MOF nanosheets during exfoliation [27–29]. Soft-physical exfoliation is one of the most often utilized synthetic techniques for obtaining ultrathin nanosheets due to its ease of usage and amiable circumstances. In neutral layered MOFs, the weak connections between layers can then be selectively torn apart by ultrasonic vibration to accomplish exfoliation.

Han et al. synthesized a novel layered bulk 2D MOF ZSB-1 ($Zn_2(SBA)_2(BPTP)$, SBA = 4,4′-sulfonylbibenzoic acid, BPTP = 3,5-bis(5-(pyridin-4-yl) thiophen-2-yl)pyridine) using the top-down physical exfoliation strategy [30]. Using a top-down liquid ultrasonication exfoliation technique, ZSB-1 nanosheets were prepared, where wet powder of ZSB-1 (10 mg, ground for 1 hour in n-hexyl alcohol) was ultrasonically processed in n-hexyl alcohol (80 mL) for 36 hours at room temperature. The upper-layer colloidal suspension was obtained by centrifuging the milky colloidal suspension at 4000 rpm for 10 minutes, and the ZSB-1 nanosheet materials were obtained by centrifuging at 14000 rpm for 5 minutes. The schematic representation of the physical exfoliation method using solvothermal synthesis is depicted in Fig. 4(a).

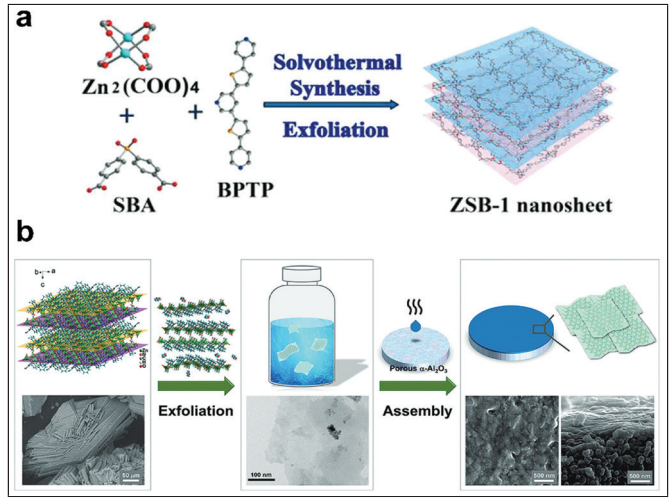

Fig. 4 (a) Schematic illustration of the synthesis process of ZSB-1 nanosheets employing top-down physical exfoliation. [30] (b) Precursor exfoliation and nanosheet assembly processes of $Zn_2(Bim)_3$ nanosheets. [31]

For the first time, $[Zn_2(benzimidazole)_3(OH)(H_2O)]_n$ nanosheets ($Zn_2(Bim)_3$) were prepared by Peng et al. using a modified top-down technique from layered $Zn_2(Bim)_3$ precursors [31]. Each Zn ion acts as a metallic node in the layered structure, coupled by three benzimidazole ligands, and each benzimidazole connects two Zn ions by a bis-monodendate connection, generating a structure resembling a six-membered ring pore opening. Each Zn ion's remaining dangling bond is filled with H_2O molecules, which primarily come from zinc nitrate hexahydrate. In the interlayer gap of bulk precursors, free water molecules and N,N-

dimethylformamide (DMF) are present. All the benzimidazole ligands are placed on one side of a single-layered nanosheet, and the coordinated water is arranged on the opposite side. They attempted to build these nanosheets on asymmetric α-Al_2O_3 porous substrates using a simple hot-drop coating approach at various coating temperatures after successfully disintegrating $Zn_2(Bim)_3$ precursors into nanosheets. For a better comprehension of the exfoliation and nanosheet building processes, a flowchart is provided in Fig. 4(b).

2.1.2 Chemical and electrochemical exfoliation methods

Current research efforts in MOF exfoliation have mainly concentrated on isolating 2D frameworks held together by interlayer van der Waals forces or hydrogen bonding in bulk crystals [14,32–35]. However, the lack of precise control over the mechanical or solvent-driven exfoliation process, which relies on weakening interlayer interactions in MOF crystals, often results in the production of 2D nanosheets with varying thicknesses and low yields. To address this issue, there is a growing need for a more dependable exfoliation approach that leverages controlled chemical reactions to modulate interlayer interactions. One efficient method for producing ultrathin 2D inorganic nanosheets involves the exfoliation of layered inorganic solids that have been pre-intercalated through chemical means [36,37].

Specifically, Ding et al. presented a novel method for the high-yield production of 2D MOF nanosheets from intercalated MOF crystals via chemical exfoliation [38]. They added a chemically labile dipyridyl ligand, 4,4′-dipyridyl disulfide (DPDS), to the layered MOF crystals to create new intercalated MOFs in order to create chemically sensitive MOFs. MOFs may be readily exfoliated into ultrathin 1 nm nanosheets in high yield (~57%) because the interlayer contacts between expanding 2D layers are decreased following scissoring of DPDS by chemically reducing the disulfide bond using trimethylphosphine (TMP). They also showed that the nanosheets as made had extremely high singlet oxygen ($^1O_2$) production efficiency for heterogeneous photocatalysis.

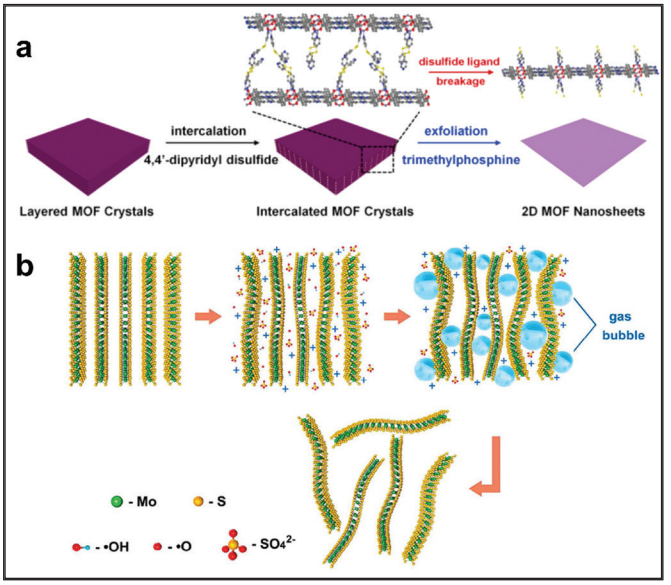

Fig. 5 (a) Standard method designed to create 2D MOF nanosheets by chemical exfoliation and intercalation approach. [38] (b) Mechanism of electrochemical exfoliation of MoS_2 flakes using Na_2SO_4 solution. [39]

Fig. 5(b) explains the electrochemical exfoliation process of MoS_2 crystals using electrochemical exfoliation approach, adopted by Liu et al [39]. First, the oxidation of water results in OH and O radicals gathered around the MoS_2 crystal when a positive bias is applied to the working electrode. The van der Waals contacts between the MoS_2 layers are weakened as a result of the OH and O radicals and/or SO_4^{2-} anions inserting themselves between the layers. Second, the release of O_2 and/or SO_2 from the oxidation of the radicals and/or anions results in a significant expansion of the MoS_2 interlayers. Finally, the exploding gas separates the MoS_2 flakes from the MoS_2 crystal, which are subsequently suspended in the solution. The generalized electrochemical exfoliation approach can, therefore, be extended for the top-down synthesis of 2D MOFs as well.

2.2 Bottom-up approach

2.2.1 Template-assisted methods

The bottom-up template-assisted method offers precise control over the structure and properties of MOFs, making it a valuable tool in materials science and chemistry. By selecting the appropriate template and building blocks, researchers can tailor

the MOF to meet specific application requirements. This method allows for the creation of MOFs with well-defined pore sizes, surface areas, and chemical functionalities, enhancing their performance in various industrial and scientific applications. The creation of an N,O-doped mesoporous carbon nanosheet using a template-assisted technique for morphology assembly from a solvent dispersible hydroxyquinoline-Zn combination was initially described by Wei et al. A self-assembled $Mg(OH)_2$ with a sheet-like shape was used as the template, and 5,7-dibromo-8-hydroxyquinoline-Zn was created and used as the precursor. The hydroxyquinoline-Zn combination serves as both a carbon supply and a sacrificial template in the design, employing the ZnO nanoparticles produced during carbonization as a model for the development of mesoporosity, the schematic for which is depicted in Fig. 6(a).

H_2pyip has a carboxylate O atom and a pyridine N atom, which results in a variety of coordination modes and strong coordination abilities with regard to metal ions, making it an effective ligand for creating MOFs with intriguing structures and potential features. When $MnCl_{24}H_2O$ and 4,4′-bipyridyl were used as a template by Liu et al., $[Mn_3(pyip)_2(HCOO)_2(H_2O)_2]_n$ was produced at 120 °C [40]. Using $Co(NO_3)_2.6H_2O$ and cyanoacetic acid as a template, $\{[Co(pyip)(H_2O)].H_2O\}_n$ was produced at 130 °C. No crystals or precipitates formed during the reactions when the templating agent was not present. This observation suggests that the role of the templating agents in the development of these MOFs was significant.

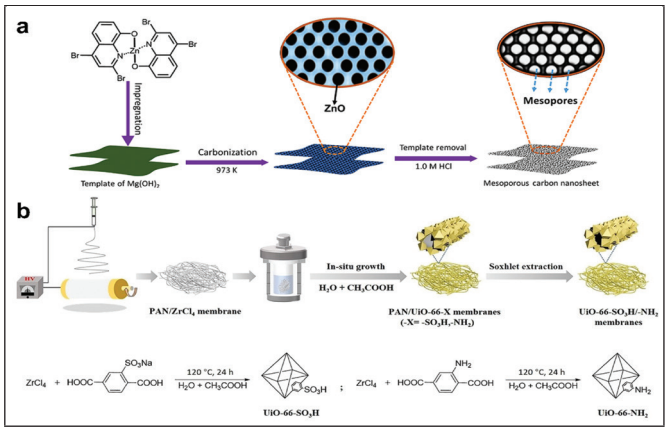

Fig. 6 (a) Schematic of hydroxyquinoline-Zn combination used to create mesoporous carbon nanosheets. [40] (b) The technique to construct the self-standing UiO-66-SO_3H and UiO-66-NH_2 membranes, as well as the procedure for making the matching MOFs. [41]

Fig. 6(b) depicts the process used to create individual porous membranes with base-functionalized MOF (UiO-66-NH_2) and acid-functionalized MOF (UiO-66-SO_3H) structures, as investigated by Du et al [41]. First, by electrospinning a combined solution of $ZrCl_4$ and PAN in DMF, a fiber membrane made of polyacrylonitrile (PAN) and $ZrCl_4$ was created. The non-woven membrane was created by the random deposition of fibers with an average diameter of 500 nm and a thickness of ~80 μm. Then, using the in-situ growth approach, MOF (UiO-66-SO_3H and UiO-66-NH_2) were formed on PAN membrane using either the 2-aminobenzenedicarboxylic acid (BDC-NH_2) or 2-sulfobenzenedicarboxylic acid monosodium salt (BDC-SO_3Na) and an acetic acid catalyst in the water. The membranes effectively accelerated the two phases of a cascade one-pot reaction, namely the reaction of the active methylene molecules malononitrile and ethyl cyanoacetate with benzaldehyde and the deacetylation of benzaldehyde dimethyl acetal to benzaldehyde. The end product might have a high overall yield. As catalysts for the reaction of benzaldehyde with active methylene compounds possessing high p*K*a, such as diethyl malonate, MOF membranes containing -NH_2 base groups are only often used [42,43].

2.2.2 Interfacial or Intermediate layer growth methods

In this method, 2D MOFs are synthesized by carefully controlling the growth of MOF layers at the interface of two immiscible phases. This technique allows for precise control over the formation of 2D MOF nanosheets with tailored properties. Like in other MOF synthesis methods, the first step involves selecting suitable metal ions (or metal clusters) and organic ligands (or linkers) that will constitute the 2D MOF [44,45]. These components are chosen based on the desired MOF structure and properties. The key feature is the use of two immiscible phases, typically a liquid-liquid or liquid-solid interface.

One phase contains the metal ions or clusters, while the other phase contains the organic ligands or linkers. A precursor solution is prepared by dissolving the metal ions or clusters in one phase and the organic ligands in the other phase [46,47]. These solutions are designed to react and form the MOF at the interface. The two immiscible phases are brought into contact at the interface, typically in a controlled manner.

Notably, Cu-MOF nanosheets were produced by sonication exfoliation of Cu-MOF membranes after first being created by interfacial growth, which layers the organic phase on the aqueous phase by Wu et al [48]. Four $Cu_2(COO)_4$ paddlewheel metal nodes connected crystals of Cu-MOF nanosheets bearing tetrakis(4-carboxyphenyl)porphyrin (TCPP) ligands to create a layered, checkerboard-like structure, as observed in Fig. 7(a). As anticipated, after 3 days, discolouration of the organic and aqueous phase was seen, as depicted in Fig. 7(b), indicating that metal ions and TCPP had interacted at the interface of two immiscible solvents. Large and free-standing Cu-MOF membranes that had developed at the contact were transferred to a glass slide, where optical microscopy revealed a claret-colored membrane with a rough surface, as illustrated in Fig. 7(c). Cu-MOF membranes' PXRD spectrum revealed four characteristic peaks - (100), (110), (002), and (004), which were closely matched to their bulk MOF counterparts and therefore suggested that they had a comparable crystal structure, represented in Fig. 7(d).

A subphase of metal ion joints (aqueous solution of $Cu(NO)_3.3H_2O$) at the air/water interface of a Langmuir trough is coated with a solution of molecular building blocks (metalloporphyrin, 5,10,15,20-tetrakis(4-carboxyphenyl)-porphyrinato-palladium(II) (PdTCPP) in chloroform/ methanol) was experimentally performed by Makiura and Konovalov [49]. As the surface is compressed to a pressure of 40 mN/m by moving the barrier walls of the trough at a constant speed, the two-dimensional (2D) copper-mediated PdTCPP arrays (NAFS-13) are formed. The surface pressure - mean molecular area (p-A) isotherm is then measured, as shown by the red line in Fig. 7(e). The CoTCPP-py-Cu (NAFS-1), H_2TCPP-Cu (NAFS-2) and NAFS-13 PdTCPP-Cu sheets' observed p-A isotherms are in good agreement, demonstrating that the linkage motif responsible for sheet formation is also the same. In particular, the linking of the tetratopic PdTCPP molecules occurs via copper ion joints, and the resulting arrays lie flat on the air/water interface. The mean molecular area, A measured at the same surface pressure, p was much less when the same PdTCPP solution was applied to a pure water subphase in the Langmuir trough for comparison and compressed at the same barrier speed, represented by the black line in Fig. 7(e).

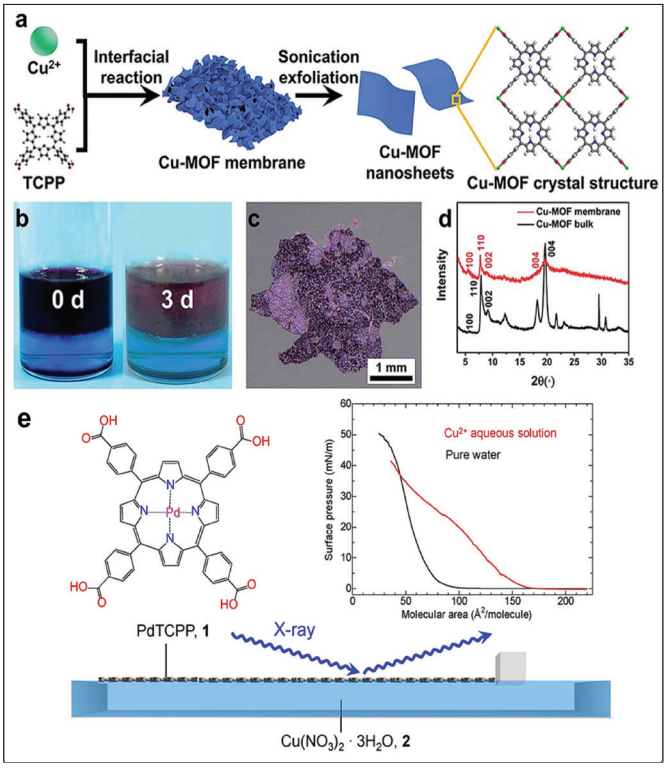

Fig. 7 (a) Synthesis of Cu-MOF nanosheets and crystal structure. [48] (b) Images of two immiscible phases and their color changes both before and after the interaction. (c) A Cu-MOF membrane micrograph. (d) PXRD spectra of bulk analogues of Cu-MOF and a Cu-MOF membrane. (e) PdTCPP-Cu metal-organic framework nanosheets (NAFS-13) assembly is schematically illustrated and is being observed by in-situ grazing incidence XRD (GIXRD) investigations at the air/liquid interface. [49]

2.2.3. Surfactant assisted methods

Surfactant-assisted methods are innovative and versatile approaches for the synthesis of two-dimensional metal-organic frameworks (2D MOFs). These methods utilize surfactants, which are amphiphilic molecules possessing both hydrophilic and hydrophobic segments, to facilitate the controlled formation of 2D MOF nanosheets with specific properties and structures [50–52]. At the heart of these methods is the incorporation of surfactants into the MOF synthesis process. Surfactants play a pivotal role by interacting with both the hydrophilic and hydrophobic components of MOF precursors. They can modify the interfacial properties of the reaction system and impact the nucleation and growth of MOF nanosheets. The surfactant molecules can self-assemble at interfaces, creating a microenvironment that guides the nucleation and growth of MOF nanosheets. Moreover, they can help control the size, shape, and orientation of the resulting nanosheets. Surfactant-assisted methods offer precise control over the growth of 2D MOFs by adjusting surfactant concentration, reaction conditions, and surfactant structure [13,51,53]. These parameters can be fine-tuned to tailor the properties of the synthesized nanosheets, such as size, thickness, porosity, and surface functionality.

Wang et al. used a surfactant-assisted solution synthesis technique to create ultrathin HHB-Cu NSs (hexahydroxybenzene) [2]. The anionic surfactant sodium dodecyl sulfate (SDS) was used for the first time to create consistent, ultrathin 2D c-MOF nanosheets. In a typical synthesis, tetrahydroxy-1,4-quinone (THQ) ligands were added after the $Cu(OAc)_2$ salts and SDS aqueous solution (1.7 mM) were prepared, after which the mixture was sonicated at 50 ºC for 30 minutes. Through electrostatic contact, the SDS molecules' negatively charged hydrophilic tails preferentially cling to the surface of MOFs. As a result, the adsorbed SDS molecules can act as structure-directing agents to significantly reduce layer stacking, which causes the MOFs to develop anisotropically in the 2D direction and, as a result, produce ultrathin and large-sized nanosheets. Additionally, during the sonication treatment, the hydrophobic chains of SDS might reduce the contacts between interlayers, breakdown to create ultrathin nanosheets, and assist stabilize the as-synthesised HHB-Cu MOF NSs in solution to avoid further agglomeration, with the schematic represented in Fig. 8(a).

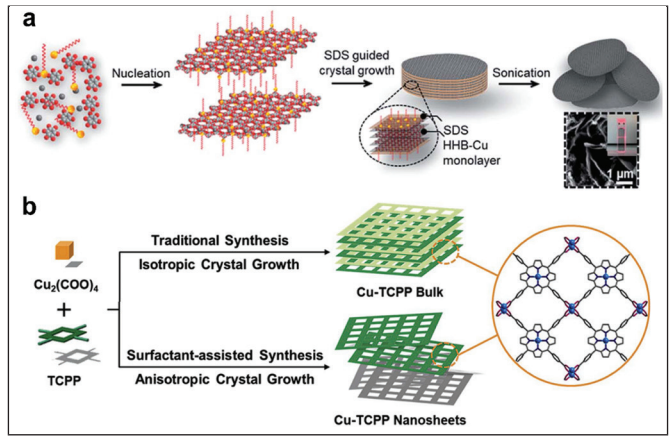

Fig. 8 (a) Using a solution synthesis technique using surfactants, a synthetic approach for ultrathin HHB-Cu NSs is shown. SEM picture of HHB-Cu NSs with the Tyndall effect of a diluent colloidal solution is depicted in the inset. [2] (b) Cu-TCPP MOFs being prepared using conventional and surfactant-aided techniques. [54]

A modified surfactant-assisted technique was used to create Cu-TCPP nanosheets by Qiu et al. [54]. DMF and ethanol were combined at a 3:1 V:V ratio. With magnetic stirring, 300 mL of the aforementioned solution was used to dissolve $Cu(NO_3)_2.3H_2O$, 200 µL of a 1.0 M TFA solution, and 200 mg of PVP, as shown in Fig. 8(b). Additionally, TCPP (100 mg, 0.18 mmol) was dissolved using ultrasound in 100 mL of the produced mixture. TCPP solution was then dropped into the metal-ions solution while being stirred, and the mixture was sonicated for 60 minutes. The completed purple solution was put into a 500 mL sealed container and left at 80 °C for 12 hours. The resultant Cu-TCPP nanosheets were centrifuged at 8000 rpm for 30 minutes before being cleaned with ethanol. Cu-TCPP nanosheets had a 57% yield.

2.2.4. Molecule pre-coordination methods

Bottom-up molecule precoordination methods are innovative approaches in the synthesis of two-dimensional metal-organic frameworks (2D MOFs). These methods enable the controlled assembly of 2D MOF nanosheets by precoordination of metal ions or clusters with organic ligands before the actual framework formation, allowing for precise

control over the structure and properties of the resulting nanosheets [55–57]. To implement this method, suitable metal ions or clusters and organic ligands are carefully chosen based on the desired MOF structure and properties. The precoordination strategy involves designing precursor complexes with a predetermined coordination geometry and ligand binding affinities [58,59].

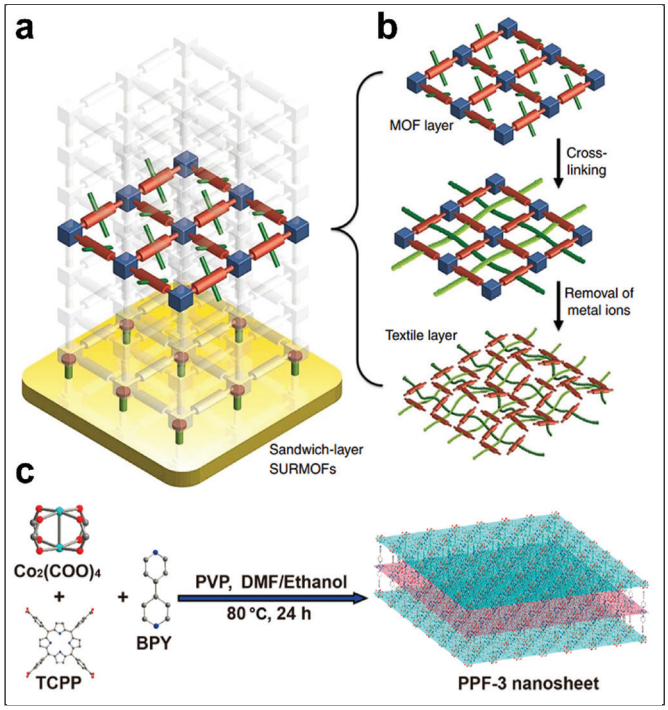

Fig. 9 (a) The heteroepitaxial sandwich-layer surface-mounted MOF (SURMOF) system is shown in a schematic diagram. (b) Cross-linking and metal-removal steps for molecular cross weaving. [60] (c) The development of PPF-3 nanosheets depicted graphically. [61]

A sandwich structure may be created using the molecule pre-coordination method developed by Wang et al. through sandwiching an active layer between two sacrificial layers, shown in Fig. 9(a-b) [60]. By attaching the appropriate node anchoring groups (NAGs), the monomers are properly pre-oriented in the MOF before they polymerize to produce the desired fabric. The crystalline MOF materials are formed by connecting the NAGs to appropriate metal-containing nodes. These 4t-monomers are prearranged in the MOF such that their cross-linking reaction produces flat sheets.

The newly created synthetic approach by Cao et al. was used to successfully create 2D porphyrin paddlewheel framework-3 (PPF-3) MOF nanosheets for the first time [61]. CoSNC, a 2D nanocomposite made of nitrogen-doped carbon and $CoS_{1.097}$ nanoparticles (NPs), is created by simultaneously sulfidating and carbonizing PPF-3 MOF nanosheets. The novel 2D CoSNC nanocomposite was further utilized as an electrode material for supercapacitors as a proof-of-concept application by the group. The formation of 2D PPF-3 nanosheets was controlled by the surfactant molecule polyvinylpyrrolidone (PVP), which was specifically attached to the surface of PPF-3 MOFs in the experiment. In the obtained PPF-3 nanosheet, one 5,10,15,20-tetrakis(4-carboxylphenyl)porphyrin (TCPP) ligand was metalated by one cobalt ion and linked by four $Co_2(COO)_4$ paddlewheel metal nodes to form a "checkerboard-like" layered structure, which was further pillared by 4,4′-bipyridine (BPY) molecules in an AB stacking pattern to form the final structure with space group of *I4/mmm*.

For the production of MOF nanosheets, numerous additional methods, including chemical vapor deposition, hydro- or solvothermal synthesis, etc., have also been reported [62,63]. Post-synthesis pyrolysis of MOFs also represents a transformative approach in tailoring the structure and morphology of carbonaceous materials for advanced applications. This thermal treatment involves subjecting MOF precursors to high temperatures under an inert atmosphere, resulting in the carbonization of organic ligands and the creation of unique carbon-based structures. One of the remarkable outcomes of this process is the retention of the 2D nature of the original MOF, leading to the formation of carbon nanosheets or nanoribbons [64–66]. The preservation of the layered structure is particularly advantageous for applications requiring anisotropic properties and enhanced surface interactions. The pyrolysis-induced carbonization process significantly influences the structural characteristics of the resulting materials. The removal of organic ligands is accompanied by the preservation of inorganic metal nodes, contributing to the formation of carbon frameworks with inherent metal content. This composition may impart additional functionalities to the carbon material, influencing

its chemical and electronic properties. In addition to structural aspects, post-synthesis pyrolysis profoundly impacts the morphology of the carbon materials derived from 2D MOFs. The removal of organic components can create voids or pores within the carbon matrix, leading to the formation of hierarchical porous structures. These structures exhibit interconnected pores at various length scales, offering enhanced surface area and improved accessibility for guest species [65,66]. The resulting hierarchical porosity is particularly advantageous for applications such as gas adsorption, where the tailored pore size distribution facilitates efficient adsorption and desorption processes.

In conclusion, every synthesis technique has advantages and disadvantages. Synthesizing 2D MOFs with desired properties and appropriate for specific applications requires careful process selection and extensive reaction parameter tuning. The discussed synthetic strategies with their individual advantages and limitations are represented in Table 1.

Table 1 Synthetic strategies of 2D MOFs with their key advantages and limitations.

Synthetic method	Advantages	Limitations	References
Physical exfoliation	• Control over Layer Thickness: Physical exfoliation allows precise control over the thickness of the resulting 2D MOF nanosheets. • High Surface Area: The exfoliation process can lead to an increase in the specific surface area of the 2D MOFs. • Enhanced Reactivity: The exposed edges and defects in the exfoliated nanosheets can result in increased reactivity compared to bulk materials. This enhanced reactivity is advantageous for catalytic and sensing applications. • Improved Dispersion: Exfoliated 2D MOF nanosheets can be easily dispersed in various solvents, facilitating their integration into different matrices or devices. This dispersion property enhances the material's applicability in coatings, composites, and films. • Customizable Functionalities: The physical exfoliation method allows for the incorporation of different functional groups during or after the exfoliation process, enabling the customization of the 2D MOF's chemical and physical properties.	• Loss of Crystallinity: The mechanical forces involved in physical exfoliation may lead to a loss of crystallinity in the resulting nanosheets. • Scalability Challenges: Scaling up the physical exfoliation process to produce large quantities of 2D MOF nanosheets can be challenging. The efficiency of the process may decrease at larger scales, limiting the practical applicability for some industrial applications. • Energy Intensive: The physical exfoliation process can be energy-intensive, especially if high shear forces or ultrasonic energy are used. This may affect the overall sustainability and cost-effectiveness of the production process. • Contamination Risk: The introduction of impurities or contaminants during the mechanical exfoliation process can be a concern. This is particularly important for applications requiring high purity, such as in electronic devices. • Limited Control over Orientation: Achieving a specific orientation of the exfoliated nanosheets can be challenging. This lack of control over orientation may impact the material's performance in certain applications.	[67,68]

Synthetic method	Advantages	Limitations	References
Chemical and electrochemical exfoliation	• Precise Control over Thickness: Electrochemical exfoliation enables precise control over layer thickness by adjusting parameters such as applied potential and electrolyte composition. • Preservation of Crystallinity: Chemical and electrochemical exfoliation may better preserve the crystallinity of the 2D MOF layers compared to mechanical methods. • Scalability Potential: Electrochemical methods can be adapted for scalable production, and continuous processes may be developed for industrial-scale production. • Reduced Energy Consumption: In some cases, electrochemical exfoliation methods may have lower energy consumption compared to certain mechanical methods, contributing to sustainability.	• Electrolyte Compatibility: The choice of electrolyte is crucial, and compatibility issues with certain MOFs may limit the applicability of electrochemical exfoliation for specific materials. • Equipment Complexity: Setups can be complex, and the need for specialized equipment may pose challenges, especially for researchers without access to advanced facilities. • Potential Electrode Interference: The presence of electrodes in the electrochemical process may introduce impurities or unwanted reactions, affecting the quality of the exfoliated 2D MOF. • Rate Limiting Steps: The kinetics of the exfoliation process can be a limiting factor, and achieving high production rates may require optimization of reaction conditions.	[63,69]
Template-assisted methods	• Controlled Pore Size and Shape: Template-assisted methods allow for precise control over the pore size and shape of the resulting 2D MOFs. This control is crucial for tailoring the material for specific applications, such as gas adsorption or catalysis. • High Surface Area: The templating process can lead to the formation of 2D MOFs with high surface areas, which is advantageous for applications requiring a large surface area for interactions with other substances. • Enhanced Structural Regularity: Using templates helps achieve enhanced structural regularity in the synthesized 2D MOFs, leading to uniform layers and improved crystallinity.	• Template Removal Challenges: The removal of templates after MOF synthesis can be challenging and may require harsh conditions, potentially leading to damage or alterations in the final structure of the 2D MOF. • Limited Templating Materials: The availability of suitable templates can be limited, and the choice of template material may affect the scalability and applicability of the method. • Possibility of Template Residue: Even after template removal, traces of the template material may remain within the MOF structure, posing potential contamination issues and affecting the material's properties. • Complex Synthesis Procedure: Template-assisted methods often involve more complex synthesis procedures compared to some other methods, which may hinder their widespread adoption.	[14, 32-34]

Synthetic method	Advantages	Limitations	References
Template-assisted methods	• Ordered Nanostructures: Template-assisted methods can result in the formation of ordered nanostructures, such as nanosheets or nanoribbons, which can exhibit unique properties and behaviors compared to disordered structures. • Multifunctionality: The use of templates allows for the incorporation of multiple components or functionalities, enabling the design of multifunctional 2D MOF materials for diverse applications.	• Less Control Over Layer Thickness: Achieving precise control over the layer thickness in template-assisted methods can be challenging compared to top-down methods, limiting the tunability of certain properties. • Limited Scalability: The scalability of template-assisted methods may be limited, particularly when dealing with intricate templates or when attempting to produce large quantities of 2D MOFs.	[14, 32-34]
Interfacial or intermediate layer growth methods	• Controlled Layer Thickness: Interfacial or intermediate layer growth methods allow for precise control over the thickness of the 2D MOF layers. • Uniform and Ordered Structures: These methods often result in the formation of uniform and ordered structures, with well-defined layer arrangements. This structural regularity can lead to improved crystallinity and enhanced material properties. • Versatility in Substrate Choice: Interfacial growth methods can be applied on a variety of substrates, providing versatility in terms of the materials and surfaces on which the 2D MOF layers can be grown. • Potential for Multilayered Structures: The growth process allows for the creation of multilayered structures with controlled interlayer distances, enabling the design of materials with specific functionalities. • Incorporation of Additional Components: Intermediate layer growth methods provide opportunities to incorporate additional components or functionalities during the growth process, leading to multifunctional 2D MOF materials.	• Limited Scalability: The scalability of layer growth methods may be limited, especially when dealing with complex substrates or intricate growth conditions. • Substrate Compatibility: The choice of substrate is critical, and not all substrates are compatible with these methods. Ensuring good adhesion and uniform growth can be challenging on certain surfaces. • Dependence on Interfacial Chemistry: The success of interfacial growth methods often depends on the specific chemistry at the interface. Variations in interfacial conditions can lead to non-uniform growth or incomplete coverage. • Limited Variety of Intermediate Layers: The range of materials that can be used as intermediate layers may be limited, restricting the variety of 2D MOFs that can be synthesized using this approach. • Possible Intercalation Challenges: Achieving controlled intercalation between layers may be challenging, and undesired interactions between adjacent layers may occur, affecting the material's properties. • Template Removal Issues: Similar to other bottom-up methods, the removal of templates or intermediate layers after MOF synthesis can be challenging and may require harsh conditions.	[14,36,37,40,41]

Synthetic method	Advantages	Limitations	References
Surfactant assisted methods	• Controlled Morphology and Size: Surfactants can act as shape-directing agents, allowing for the controlled morphology and size of the resulting 2D MOF structures. • Improved Dispersion: Surfactants can enhance the dispersion of 2D MOFs in solution, leading to more uniform and stable suspensions. This property is advantageous for subsequent processing and applications such as coatings and films. • Stabilization of Intermediates: Surfactants can stabilize intermediate species during the MOF synthesis, preventing uncontrolled aggregation and promoting the formation of well-defined 2D structures. • Tunable Surface Chemistry: The choice of surfactant can allow for the introduction of specific functional groups or surface modifications on the 2D MOF. • Facilitates Nucleation and Growth: Surfactants can act as templates or nucleation sites, promoting the controlled growth of 2D MOF layers and preventing uncontrolled crystal growth.	• Surfactant Removal Challenges: The removal of surfactants after MOF synthesis can be challenging and may require additional purification steps, potentially impacting the final structure and properties of the 2D MOF. • Potential Contamination: Residual surfactants in the final 2D MOF product may lead to contamination, affecting the material's purity and performance in applications where high purity is essential. • Surfactant-Sensitive Synthesis Conditions: The effectiveness of surfactants may be sensitive to synthesis conditions and optimizing these conditions for specific MOFs can be challenging. • Limited Control Over Layer Thickness: Achieving precise control over the layer thickness may be challenging in some cases, as surfactant-assisted methods may result in variations in layer thickness. • Compatibility Issues with Some MOFs: Not all MOFs may be compatible with surfactant-assisted methods, limiting the range of materials that can be synthesized using this approach.	[62]
Molecule pre-coor-dination methods	• Enhanced Control Over Coordination Environment: Molecule precoordination allows for precise control over the coordination environment of metal ions, influencing the subsequent formation of 2D MOF structures with tailored properties. • Improved Crystallinity: Precoordination can lead to improved crystallinity in the resulting 2D MOF, as the controlled coordination of metal ions with ligands can promote the formation of well-defined and ordered structures.	• Complex Synthesis Process: Molecule precoordination methods often involve complex synthesis procedures, requiring precise control over reaction conditions. This complexity may limit the practicality of these methods for large-scale production. • Limited Metal and Ligand Compatibility: The choice of metal ions and ligands for precoordination may be limited by their compatibility with the desired 2D MOF structure. Finding suitable combinations can be a challenge for certain applications.	[47,49,50-53]

Synthetic method	Advantages	Limitations	References
Molecule pre-coordination methods	• Facilitated Nucleation and Growth: Precoordination may act as a nucleation step, providing a favorable environment for the subsequent growth of 2D MOF layers. • Controlled Morphology and Size: The precoordination step can influence the morphology and size of the final 2D MOF, allowing for better control over these structural aspects for specific applications. • Tunable Properties: By carefully selecting the metal ions and ligands during the precoordination step, it is possible to tune the physical and chemical properties of the resulting 2D MOF, making it suitable for various applications.	• Precursor Stability Issues: The stability of precoordination precursors may be a concern, as certain combinations may be prone to decomposition or side reactions, affecting the overall success of the synthesis. • Template Removal Challenges: Similar to other bottom-up methods, the removal of templates or precursors after MOF synthesis can be challenging and may require careful optimization to avoid damage to the final 2D MOF structure. • Scale-Up Challenges: Scaling up molecule precoordination methods for large-scale production may be challenging due to the intricate control needed over precursor stability, reaction conditions, and other parameters.	[47,49,50-53]

3. 2D MOFs for electrochemical energy storage

3.1 Applications of 2D MOFs in supercapacitors

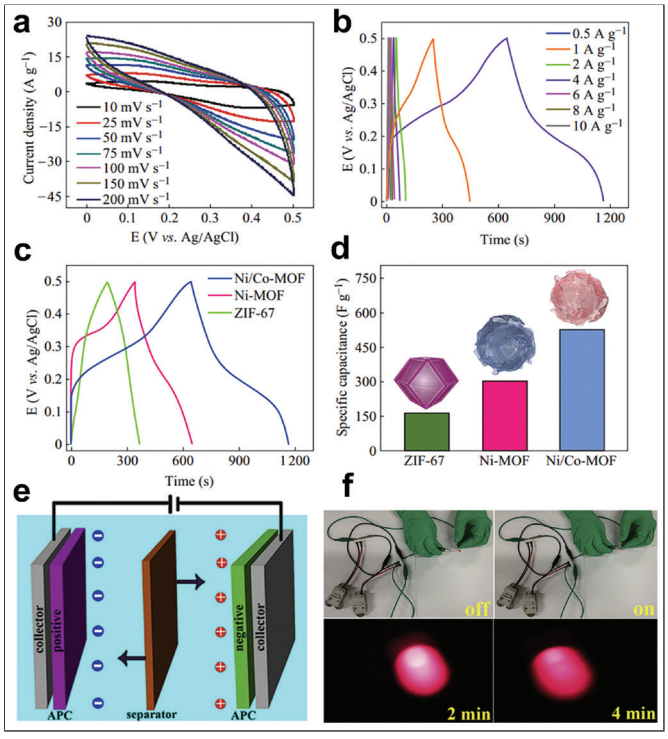

Fig. 10 (a) Cyclic voltammograms of Ni/Co-MOF nanoflake electrodes in 1 M LiOH solution at various scan speeds. (b) Ni/Co-MOF nanoflakes' galvanostatic charge-discharge curves at various currents in 1 M LiOH solution. (c) Ni/Co-MOF nanoflakes, ZIF-67, and Ni/Co-MOF nanoflakes at different current densities in 1 M LiOH solution are compared using galvanostatic charge-discharge curves. (d) Ni/Co-MOF nanoflakes, Ni-MOF nanoflakes, and ZIF-67 electrodes' individual capacitances at 0.5 Ag^{-1}. [70] (e) Schematic of activated porous carbon-based symmetric supercapacitor (SSC) (f) Glowing of LED using the SSC. [71]

Two-dimensional metal-organic frameworks have gained significant attention in the field of supercapacitors due to their unique properties and potential for energy storage applications [3,72]. The distinctive structure of both Ni/Co-MOF nanoflakes and Ni-MOF nanoflakes intrigued Xia et al. to assess their electrochemical performance in the context of a supercapacitor using a three-electrode system in a 1 M LiOH aqueous electrolyte [70]. As depicted in Fig. 10(a), the cyclic voltammetry (CV) curves of the Ni/Co-MOF nanoflakes exhibit approximately rectangular shapes with reversible peaks, indicative of a combination of electric double-layer capacitance (EDLC) and pseudocapacitive reactions [73,74]. Importantly, it is worth noting that even at a high potential scan rate of 200 mVs^{-1}, the roughly rectangular shape of the Ni/Co-MOF nanoflake

CVs is preserved, suggesting a predominantly EDLC behavior and the rapid establishment of the double layer, even under high-rate conditions. The nearly symmetric galvanostatic charge-discharge curves presented in Fig. 10(b) imply that this unique electrode experiences low polarization and exhibits high charge-discharge columbic efficiency. Remarkably, as depicted in Figs. 10(c, d), the Ni/Co-MOF nanoflakes demonstrate a remarkable specific capacitance of 530.4 Fg^{-1} at 0.5 Ag^{-1}, surpassing the specific capacitance values of the Ni-MOF nanoflakes (306.8 Fg^{-1}) and ZIF-67 (168.3 Fg^{-1}) by factors of 3.15 and 1.72, respectively.

In a study by Li et al., a novel Cu-based Metal-Organic Framework (Cu-MOF) with a translational 2D structure characterized by (4,4) layers have been designed [71]. This MOF exhibits hierarchical stacking lamellae with spaces in between, represented in Fig. 10(e). Initially, Cu-MOF was used as a precursor to synthesize a Cu@C composite through a process involving calcination and thermolysis. Subsequently, the Cu@C composite underwent etching with HCl and activation using KOH to yield an Activated Porous Carbon (APC) material with a nanosheet morphology. Notably, this APC nanosheet possessed an exceptionally high BET specific surface area of 2491 m^2/g and a pore volume of 1.50 cm^3/g (comprising 0.12 cm^3/g of micropores and 1.38 cm^3/g of meso- and macropores). Importantly, the APC nanosheet exhibits an impressive specific capacitance of 260.5 F/g when tested at 0.5 A/g with a mass loading of 8 mg/cm^2. The resulting Symmetric Supercapacitor (SSC) based on APC achieves an outstanding specific energy density of 18.38 Wh/kg at a specific power density of 350 W/kg. Moreover, this SSC retains 91.1% of its original capacitance even after undergoing 5000 charge-discharge cycles, demonstrating remarkable long-term cycling stability and reversibility. Remarkably, using three of these SSCs can power a red LED for over 12 minutes, as shown in Fig. 10(f). Consequently, the APC nanosheet emerges as a strong and promising candidate for the fabrication of high-performance supercapacitor cells. The major MOFs used in supercapacitors have been tabulated in terms of porosity, specific surface area, specific capacitance, and retention in Table 2.

Table 2 Material parameters of major MOFs used in supercapacitors.

Material	Pore size (nm)	Specific surface area (m^2/g)	Specific capacitance	Retention (%/ cycles)	Reference
Co-BDC NSs	Broad	260	1159 @ 0.5 A/g, 1052 @ 5 A/g	96.7/6000	[75]
Co-BTC/D-E	Broad	23.1	958.1 @ 2 A/g, 627.6 @ 30 A/g	92.3/3000	[76]
2D Ni-HAB MOFs	0.87 and >15	180-350	420 @ 1 mV/s, 273 @ 100 mV/s	90/12000	[77]
Zn-doped Ni-PTA (MOF-2)	Broad	47.9	1620 @ 0.25 A/g, 854 @ 10 A/g	91/3000	[78]
437-MOF (In)	2.8 and 3.6	2379	150.2 @ 0.2 A/g, 56 @ 8 A/g	~100/6000	[79]
ZnO/NiO MSs (ZnNi-BTC)	7.5-25	170	172.9 @ 0.5 A/g, 107.8 @ 3 A/g	97.4/2000	[80]
NiCo-O (CoNi-MOF-74)	Broad	77.3	305 @ 1 A/g, 218 @ 10 A/g	90.5/10000	[21]
Double shelled Zn-Co-S RDCs (CoZn-ZIF-8)	-	-	1266 @ 1 A/g, 720 @ 20 A/g	91/10000	[81]
Hollow porous NiPO (Ni-BTC)	Broad	142.2	1627 @ 1 A/g, 1044.4 @ 20 A/g	76.8/2000	[19]
Activated porous carbon NSs APC (Cu-BIB)	<6	2491	260.5 @ 0.5 A/g, 165 @ 10 A/g	91.1/5000	[82]
Carbon nanocubes CNC (Zn-BIM)	Broad	1132	255 @ 0.5 A/g, 130 @ 20 A/g	98.2/5000	[83]
2D Ni/Co-MOF nanoflakes	Broad	-	530.4 @ 0.5 A/g	99.75/2000	[84]

3.2. Applications of 2D MOFs in batteries

2D MOFs offer a versatile platform for enhancing various aspects of battery technology, including energy density, rate capability, safety, and cycle life [85–87]. Their versatility, tunability, and unique properties make them a promising avenue for advancing the next generation of energy storage systems.

The exceptional stability and enhanced energy density of lithium-ion batteries have prompted extensive research [88–91]. However, there are numerous issues with the application process, including poor rate performance, low specific capacity, and significant electrode volume expansion. The capacity contribution of lithium/potassium ion batteries can be explained by two primary storage mechanisms for the anode materials: the diffusion-controlled intercalation process and the capacitive process, which is dominated by surface-induced capacitance [92,93]. 2D MOFs with an ultrathin nanosheet structure have emerged as an attempt to increase the number of active sites for the lithium-ion reaction and enhance its specific capacity even further. Because of its high porosity, large specific surface area, enough redox-active metal sites, and short ion diffusion distance, two-dimensional metal-organic frameworks (MOFs) have garnered significant interest as electrode materials for lithium-ion batteries.

2D Cu-BDC MOF nanosheets were meticulously designed and synthesized by precise control of the reaction duration, carried out by Zheng et al. [94]. Subsequently, they underwent annealing at varying pyrolysis temperatures. The end result was the production of MOF-derived carbon materials, namely C500 (referring to the final product obtained at 500°C) and C700 (the final product obtained at 700°C), which were achieved through acid etching. Both carbon derivatives exhibited an abundance of mesoporous structures, which are highly advantageous for facilitating ion migration and promoting the storage of lithium and potassium ions. In the context of lithium-ion and potassium-ion batteries, C500 and C700 displayed distinct dominant kinetic behaviors. Specifically, C500, influenced by a diffusion-controlled process, demonstrated superior performance when employed as an anode material in lithium-ion batteries (LIBs). The C500 anode exhibited an impressive reversible specific capacity of 690.4 milliampere-hours per gram (mAh/g) at a low current density of 0.1 amperes per gram (A/g). Remarkably, even after undergoing 500 charge-discharge cycles at a higher current density of 5.0 A/g, it managed to maintain a substantial specific capacity of 210.3 mAh/g.

Lithium-sulfur (Li-S) batteries hold great potential for the future because of their high theoretical specific capacity (1675 mAh/g) and energy density (2600 Wh/kg) [95,96]. One of the major issues limits the commercialization is the prominent shuttle effect which results from the breakdown of lithium polysulphide and infinite transport/ shuttle between cathode and anode throughout the redox cycle. These occurrences significantly decrease in cycling stability and anode corrosion [96,97]. The breakdown of polysulfide in the organic liquid-based electrolyte is the primary cause of the shuttle effect in Li-S batteries. The physical state of sulfur during the charging and discharging operation will go through a solid-liquid-solid transition process depending on solubility the various sulfur species present in the electrolyte. Elemental sulfur in the solid state will dissolve in the electrolyte and react with the lithium anode to produce low order polysulfide when it is discharged to high order polysulfide. After producing high order polysulfide during charging, the low order polysulfide will then diffuse back to the cathode, and the high order polysulfide will then diffuse to the anode side once more. One practical, yet effective, method to reduce the shuttle effect is to modify the separator. 2D MOF can become a promising candidate as separator or a cathode material which is both chemically and physically and thermally stable, as a physical barrier to prevent soluble polysulfides [97].

While lithium-sulfur (Li-S) batteries offer numerous advantages, such as high energy density, they face practical limitations due to the unwanted shuttle effect and their insulating nature [98]. In response to these

challenges, a conductive metal-organic framework (MOF)-modified separator was developed using a straightforward filtration method by Chen et al. [99]. This modified separator possessed inherent microporous structures, hydrophilic properties, and conductivity, facilitating efficient contact with and retention of polysulfides while promoting faster electrochemical reactions. The physical and chemical attributes of the resulting separator played a crucial role in mitigating the shuttle effect and enhancing the battery's rate capability. Consequently, the Li-S battery equipped with the MOF-modified separator exhibited significantly improved electrochemical performance. Summarily, major 2D MOFs used in batteries have been tabulated and discussed in Table 3, in terms of various parameters.

Table 3 Material parameters of major 2D MOFs used in batteries.

Material	Pore size (nm)	Specific surface area (m^2/g)	Testing potential (V)	Reversible capacity (mAh/g)	Retention (%/cycles)	References
$Cu_3(HHTP)_2$	1.9	506.1	1.7-3.5	95 @ 1 C, 86 @ 20 C	50/500	[100]
Cu-TCA	-	180	1.4-4.3	60 @ 0.5 C, 55 @ 2 C	54.2/200	[91]
Ni-Me4BPZ	Broad	67	0.01-3	140 @ 0.05 A/g	85.7/100	[88]
H-Co-BDC microflowers	5-50	49.9	0.01-3	1345 @ 0.1 A/g, 798 @ 2 A/g	98.8/100	[90]
Mn-BTC	Broad	23.8	0.01-2	694 @ 0.103 A/g, 250 @ 2.06 A/g	83/100	[101]
$AlCl_3$-FumA	Broad	260.1	0.01-3	409 @ 0.0375 A/g, 258 @ 37.5 A/g	93.8/100	[102]
Ti-DOBDC	-	621	0.01-3.0	527 @ 0.1 A/g, 120 @ 0.8 A/g	85/500	[103]
h-ZIF-8@ZnO	1 and 5-8	596.6	0.001-3	805.4 @ 0.2 A/g, 388.6 @ 5 A/g	92.7/100	[104]
ZnO/C NCs (Zn-BDC)	Broad	110	0.01-3	750 @ 0.1 A/g, 351 @ 2 A/g	74.3/100	[105]
CoO@C dandelions (Co-BDC)	~4 and 14	60.3	0.01-3	866 @ 0.1 A/g, 400 @ 5 A/g	110/300	[106]
N-C-800 (ZIF-8)	2	730.1	0.01-3	2037 @ 0.1 A/g, 780 @ 5 A/g	99.2/50	[107]
Zn(BIM)(OAc)	Broad	1535.2	0.001-3	1200 @ 0.1 A/g, 553 @ 10 A/g	110.1/1000	[108]

4. Conclusions and future perspectives

Two-dimensional metal-organic frameworks (2D MOFs) have emerged as promising materials for electrochemical energy storage applications, including batteries and supercapacitors. Their unique properties, such as high surface area, tunable porosity, and versatile chemistry, make them attractive candidates for addressing the growing demand for high-performance and sustainable energy storage solutions. In recent years, significant progress has been made in the synthesis, characterization, and application of 2D MOFs in energy storage systems. These materials have demonstrated impressive performance in terms of energy density, rate capability, and long-term stability. However, several challenges and limitations still need to be addressed to fully unlock their potential.

Future Perspectives:

- Synthesis and Scalability: Developing scalable and cost-effective synthesis methods for large-scale production of 2D MOFs is crucial for practical applications. Exploring innovative techniques and improving the reproducibility of synthesis processes will be a focus area.
- Structural Design: Tailoring the structure of 2D MOFs by fine-tuning metal ions and organic linkers will continue to be explored. Design strategies that enhance ion transport and diffusion within the material while maintaining stability are essential.

- Stability and Durability: Ensuring the long-term stability and durability of 2D MOFs in real-world applications remains a challenge. Research efforts should focus on mitigating degradation mechanisms, particularly in aqueous environments.
- Integration with Current Technologies: Integrating 2D MOFs with existing battery and supercapacitor technologies is crucial for practical implementation. Compatibility with different electrode materials and electrolytes needs further investigation.
- Electrical Conductivity: Improving the electrical conductivity of 2D MOFs is essential for enhancing their rate performance. Strategies such as incorporating conductive additives or creating hybrid materials should be explored.

Challenges and Limitations:

- Low Energy Density: 2D MOFs, like other porous materials, often have lower energy density compared to traditional battery materials. Finding ways to increase their energy density without sacrificing other performance metrics is a challenge.
- Synthesis Control: Achieving precise control over the synthesis of 2D MOFs, including size, shape, and composition, can be challenging. Variability in synthesis can affect their performance.
- Scalability: Transitioning from laboratory-scale synthesis to large-scale production of 2D MOFs can present scalability issues and cost challenges that need to be addressed.
- Structural Stability: Some 2D MOFs may suffer from structural instability during cycling, which can limit their long-term performance. Developing strategies to mitigate this issue is essential.
- Commercial Viability: Demonstrating the commercial viability and cost-effectiveness of 2D MOFs for energy storage applications is a significant hurdle that requires further research and development.

Summarily, 2D MOFs hold great promise for advancing electrochemical energy storage technologies. While substantial progress has been made, addressing the outlined challenges and limitations and pursuing future research directions will be essential to fully harness their potential and facilitate their integration into practical energy storage systems.

Acknowledgements

RM acknowledges CSIR-GATE SRF program for his Ph.D. fellowship. UM is thankful to CSIR, India (Project No. OLP-102) for providing the financial assistance.

Notes

The authors declare no competing financial interests.

References

[1] O.M. Yaghi, G. Li, H. Li, Selective binding and removal of guests in a microporous metal–organic framework, Nature. 378 (1995) 703–706. https://doi.org/10.1038/378703a0.

[2] Z. Wang, G. Wang, H. Qi, M. Wang, M. Wang, S. Park, H. Wang, M. Yu, U. Kaiser, A. Fery, S. Zhou, R. Dong, X. Feng, Ultrathin two-dimensional conjugated metal–organic framework single-crystalline nanosheets enabled by surfactant-assisted synthesis, Chemical Science. 11 (2020) 7665–7671. https://doi.org/10.1039/D0SC01408G.

[3] J. Liu, Y. Zhou, Z. Xie, Y. Li, Y. Liu, J. Sun, Y. Ma, O. Terasaki, L. Chen, Conjugated Copper–Catecholate Framework Electrodes for Efficient Energy Storage, Angewandte Chemie International Edition. 59 (2020) 1081–1086. https://doi.org/10.1002/anie.201912642.

[4] Y. Wang, Z. Deng, J. Huang, H. Li, Z. Li, X. Peng, Y. Tian, J. Lu, H. Tang, L. Chen, Z. Ye, 2D Zr-Fc metal-organic frameworks with highly efficient anchoring and catalytic conversion ability towards polysulfides for advanced Li-S battery, Energy Storage Materials. 36 (2021) 466–477. https://doi.org/10.1016/j.ensm.2021.01.025.

[5] X. Cui, L. Zhang, J. Zhang, L. Gong, M. Gao, P. Zheng, L. Xiang, W. Wang, W. Hu, Q. Xu, W. Wei, H. Zeng, A novel metal-organic layered material with superior supercapacitive performance through ultrafast and reversible tetraethylammonium intercalation, Nano Energy. 59 (2019) 102–109. https://doi.org/10.1016/j.nanoen.2019.02.034.

[6] B. Liu, H. Shioyama, T. Akita, Q. Xu, Metal-Organic Framework as a Template for Porous Carbon Synthesis, Journal of the American Chemical Society. 130 (2008) 5390–5391. https://doi.org/10.1021/ja7106146.

[7] K.J. Erickson, F. Léonard, V. Stavila, M.E. Foster, C.D. Spataru, R.E. Jones, B.M. Foley, P.E. Hopkins, M.D. Allendorf, A.A. Talin, Thin Film Thermoelectric Metal–Organic Framework with High Seebeck Coefficient and Low Thermal Conductivity, Advanced Materials. 27 (2015) 3453–3459. https://doi.org/10.1002/adma.201501078.

[8] X. Song, X. Wang, Y. Li, C. Zheng, B. Zhang, C. Di, F. Li, C. Jin, W. Mi, L. Chen, W. Hu, 2D Semiconducting Metal–Organic Framework Thin Films for Organic Spin Valves, Angewandte Chemie International Edition. 59 (2020) 1118–1123. https://doi.org/10.1002/anie.201911543.

[9] D. Sheberla, J.C. Bachman, J.S. Elias, C.-J. Sun, Y. Shao-Horn, M. Dincă, Conductive MOF electrodes for stable supercapacitors with high areal capacitance, Nature Materials. 16 (2017) 220–224. https://doi.org/10.1038/nmat4766.

[10] T.C. Narayan, T. Miyakai, S. Seki, M. Dincă, High Charge Mobility in a Tetrathiafulvalene-Based Microporous Metal–Organic Framework, Journal of the American Chemical Society. 134 (2012) 12932–12935. https://doi.org/10.1021/ja3059827.

[11] R. Freund, O. Zaremba, G. Arnauts, R. Ameloot, G. Skorupskii, M. Dincă, A. Bavykina, J. Gascon, A. Ejsmont, J. Goscianska, M. Kalmutzki, U. Lächelt, E. Ploetz, C.S. Diercks, S. Wuttke, The Current Status of MOF and COF Applications, Angewandte Chemie International Edition. 60 (2021) 23975–24001. https://doi.org/10.1002/anie.202106259.

[12] J.Wang,N.Li,Y.Xu,H.Pang,Two-Dimensional MOF and COF Nanosheets: Synthesis and Applications in Electrochemistry, Chemistry - A European Journal. 26 (2020) 6402–6422. https://doi.org/10.1002/chem.202000294.

[13] Y. Pan, R. Abazari, J. Yao, J. Gao, Recent progress in 2D metal-organic framework photocatalysts: Synthesis, photocatalytic mechanism and applications, JPhys Energy. 3 (2021). https://doi.org/10.1088/2515-7655/abf721.

[14] K.A.S. Usman, J.W. Maina, S. Seyedin, M.T. Conato, L.M. Payawan, L.F. Dumée, J.M. Razal, Downsizing metal–organic frameworks by bottom-up and top-down methods, NPG Asia Materials. 12 (2020). https://doi.org/10.1038/s41427-020-00240-5.

[15] O. Shekhah, J. Liu, R.A. Fischer, Ch. Wöll, MOF thin films: existing and future applications, Chemical Society Reviews. 40 (2011) 1081. https://doi.org/10.1039/c0cs00147c.

[16] C. Liu, J. Wang, J. Wan, C. Yu, MOF-on-MOF hybrids: Synthesis and applications, Coordination Chemistry Reviews. 432 (2021) 213743. https://doi.org/10.1016/j.ccr.2020.213743.

[17] Q.-Q. Huang, Y.-J. Lin, R. Zheng, W.-H. Deng, C. Kashi, P.N. Kumar, G.-E. Wang, G. Xu, Tunable electrical conductivity of a new 3D MOFs: Cu-TATAB, Inorganic Chemistry Communications. 105 (2019) 119–124. https://doi.org/10.1016/j.inoche.2019.04.037.

[18] Y. Wen, Q. Liu, S. Su, Y. Yang, X. Li, Q.-L. Zhu, X. Wu, Coordination tailoring of water-labile 3D MOFs to fabricate ultrathin 2D MOF nanosheets, Nanoscale. 12 (2020) 12767–12772. https://doi.org/10.1039/D0NR02956D.

[19] R. Bendi, V. Kumar, V. Bhavanasi, K. Parida, P.S. Lee, Metal Organic Framework-Derived Metal Phosphates as Electrode Materials for Supercapacitors, Adv Energy Mater. 6 (2016). https://doi.org/10.1002/aenm.201501833.

[20] D. Sheberla, J.C. Bachman, J.S. Elias, C.-J. Sun, Y. Shao-Horn, M. Dincă, Conductive MOF electrodes for stable supercapacitors with high areal capacitance, Nat Mater. 16 (2017) 220–224. https://doi.org/10.1038/nmat4766.

[21] J. Yu, X. Gao, Z. Cui, Y. Jiao, Q. Zhang, H. Dong, L. Yu, L. Dong, Facile Synthesis of Binary Transition Metal Sulfide Tubes Derived from NiCo-MOF-74 for High-Performance Supercapacitors, Energy Technology. 7 (2019). https://doi.org/10.1002/ente.201900018.

[22] O. Padmaraj, M. Venkateswarlu, N. Satyanarayana, Effect of ZnO filler concentration on the conductivity, structure and morphology of PVdF-HFP nanocomposite solid polymer electrolyte for lithium battery application, Ionics (Kiel). 19 (2013) 1835–1842. https://doi.org/10.1007/s11581-013-0922-1.

[23] Y. Wang, Z. Deng, J. Huang, H. Li, Z. Li, X. Peng, Y. Tian, J. Lu, H. Tang, L. Chen, Z. Ye, 2D Zr-Fc metal-organic frameworks with highly efficient anchoring and catalytic conversion ability towards polysulfides for advanced Li-S battery, Energy Storage Mater. 36 (2021) 466–477. https://doi.org/10.1016/j.ensm.2021.01.025.

[24] K.W. Nam, S.S. Park, R. dos Reis, V.P. Dravid, H. Kim, C.A. Mirkin, J.F. Stoddart, Conductive 2D metal-organic framework for high-performance cathodes in aqueous rechargeable zinc batteries, Nat Commun. 10 (2019) 4948. https://doi.org/10.1038/s41467-019-12857-4.

[25] F. Wang, H. Lu, H. Li, J. Li, L. Wang, D. Han, J. Gao, C. Geng, C. Cui, Z. Zhang, Z. Weng, C. Yang, J. Lu, F. Kang, Q.-H. Yang, Demonstrating U-shaped zinc deposition with 2D metal-organic framework nanoarrays for dendrite-free zinc batteries, Energy Storage Mater. 50 (2022) 641–647. https://doi.org/10.1016/j.ensm.2022.06.005.

[26] M. Yuan, R. Wang, W. Fu, L. Lin, Z. Sun, X. Long, S. Zhang, C. Nan, G. Sun, H. Li, S. Ma, Ultrathin Two-Dimensional Metal–Organic Framework Nanosheets with the Inherent Open Active Sites as Electrocatalysts in Aprotic Li–O 2 Batteries, ACS Appl Mater Interfaces. 11 (2019) 11403–11413. https://doi.org/10.1021/acsami.8b21808.

[27] L. Han, D. Zheng, S. Chen, H. Zheng, J. Ma, A Highly Solvent-Stable Metal–Organic Framework Nanosheet: Morphology Control, Exfoliation, and Luminescent Property, Small. 14 (2018). https://doi.org/10.1002/smll.201703873.

[28] Q. Liu, X. Li, Y. Wen, Q. Xu, X. Wu, Q. Zhu, Twofold Interpenetrated 2D MOF Nanosheets Generated by an Instant In Situ Exfoliation Method: Morphology Control and Fluorescent Sensing, Advanced Materials Interfaces. 7 (2020). https://doi.org/10.1002/admi.202000813.

[29] Y. Peng, Y. Li, Y. Ban, W. Yang, Two-Dimensional Metal–Organic Framework Nanosheets for Membrane-Based Gas Separation, Angewandte Chemie. 129 (2017) 9889–9893. https://doi.org/10.1002/ange.201703959.

[30] L. Han, D. Zheng, S. Chen, H. Zheng, J. Ma, A Highly Solvent-Stable Metal–Organic Framework Nanosheet: Morphology Control, Exfoliation, and Luminescent Property, Small. 14 (2018). https://doi.org/10.1002/smll.201703873.

[31] Y. Peng, Y. Li, Y. Ban, W. Yang, Two-Dimensional Metal–Organic Framework Nanosheets for Membrane-Based Gas Separation, Angewandte Chemie International Edition. 56 (2017) 9757–9761. https://doi.org/10.1002/anie.201703959.

[32] R. Mitra, U. Manju, Negative Capacitance and Intrinsic Ferroelectric Behavior in α-MoO_3 Culminating as a Robust Piezoelectric Energy Harvester, ACS Applied Electronic Materials. 5 (2023) 3130–3143. https://doi.org/10.1021/acsaelm.3c00203.

[33] K.S. Novoselov, A. Mishchenko, A. Carvalho, A.H. Castro Neto, 2D materials and van der Waals heterostructures, Science. 353 (2016). https://doi.org/10.1126/science.aac9439.

[34] M.R. Momeni, Z. Zhang, D. Dell'Angelo, F.A. Shakib, Correction: Gauging van der Waals interactions in aqueous solutions of 2D MOFs: when water likes organic linkers more than open-metal sites, Physical Chemistry Chemical Physics. 24 (2022) 25673–25674. https://doi.org/10.1039/D2CP90191A.

[35] M. Yao, J. Xiu, Q. Huang, W. Li, W. Wu, A. Wu, L. Cao, W. Deng, G. Wang, G. Xu, Van der Waals Heterostructured MOF-on-MOF Thin Films: Cascading Functionality to Realize Advanced Chemiresistive Sensing, Angewandte Chemie. 131 (2019) 15057–15061. https://doi.org/10.1002/ange.201907772.

[36] F. Liu, C. Wang, X. Sui, M.A. Riaz, M. Xu, L. Wei, Y. Chen, Synthesis of graphene materials by electrochemical exfoliation: Recent progress and future potential, Carbon Energy. 1 (2019) 173–199. https://doi.org/10.1002/cey2.14.

[37] Y. Yang, H. Hou, G. Zou, W. Shi, H. Shuai, J. Li, X. Ji, Electrochemical exfoliation of graphene-like two-dimensional nanomaterials, Nanoscale. 11 (2019) 16–33. https://doi.org/10.1039/C8NR08227H.

[38] Y. Ding, Y.-P. Chen, X. Zhang, L. Chen, Z. Dong, H.-L. Jiang, H. Xu, H.-C. Zhou, Controlled Intercalation and Chemical Exfoliation of Layered Metal–Organic Frameworks Using a Chemically Labile Intercalating Agent, Journal of the American Chemical Society. 139 (2017) 9136–9139. https://doi.org/10.1021/jacs.7b04829.

[39] N. Liu, P. Kim, J.H. Kim, J.H. Ye, S. Kim, C.J. Lee, Large-Area Atomically Thin MoS 2 Nanosheets Prepared Using Electrochemical Exfoliation, ACS Nano. 8 (2014) 6902–6910. https://doi.org/10.1021/nn5016242.

[40] Y. Liu, H. Li, Y. Han, X. Lv, H. Hou, Y. Fan, Template-Assisted Synthesis of Co,Mn-MOFs with Magnetic Properties Based on Pyridinedicarboxylic Acid, Crystal Growth & Design. 12 (2012) 3505–3513. https://doi.org/10.1021/cg300237e.

[41] Y. Du, C. Ding, J. Timm, R. Marschall, S. Agarwal, Template-assisted Preparation of Self-standing 2D-MOF Membranes for Application in Cascade Reactions, ChemCatChem. 14 (2022). https://doi.org/10.1002/cctc.202201040.

[42] X. Yan, G. Du, H. Chen, Q. Zhao, Q. Guo, J. Wang, Z. Wang, W. Song, Q. Sheng, Y. Luo, Y. Yuan, T. Yue, Label-free fluorescence aptasensor for the detection of patulin using target-induced DNA gates and TCPP/BDC-NH_2 mixed ligands functionalized Zr-MOF systems, Biosensors and Bioelectronics. 217 (2022) 114723. https://doi.org/10.1016/j.bios.2022.114723.

[43] H.G. Zaman, L. Baloo, S.R. Kutty, M. Altaf, Post Synthetic Modification of NH2-(Zr-MOF) via Rapid Microwave-promoted Synthesis for Effective Adsorption of Pb(II) and Cd(II), Arabian Journal of Chemistry. 16 (2023) 104122. https://doi.org/10.1016/j.arabjc.2022.104122.

[44] H. Wang, Q. Wu, H. Fu, L.-Z. Wu, X. Feng, Controlled growth of organic 2D layered material thin films via interfacial methods, Chemical Communications. 58 (2022) 12384–12398. https://doi.org/10.1039/D2CC03941A.

[45] S. Jiang, X. Shi, Y. Zu, F. Sun, G. Zhu, Interfacial growth of 2D MOF membranes via contra-diffusion for CO_2 separation, Materials Chemistry Frontiers. 5 (2021) 5150–5157. https://doi.org/10.1039/D1QM00154J.

[46] J. Ji, B. Liu, H. Huang, X. Wang, L. Yan, S. Qu, X. Liu, H. Jiang, M. Duan, Y. Li, M. Li, Nondestructive passivation of the TiO 2 electron transport layer in perovskite solar cells by the PEIE-2D MOF interfacial modified layer, Journal of Materials Chemistry C. 9 (2021) 7057–7064. https://doi.org/10.1039/D1TC00036E.

[47] E.A. Flügel, A. Ranft, F. Haase, B. V. Lotsch, Synthetic routes toward MOF nanomorphologies, Journal of Materials Chemistry. 22 (2012) 10119. https://doi.org/10.1039/c2jm15675j.

[48] S. Wu, L. Qin, K. Zhang, Z. Xin, S. Zhao, Ultrathin 2D metal–organic framework nanosheets prepared via sonication exfoliation of membranes from interfacial growth and exhibition of enhanced catalytic activity by their gold nanocomposites, RSC Advances. 9 (2019) 9386–9391. https://doi.org/10.1039/C9RA00662A.

[49] R. Makiura, O. Konovalov, Interfacial growth of large-area single-layer metal-organic framework nanosheets, Scientific Reports. 3 (2013) 2506. https://doi.org/10.1038/srep02506.

[50] C. Avci, Y. Liu, J.A. Pariente, A. Blanco, C. Lopez, I. Imaz, D. Maspoch, Template-Free, Surfactant-Mediated Orientation of Self-Assembled Supercrystals of Metal–Organic Framework Particles, Small. 15 (2019). https://doi.org/10.1002/smll.201902520.

[51] A. Pustovarenko, M.G. Goesten, S. Sachdeva, M. Shan, Z. Amghouz, Y. Belmabkhout, A. Dikhtiarenko, T. Rodenas, D. Keskin, I.K. Voets, B.M. Weckhuysen, M. Eddaoudi, L.C.P.M. de Smet, E.J.R. Sudhölter, F. Kapteijn, B. Seoane, J. Gascon, Nanosheets of Nonlayered Aluminum Metal–Organic Frameworks through a Surfactant-Assisted Method, Advanced Materials. 30 (2018). https://doi.org/10.1002/adma.201707234.

[52] X. Zhang, P. Zhang, C. Chen, J. Zhang, G. Yang, L. Zheng, J. Zhang, B. Han, Fabrication of 2D metal–organic framework nanosheets with tailorable thickness using bio-based surfactants and their application in catalysis, Green Chemistry. 21 (2019) 54–58. https://doi.org/10.1039/C8GC02835D.

[53] R. Marsalek, Particle Size and Zeta Potential of ZnO, APCBEE Procedia. 9 (2014) 13–17. https://doi.org/10.1016/j.apcbee.2014.01.003.

[54] S. Qiu, Y. Su, H. Zhao, L. Wang, Q. Xue, Ultrathin metal-organic framework nanosheets prepared via surfactant-assisted method and exhibition of enhanced anticorrosion for composite coatings, Corrosion Science. 178 (2021) 109090. https://doi.org/10.1016/j.corsci.2020.109090.

[55] D. Zacher, R. Nayuk, R. Schweins, R.A. Fischer, K. Huber, Monitoring the Coordination Modulator Shell at MOF Nanocrystals, Crystal Growth & Design. 14 (2014) 4859–4863. https://doi.org/10.1021/cg501025g.

[56] B. Li, X. You, H. Wu, R. Li, K. Xiao, Y. Ren, H. Wang, S. Song, Y. Wang, Y. Pu, X. Huang, Z. Jiang, A facile metal ion pre-anchored strategy for fabrication of defect-free MOF membranes on polymeric substrates, Journal of Membrane Science. 650 (2022) 120419. https://doi.org/10.1016/j.memsci.2022.120419.

[57] S. Chand, S.C. Pal, D.-W. Lim, K. Otsubo, A. Pal, H. Kitagawa, M.C. Das, A 2D Mg(II)-MOF with High Density of Coordinated Waters as Sole Intrinsic Proton Sources for Ultrahigh Superprotonic Conduction, ACS Materials Letters. 2 (2020) 1343–1350. https://doi.org/10.1021/acsmaterialslett.0c00358.

[58] T. Wu, Y. Shi, Z. Wang, C. Liu, J. Bi, Y. Yu, L. Wu, Unsaturated Ni II Centers Mediated the Coordination Activation of Benzylamine for Enhancing Photocatalytic Activity over Ultrathin Ni MOF-74 Nanosheets, ACS Applied Materials & Interfaces. 13 (2021) 61286–61295. https://doi.org/10.1021/acsami.1c20128.

[59] X. Wang, M. Sun, L. Liu, On the construction and performance of pre-oxidized probe inserted into charged MOF for the in vitro

vitamin C detection: A highly selective emission turn-on sensing, Spectrochimica Acta Part A: Molecular and Biomolecular Spectroscopy. 297 (2023) 122705. https://doi.org/10.1016/j.saa.2023.122705.

[60] Z. Wang, A. Błaszczyk, O. Fuhr, S. Heissler, C. Wöll, M. Mayor, Molecular weaving via surface-templated epitaxy of crystalline coordination networks., Nature Communications. 8 (2017) 14442. https://doi.org/10.1038/ncomms14442.

[61] F. Cao, M. Zhao, Y. Yu, B. Chen, Y. Huang, J. Yang, X. Cao, Q. Lu, X. Zhang, Z. Zhang, C. Tan, H. Zhang, Synthesis of Two-Dimensional CoS 1.097 /Nitrogen-Doped Carbon Nanocomposites Using Metal–Organic Framework Nanosheets as Precursors for Supercapacitor Application, Journal of the American Chemical Society. 138 (2016) 6924–6927. https://doi.org/10.1021/jacs.6b02540.

[62] J. Hwang, A. Ejsmont, R. Freund, J. Goscianska, B.V.K.J. Schmidt, S. Wuttke, Controlling the morphology of metal–organic frameworks and porous carbon materials: metal oxides as primary architecture-directing agents, Chem Soc Rev. 49 (2020) 3348–3422. https://doi.org/10.1039/C9CS00871C.

[63] V.M.V., G. Nageswaran, Review—2D Layered Metal Organic Framework Nanosheets as an Emerging Platform for Electrochemical Sensing, J Electrochem Soc. 167 (2020) 136502. https://doi.org/10.1149/1945-7111/abb4f5.

[64] L. Chai, L. Zhang, X. Wang, L. Xu, C. Han, T.-T. Li, Y. Hu, J. Qian, S. Huang, Bottom-up synthesis of MOF-derived hollow N-doped carbon materials for enhanced ORR performance, Carbon NY. 146 (2019) 248–256. https://doi.org/10.1016/j.carbon.2019.02.006.

[65] K. Zhao, S. Liu, G. Ye, Q. Gan, Z. Zhou, Z. He, High-yield bottom-up synthesis of 2D metal–organic frameworks and their derived ultrathin carbon nanosheets for energy storage, J Mater Chem A Mater. 6 (2018) 2166–2175. https://doi.org/10.1039/C7TA06916B.

[66] Y.-C. Han, M.-L. Liu, L. Sun, X.-C. Li, Y. Yao, C. Zhang, S.-Y. Ding, H.-G. Liao, L. Zhang, F.R. Fan, M. Moskovits, Z.-Q. Tian, A general strategy for overcoming the trade-off between ultrasmall size and high loading of MOF-derived metal nanoparticles by millisecond pyrolysis, Nano Energy. 97 (2022) 107125. https://doi.org/10.1016/j.nanoen.2022.107125.

[67] K. Cheng, Y. Li, Z. Gao, F. Chen, C. You, B. Sun, Two-dimensional metal organic framework for effective gas absorption, Inorg Chem Commun. 101 (2019) 27–31. https://doi.org/10.1016/j.inoche.2018.12.003.

[68] C. Li, C. Wu, B. Zhang, Enhanced CO_2 / CH_4 Separation Performances of Mixed Matrix Membranes Incorporated with Two-Dimensional Ni-Based MOF Nanosheets, ACS Sustain Chem Eng. 8 (2020) 642–648. https://doi.org/10.1021/acssuschemeng.9b06370.

[69] W. Pang, B. Shao, X.-Q. Tan, C. Tang, Z. Zhang, J. Huang, Exfoliation of metal–organic frameworks into efficient single-layer metal–organic nanosheet electrocatalysts by the synergistic action of host–guest interactions and sonication, Nanoscale. 12 (2020) 3623–3629. https://doi.org/10.1039/C9NR09742B.

[70] H. Xia, J. Zhang, Z. Yang, S. Guo, S. Guo, Q. Xu, 2D MOF Nanoflake-Assembled Spherical Microstructures for Enhanced Supercapacitor and Electrocatalysis Performances, Nano-Micro Letters. 9 (2017) 43. https://doi.org/10.1007/s40820-017-0144-6.

[71] Z.-X. Li, B.-L. Yang, K.-Y. Zou, L. Kong, M.-L. Yue, H.-H. Duan, Novel porous carbon nanosheet derived from a 2D Cu-MOF: Ultrahigh porosity and excellent performances in the supercapacitor cell, Carbon. 144 (2019) 540–548. https://doi.org/10.1016/j.carbon.2018.12.061.

[72] W.Y. Chen, S.N. Lai, C.C. Yen, X. Jiang, D. Peroulis, L.A. Stanciu, Surface Functionalization of Ti3C2TxMXene with Highly Reliable Superhydrophobic Protection

for Volatile Organic Compounds Sensing, ACS Nano. 14 (2020) 11490–11501. https://doi.org/10.1021/acsnano.0c03896.

[73] M.A. Borysiewicz, J.-H. Dou, I. Stassen, M. Dincă, Why conductivity is not always king – physical properties governing the capacitance of 2D metal–organic framework-based EDLC supercapacitor electrodes: a Ni 3 (HITP) 2 case study, Faraday Discussions. 231 (2021) 298–304. https://doi.org/10.1039/D1FD00028D.

[74] S. Bi, H. Banda, M. Chen, L. Niu, M. Chen, T. Wu, J. Wang, R. Wang, J. Feng, T. Chen, M. Dincă, A.A. Kornyshev, G. Feng, Molecular understanding of charge storage and charging dynamics in supercapacitors with MOF electrodes and ionic liquid electrolytes, Nature Materials. 19 (2020) 552–558. https://doi.org/10.1038/s41563-019-0598-7.

[75] Y. Zheng, S. Zheng, Y. Xu, H. Xue, C. Liu, H. Pang, Ultrathin two-dimensional cobalt-organic frameworks nanosheets for electrochemical energy storage, Chemical Engineering Journal. 373 (2019) 1319–1328. https://doi.org/10.1016/j.cej.2019.05.145.

[76] R. Ramachandran, C. Zhao, D. Luo, K. Wang, F. Wang, Morphology-dependent electrochemical properties of cobalt-based metal organic frameworks for supercapacitor electrode materials, Electrochim Acta. 267 (2018) 170–180. https://doi.org/10.1016/j.electacta.2018.02.074.

[77] D. Feng, T. Lei, M.R. Lukatskaya, J. Park, Z. Huang, M. Lee, L. Shaw, S. Chen, A.A. Yakovenko, A. Kulkarni, J. Xiao, K. Fredrickson, J.B. Tok, X. Zou, Y. Cui, Z. Bao, Robust and conductive two-dimensional metal−organic frameworks with exceptionally high volumetric and areal capacitance, Nat Energy. 3 (2018) 30–36. https://doi.org/10.1038/s41560-017-0044-5.

[78] J. Yang, C. Zheng, P. Xiong, Y. Li, M. Wei, Zn-doped Ni-MOF material with a high supercapacitive performance, J. Mater. Chem. A. 2 (2014) 19005–19010. https://doi.org/10.1039/C4TA04346D.

[79] M. Du, M. Chen, X.-G. Yang, J. Wen, X. Wang, S.-M. Fang, C.-S. Liu, A channel-type mesoporous In(<scp>iii</scp>)–carboxylate coordination framework with high physicochemical stability for use as an electrode material in supercapacitors, J. Mater. Chem. A. 2 (2014) 9828–9834. https://doi.org/10.1039/C4TA00963K.

[80] L. Zhang, J. Zhang, Y. Liu, L. Zhang, A. Yuan, Porous ZnO/NiO Microspherical Structures Prepared by Thermolysis of Heterobimetallic Metal-Organic Framework as Supercapacitor Electrodes, J Nanosci Nanotechnol. 17 (2017) 2571–2577. https://doi.org/10.1166/jnn.2017.12677.

[81] B. Zhang, Z. Xu, Q. Teng, G. Pan, M. Ma, B. Shen, A Long-Range Acting Dehydratase Domain as the Missing Link for C17-Dehydration in Iso-Migrastatin Biosynthesis, Angewandte Chemie. 129 (2017) 7353–7357. https://doi.org/10.1002/ange.201703588.

[82] Z.-X. Li, B.-L. Yang, K.-Y. Zou, L. Kong, M.-L. Yue, H.-H. Duan, Novel porous carbon nanosheet derived from a 2D Cu-MOF: Ultrahigh porosity and excellent performances in the supercapacitor cell, Carbon N Y. 144 (2019) 540–548. https://doi.org/10.1016/j.carbon.2018.12.061.

[83] K. Zhao, S. Liu, G. Ye, Q. Gan, Z. Zhou, Z. He, High-yield bottom-up synthesis of 2D metal–organic frameworks and their derived ultrathin carbon nanosheets for energy storage, J Mater Chem A Mater. 6 (2018) 2166–2175. https://doi.org/10.1039/C7TA06916B.

[84] H. Xia, J. Zhang, Z. Yang, S. Guo, S. Guo, Q. Xu, 2D MOF Nanoflake-Assembled Spherical Microstructures for Enhanced Supercapacitor and Electrocatalysis Performances, Nanomicro Lett. 9 (2017) 43. https://doi.org/10.1007/s40820-017-0144-6.

[85] K.W. Nam, S.S. Park, R. dos Reis, V.P. Dravid, H. Kim, C.A. Mirkin, J.F. Stoddart, Conductive 2D metal-organic framework for high-performance cathodes in aqueous

rechargeable zinc batteries, Nature Communications. 10 (2019) 4948. https://doi.org/10.1038/s41467-019-12857-4.

[86] X. Wang, C. Zhao, B. Liu, S. Zhao, Y. Zhang, L. Qian, Z. Chen, J. Wang, X. Wang, Z. Chen, Creating Edge Sites within the 2D Metal-Organic Framework Boosts Redox Kinetics in Lithium–Sulfur Batteries, Advanced Energy Materials. 12 (2022). https://doi.org/10.1002/aenm.202201960.

[87] F. Wang, H. Lu, H. Li, J. Li, L. Wang, D. Han, J. Gao, C. Geng, C. Cui, Z. Zhang, Z. Weng, C. Yang, J. Lu, F. Kang, Q.-H. Yang, Demonstrating U-shaped zinc deposition with 2D metal-organic framework nanoarrays for dendrite-free zinc batteries, Energy Storage Materials. 50 (2022) 641–647. https://doi.org/10.1016/j.ensm.2022.06.005.

[88] T. An, Y. Wang, J. Tang, Y. Wang, L. Zhang, G. Zheng, A flexible ligand-based wavy layered metal–organic framework for lithium-ion storage, J Colloid Interface Sci. 445 (2015) 320–325. https://doi.org/10.1016/j.jcis.2015.01.012.

[89] Y. Tong, M. Que, S. Su, L. Chen, Design of amphiphilic poly(vinylidene fluoride-co-hexafluoropropylene)-based gel electrolytes for high-performance lithium-ion batteries, Ionics (Kiel). 22 (2016) 1311–1318. https://doi.org/10.1007/s11581-016-1662-9.

[90] L. Chen, W. Yang, J. Wang, C. Chen, M. Wei, Hierarchical Cobalt-Based Metal–Organic Framework for High-Performance Lithium-Ion Batteries, Chemistry – A European Journal. 24 (2018) 13362–13367. https://doi.org/10.1002/chem.201802629.

[91] Z. Peng, X. Yi, Z. Liu, J. Shang, D. Wang, Triphenylamine-Based Metal–Organic Frameworks as Cathode Materials in Lithium-Ion Batteries with Coexistence of Redox Active Sites, High Working Voltage, and High Rate Stability, ACS Appl Mater Interfaces. 8 (2016) 14578–14585. https://doi.org/10.1021/acsami.6b03418.

[92] X. Wang, C. Zhao, B. Liu, S. Zhao, Y. Zhang, L. Qian, Z. Chen, J. Wang, X. Wang, Z. Chen, Creating Edge Sites within the 2D Metal-Organic Framework Boosts Redox Kinetics in Lithium–Sulfur Batteries, Adv Energy Mater. 12 (2022). https://doi.org/10.1002/aenm.202201960.

[93] H. Chen, Y. Xiao, C. Chen, J. Yang, C. Gao, Y. Chen, J. Wu, Y. Shen, W. Zhang, S. Li, F. Huo, B. Zheng, Conductive MOF-Modified Separator for Mitigating the Shuttle Effect of Lithium–Sulfur Battery through a Filtration Method, ACS Appl Mater Interfaces. 11 (2019) 11459–11465. https://doi.org/10.1021/acsami.8b22564.

[94] G. Zheng, Z. Xing, X. Gao, C. Nie, Z. Xu, Z. Ju, Fabrication of 2D Cu-BDC MOF and its derived porous carbon as anode material for high-performance Li/K-ion batteries, Applied Surface Science. 559 (2021) 149701. https://doi.org/10.1016/j.apsusc.2021.149701.

[95] M. Zhao, B.-Q. Li, X.-Q. Zhang, J.-Q. Huang, Q. Zhang, A Perspective toward Practical Lithium–Sulfur Batteries, ACS Cent Sci. 6 (2020) 1095–1104. https://doi.org/10.1021/acscentsci.0c00449.

[96] A. Manthiram, Y. Fu, Y.-S. Su, Challenges and Prospects of Lithium–Sulfur Batteries, Acc Chem Res. 46 (2013) 1125–1134. https://doi.org/10.1021/ar300179v.

[97] D. Chen, S. Mukherjee, C. Zhang, Y. Li, B. Xiao, C.V. Singh, Two-dimensional square metal organic framework as promising cathode material for lithium-sulfur battery with high theoretical energy density, J Colloid Interface Sci. 613 (2022) 435–446. https://doi.org/10.1016/j.jcis.2021.12.045.

[98] A. Manthiram, Y. Fu, Y.-S. Su, Challenges and Prospects of Lithium–Sulfur Batteries, Accounts of Chemical Research. 46 (2013) 1125–1134. https://doi.org/10.1021/ar300179v.

[99] H. Chen, Y. Xiao, C. Chen, J. Yang, C. Gao, Y. Chen, J. Wu, Y. Shen, W. Zhang, S.

Li, F. Huo, B. Zheng, Conductive MOF-Modified Separator for Mitigating the Shuttle Effect of Lithium–Sulfur Battery through a Filtration Method, ACS Applied Materials & Interfaces. 11 (2019) 11459–11465. https://doi.org/10.1021/acsami.8b22564.

[100] S. Gu, Z. Bai, S. Majumder, B. Huang, G. Chen, Conductive metal–organic framework with redox metal center as cathode for high rate performance lithium ion battery, J Power Sources. 429 (2019) 22–29. https://doi.org/10.1016/j.jpowsour.2019.04.087.

[101] S. Maiti, A. Pramanik, U. Manju, S. Mahanty, Reversible Lithium Storage in Manganese 1,3,5-Benzenetricarboxylate Metal–Organic Framework with High Capacity and Rate Performance, ACS Appl Mater Interfaces. 7 (2015) 16357–16363. https://doi.org/10.1021/acsami.5b03414.

[102] Y. Wang, Q. Qu, G. Liu, V.S. Battaglia, H. Zheng, Aluminum fumarate-based metal organic frameworks with tremella-like structure as ultrafast and stable anode for lithium-ion batteries, Nano Energy. 39 (2017) 200–210. https://doi.org/10.1016/j.nanoen.2017.06.007.

[103] S.-B. Xia, S.-W. Yu, L.-F. Yao, F.-S. Li, X. Li, F.-X. Cheng, X. Shen, C.-K. Sun, H. Guo, J.-J. Liu, Robust hexagonal nut-shaped titanium(IV) MOF with porous structure for ultra-high performance lithium storage, Electrochim Acta. 296 (2019) 746–754. https://doi.org/10.1016/j.electacta.2018.11.135.

[104] Y. Zhang, Y. Lu, S. Feng, D. Liu, Z. Ma, S. Wang, On-site evolution of ultrafine ZnO nanoparticles from hollow metal–organic frameworks for advanced lithium ion battery anodes, J Mater Chem A Mater. 5 (2017) 22512–22518. https://doi.org/10.1039/C7TA08284C.

[105] Y. Song, Y. Chen, J. Wu, Y. Fu, R. Zhou, S. Chen, L. Wang, Hollow metal organic frameworks-derived porous ZnO/C nanocages as anode materials for lithium-ion batteries, J Alloys Compd. 694 (2017) 1246–1253. https://doi.org/10.1016/j.jallcom.2016.10.110.

[106] F. Wu, S. Zhang, B. Xi, Z. Feng, D. Sun, X. Ma, J. Zhang, J. Feng, S. Xiong, Unusual Formation of CoO@C "Dandelions" Derived from 2D Kagóme MOLs for Efficient Lithium Storage, Adv Energy Mater. 8 (2018). https://doi.org/10.1002/aenm.201703242.

[107] F. Zheng, Y. Yang, Q. Chen, High lithium anodic performance of highly nitrogen-doped porous carbon prepared from a metal-organic framework, Nat Commun. 5 (2014) 5261. https://doi.org/10.1038/ncomms6261.

[108] K. Zhao, S. Liu, G. Ye, Q. Gan, Z. Zhou, Z. He, High-yield bottom-up synthesis of 2D metal–organic frameworks and their derived ultrathin carbon nanosheets for energy storage, J Mater Chem A Mater. 6 (2018) 2166–2175. https://doi.org/10.1039/C7TA06916B.

Tailoring ZIF-67 Carbonization: A Comprehensive Study on Structural, Morphological and Electrochemical Properties for Dual Dopamine and Uric Acid Detection

Vidyagouri Karkal[a], Rupali Mane[b], Neetu Jha[b*]

a – Centre of Green Technology, Institute of Chemical Technology, Nathalal Parekh Marg, Mumbai - 400019. India.

b – Department of Physics, Institute of Chemical Technology, Nathalal Parekh Marg, Mumbai - 400019. India.

*Corresponding Author

Email: nr.jha@ictmumbai.edu.in

Abstract

This work presents the optimization of pyrolysis temperature for Co-based Zeolite Imidazole Frameworks (ZIF67) and its application as a nonenzymatic electrochemical sensor for the simultaneous detection of dopamine and uric acid. The pyrolysis process was meticulously conducted across a range of temperatures. Structural, morphological and surface area properties of ZIF67 and its carbonized derivatives were investigated through X-ray diffraction (XRD), scanning electron microscopy (SEM) and BET N_2 absorption-desorption studies. To evaluate the performance of the synthesized materials performance for sensing application, comprehensive electrochemical analyses were conducted employing cyclic voltammetry (CV) and differential pulse voltammetry (DPV). The investigation revealed that ZIF67, carbonized at 800°C exhibited superior electrocatalytic activity compared to the other carbonized ZIF67 derivatives. In conclusion, this study underscores the significance of carbonization in enhancing the electrocatalytic properties of ZIF-67 based materials. The results demonstrates that ZIF67-800 as a promising candidate for such applications, exhibiting remarkable electrocatalytic activity, wide linear detection range, low detection limits, and excellent selectivity and stability in biological samples. These findings highlight its potential for practical applications in simultaneous dopamine and uric acid detection.

Keywords: *Electrochemical sensors, simultaneous detection, Metal organic framework, Temperature optimization, Differential pulse voltammetry, Cyclic Voltammetry, human plasma*

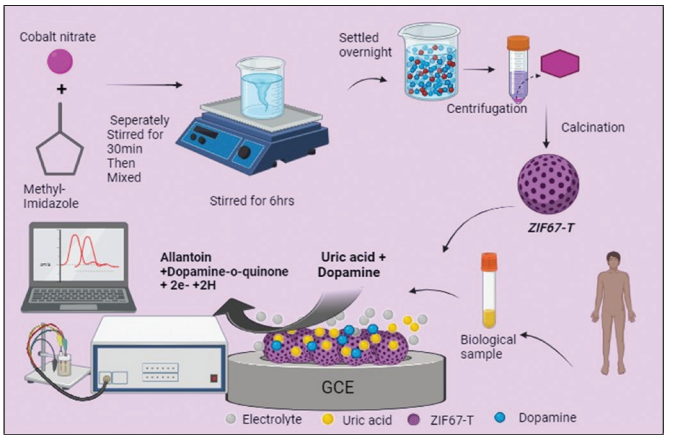

Graphical Abstract

1. Introduction

Dopamine, a neurotransmitter, plays a crucial role in numerous physiological and cognitive functions within the human brain. It is often referred to as 'feel-good' chemical due to its contributions in regulating emotions, motivation, pleasure, and reward. Dopamine functions as a chemical messenger, facilitating signal transmission between neurons and influencing information exchange across various brain regions. This neurotransmitter is vital for processes such as coordinating movement, learning and memory, attention, and maintaining hormonal balance[1]. The dysregulation of dopamine has been linked to various neurological and psychiatric disorders, including Parkinson's disease, schizophrenia, addiction, and depression. A comprehensive understanding of opamine's intricate mechanisms and roles is essential for advancing our knowledge of brain function and developing target treatments for neurological and psychiatric conditions. In general, the concentration

of dopamine in the brain is relatively low compared to other neurotransmitters. Estimates suggest that dopamine levels in the human brain typically range from approximately 0.1 to 0.3 micromoles per liter (μmol/L). However, these concentrations can vary significantly based on specific brain regions and the individual's physiological state[2].

Uric acid (UA), also known as 2,4,8 - Trihydroxypurine, serves as the final product of purine metabolism, encompassing adenine and guanine. In humans, the absence of the urate enzyme gene prevents the breakdown of uric acid, leading to its accumulation in the body. Elevated uric acid levels can lead to various diseases related to acid level fluctuations, such as gout, neurological disorders, cardiovascular issues, arthritis, and kidney diseases. Typically, the average uric acid concentration in the blood of a healthy individual ranges from 236 to 420 μmol/L. Elevated uric acid levels known as hyperuricemia, are linked to conditions like gout. Uric acid also functions as a biomarker for cardiovascular diseases, hypertension, metabolic syndrome, and diabetes[3].

Rapid development in the health care and point of care device development necessitates the creation of low-cost flexible, innovative and user friendly sensors. Conventional analytical methods, including spectroscopy[4], HPLC[5], fluorescence method[6] and colorimetry[7] have been employed for dopamine and uric acid detection but possess disadvantages such as high cost, reliance on sophisticated instruments, complex operational procedures, time consuming sample preparation and limited on-site monitoring capabilities. Consequently, there is a growing need for the development of simple, highly sensitivity, selective, real time and cost effective sensor[8].

Electrochemical sensors offer several advantages, including affordability, simplicity, high sensitivity, and rapid real-time detection. They can be employed in both enzymatic and non-enzymatic configurations[9]. Enzymatic sensors, however, have significant drawbacks, including the high cost of enzymes, limited reproducibility, challenges in immobilization, and the need for precise control of operational parameters such as pH and temperature. On the other hand, non-enzymatic sensors demonstrate superior performance, particularly when electrodes are modified with nanomaterials to enhance electron-species interaction and peak separation[10]. In non-enzymatic approaches, analyte oxidation occurs at the surface of modified electrodes. Various nanomaterials are utilized for electrode modification, including carbon-based materials such as carbon nanotubes (CNTs), graphene, graphene oxides, fullerenes, and carbon dots[11]. Inorganic nanomaterials encompass metals and metal oxides [12] while organic nanomaterials include dendrimers, micelles, liposomes, and polymers[13]. Additionally, composite materials with multiphase nanoparticles or complex structures, such as hybrid nanofibers and metal-organic frameworks [14] [15] are also employed in sensor development.

Metal-Organic Frameworks (MOFs) represent a class of hybrid porous materials with diverse applications in catalysis, gas storage, batteries, gas separation, and electrochemical sensors. Their utilization in electrochemical sensors has yielded notable benefits, including improved electrocatalytic performance, adaptable stereochemistry, and high chemical stability. MOFs offer advantages such as rapid mass transfer and ample active sites, enhancing their electrocatalytic activity. They also possess a high surface area while maintaining low density[16]. Within the MOF family, Zeolite Imidazole Frameworks (ZIFs) stand out as a subclass. An example is ZIF-67, composed of cobalt ions and 2-methylimidazole. ZIFs exhibit exceptional porosity, a large surface area, and active sites conducive to redox reactions. However, they do have drawbacks, notably poor stability and low electrical conductivity. These limitations can be addressed through the pyrolysis of materials[17],[18]

This study focuses on the simultaneous electrochemical detection of dopamine and uric acid using a glassy carbon electrode (GCE) modified with ZIF67 and compares it with carbonized ZIF67 at various temperatures. ZIF67 was subjected to carbonization within the temperature range of 500

to 900ºC to determine the optimal temperature for enhanced conductivity and stability. Altering the temperature resulted in improvements in the electronic structure, charge, and spin density of atoms, thereby reducing energy barriers and facilitating smoother electron transfer processes. The high surface area achieved after pyrolysis of ZIF67 enabled efficient oxidation of both dopamine and uric acid. Acid treatment was applied to ZIF67 to eliminate inactive species and promote the formation of an atomically dispersed network. The modified electrode exhibited excellent selectivity, sensitivity, and a wide linear detection range. This proposed method was successfully applied to the analysis of real samples, yielding satisfactory results.

2. Experimental

Materials

We sourced Cobalt nitrate hexahydrate, 2-methyl imidazole, polyvinyl pyridine, methanol, uric acid (UA), dopamine (DP), Potassium ferrocyanide, and potassium chloride from SD Finechem Ltd. To prepare a 0.1M Potassium Phosphate Buffer, we used Potassium Dihydrogen Phosphate and Dipotassium hydrogen phosphate, adjusting the pH to various values using Phosphoric acid (H3PO4) and Sodium hydroxide (NaOH). All the reagents utilized were of analytical grade, and we conducted all experiments using double-distilled water.

Instrumentation

A comprehensive array of analytical techniques was employed to investigate various aspects of the materials, including their synthesis, structure, morphology, chemical bonding, interfacial behavior, and effective surface area. To determine elemental composition and examine crystal structure, X-ray diffraction (XRD) spectroscopy was utilized, employing a Rigaku Ultima IV machine with CuKα radiation. Scanning electron microscopy (SEM), using a ZEISS Gemini SEM system, was employed for morphological studies. Fourier-transform infrared spectroscopy (FTIR) was employed to confirm chemical bonding with a L1600300 Spectrum Two LITA instrument from Perkins. Surface area and pore size were determined through Brunauer-Emmett-Teller (BET) analysis. To evaluate the interfacial behavior and effective surface area of various electrodes, electrochemical impedance spectroscopy, differential pulse voltammetry, and cyclic voltammetry were performed using a Metrohm (PGSTAT204) electrochemical workstation. Finally, the material's surface area and pore size were determined through BET analysis using a Porous Material Inc. BET-201A instrument, with N2 adsorption-desorption isotherms measured at 77K.

Preparation of ZIF67 and ZIF67-T

To synthesize ZIF67, 0.49g of Cobalt nitrate was dissolved in 20 ml of methanol, and separately, 1.25g of 2-methyl imidazole was dissolved in 20 ml of methanol. Each solution was stirred for 30 minutes. The solution containing cobalt salts was slowly added to the solution containing 2-methyl imidazole. This addition caused the color to change from colorless to purple, attributed to the introduction of the initially pink-colored Co ion solution. The resulting mixture was continuously stirred for 6 hours. After this period, the solution was left undisturbed overnight. The sediment was washed three times using methanol at 6000 rpm for 10 minutes. The resulting pellet was dried to obtain ZIF67. Subsequently, ZIF67 underwent carbonization in a tube furnace under varying temperatures in a nitrogen atmosphere. Each temperature was maintained for 1.5 hours before cooling to room temperature. The resulting samples were designated as ZIF67-500, ZIF67-600, ZIF67-700, ZIF67-800, and ZIF67-900.

Pyrolysis of ZIF led to the oxidation of volatile elements such as C, N, and H into gaseous by-products. These gases created porous, N-doped ZIF-derived metal with interconnected pores. All samples then underwent acid leaching using 0.1M HCL and were left overnight to remove any unreacted Co species, further enhancing porosity. The settled materials were subsequently centrifuged using distilled water until a neutral pH was achieved before being dried.

Electrochemical measurements

Samples of weight, 5 mg were dissolved in 1 ml of N, N-Dimethylformamide, and these slurries were then subjected to ultrasonication for 15 minutes to achieve a well-dispersed solution. Subsequently, a glassy carbon electrode (GCE) was polished using an alumina solution, and 10μL of this prepared solution was applied to the GCE and allowed to dry. The Differential Pulse Voltammetry (DPV) and Cyclic Voltammetry (CV) experiments were conducted in a phosphate buffer with a pH of 6, containing appropriate concentrations of DP (dopamine) and UA (uric acid). DPV measurements were recorded over a potential range spanning from -0.2V to +0.6V, using a pulse amplitude of 50mV and a pulse width of 50ms in the phosphate buffer. The electrode underwent potential cycling between -0.2V and 0.6V in the same phosphate buffer at a scan rate of 100mV/s until a steady state was achieved for subsequent experiments. The electrochemical behaviors of the electrodes were investigated using Electrochemical Impedance Spectroscopy (EIS) in a solution containing 5.0mM Fe $(CN)_6^{3-/4-}$ and 0.1M KCL with a frequency range between 0.1 and 10kHz. All electrochemical experiments were carried out at room temperature.

Sample analysis

Human plasma samples were generously provided by healthy volunteers. For analysis, 1 mL of each human plasma sample was diluted by a factor of 50 with phosphate buffer and subsequently analyzed using Differential Pulse Voltammetry (DPV). The recorded data included the peak currents of the analytes.

3. Result and discussion

Choice of materials

ZIF67 exhibits a large surface area and nano-porous structure, making it an ideal oxidation site for electrochemical reactions involving dopamine and uric acid. This unique structure contributes to the high current response observed for both DP and UA. Pyrolysis of ZIF67 at various temperatures enhances its surface area, chemical stability, and flexibility. Additionally, it improves the material's conductivity. During pyrolysis, the graphitic degree of the resulting samples increases with higher applied temperatures, albeit with a gradual decrease in surface area. ZIF67 contains Co species that transform into metallic Co nanoparticles during carbonization. These Co nanoparticles can act as catalysts for the graphitization of carbon. The electrochemical response for detecting DA and UA is significantly influenced by the degree of graphitization of carbon, which is why it was chosen as the platform for the determination of DP and UA.

Material Characterization of ZIF67-T

The prepared samples, including ZIF67, ZIF67-500, ZIF67-600, ZIF67-700, ZIF67-800, and ZIF67-900, were characterized for structure, functional groups, morphology and surface area using techniques XRD, FTIR, SEM, and BET, respectively. The XRD patterns, presented in Fig 1A, demonstrated that all the peaks are aligned perfectly with the standard simulated pattern of ZIF67, indicating the absence of impurities[19]. Fig 1B illustrates that all the samples underwent structural transformations after carbonization. As the temperature increased up to 900°C, the diffraction peak around 25°, corresponding to the carbon (002) interlayer, became more distinct and intense, signifying the development of highly graphitized carbon. However, the (111) and (200) diffractions of the Co crystal at 44.2° and 51.6°, respectively, were still observable, suggesting the presence of some Co nanoparticles even after acid treatment. SEM images (Fig 1C) revealed that the polyhedral morphology of ZIF67 with particle sizes ranging from 1 to 2 μm. Post carbonization, Co species aggregates leading to the formation of metallic nanoparticles[20]. SEM images of ZIF67 after pyrolysis at 800 °C are shown in Fig 1D. This confirms highly porous structure of ZIF67-800, which also leads to increase in surface area. The overall particle shape and size of the original ZIF67 precursor were preserved, but a higher degree of distortion was observed due to pyrolysis [21].

For the investigation of the surface area and porosity of the catalyst, N_2 absorption-desorption and Barrett-Joyner-Halenda (BJH) measurements were conducted. Notably, the surface area of the catalyst increased as the pyrolysis temperature increased. The surface area values for ZIF67-600, ZIF67-700, ZIF67-800, and ZIF67-900 were obtained to be 290, 410, 471, and 530 m^2/g, respectively (Fig 1E). This

increase in surface area with temperature can be attributed to two factors: post-acid treatment, which removed agglomerated and unreacted Co atoms embedded in the carbon system, and the presence of micropores. The average pore size for ZIF67 was 1.69 nm, which decreased to 1.26 nm after pyrolysis at 600°C. At 700°C, the pore size increased to 1.28 nm, further expanding to 1.49 nm at 800°C, and then returning to 1.28 nm at 900°C. These micropores contribute to improved mass transport and provide a high density of active Co sites. However, it was observed that ZIF67-800 exhibited a larger pore size than ZIF67-900, possibly due to structural defects. At high temperatures, the material tends to expose more metallic Co, forming closed and unresolved graphitic shells that hinders the access of N_2 molecule [22].

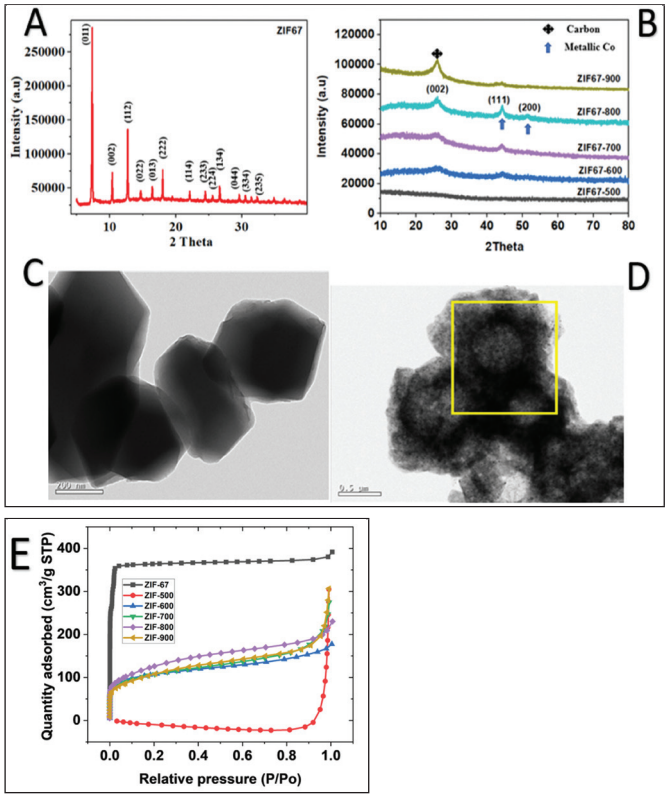

Fig 1A. XRD spectra of pure ZIF67, 3B. XRD spectra of all carbonized ZIF67, 3C. SEM images of ZIF67-800, 3D. High resolution SEM image of ZIF67-800, 3E. N_2 absorption-desorption isotherms of all the ZIF67 materials

Electrochemical Characterization of modified electrodes

The electrochemical properties of various electrodes were studied using $K_3[Fe(CN)_6]$ as a probe via cyclic voltammetry. In Fig 2A, cyclic voltammograms of the bare Glassy Carbon Electrode (GCE), ZIF67, ZIF67-500, ZIF67-600, ZIF67-700, ZIF67-800, and ZIF67-900 in a solution containing 5.0 mM $[Fe(CN)_6]^{3-/4-}$ and 0.1 M KCl are presented. The anodic peak current (Ipa) obtained with ZIF67-800 was at much higher current density compared to other electrodes. This is attributed to its larger surface area and enhanced conductivity of the modified electrode.

For a reversible process, the peak current (I_{pa}) is linearly proportional to the square root of the scan rate ($v_{1/2}$), as described by the Randles-Sevcik formula:

$$I_{pa} = 2.69\times10^5 n^{3/2} A D^{1/2} C v^{1/2}$$

Where I_{pa} is the peak current, n is the number of electrons involved (n=1), A is the surface area of electrode, C is the concentration of the reactant in electrolyte. D is the diffusion coefficient of the $[Fe(CN)_6]^{3-/4-}$ and v is the scan rate. Thus, from the slope of the anodic peak current (I_{pa}) vs square root of scan rate($v^{1/2}$) relation, the value of A for ZIF67-800 was obtained and was found to be much larger than that of non-pyrolyzed ZIF67 and bare GCE. This indicates increase in electroactive surface area of the modified electrode due to the pyrolysis of ZIF67 at high temperature. Electrochemical effective surface area of bare GC, ZIF67, ZIF67-500, ZIF67-600, ZIF67-700, ZIF67-800, ZIF67- 900 are 0.3166 m², 0.478 m², 0.368 m²,0.688 m², 1.982 m², 4.990 m² and 3.651 m² respectively.

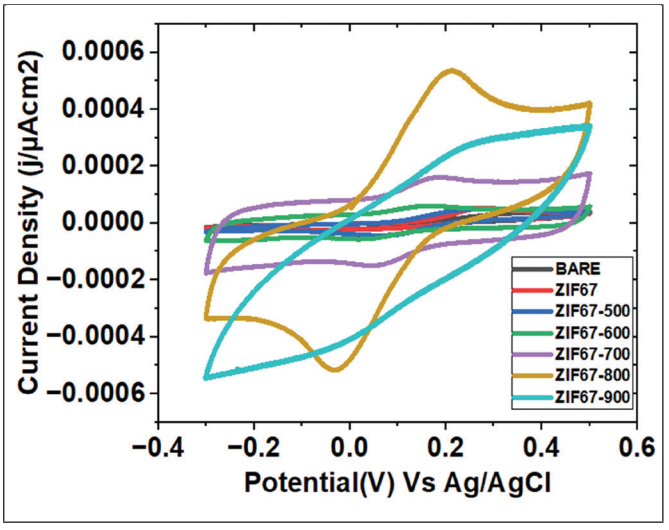

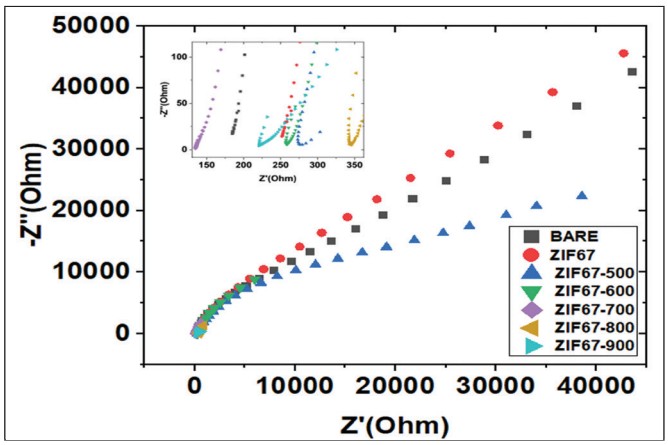

Fig 2 Electrochemical Charcterization of bare GCE, ZIF67, ZIF67-500, ZIF67-600, ZIF67-700, ZIF67-800 and ZIF67-900 in 5.0 mM $[Fe(CN)_6]^{3-/4-}$ containing 0.1 M KCl(A)Cyclic Voltametry B) Electrochemical impedance spectroscopy to determine the x-intercept for R_{ct}(shown in the inset)

Electrochemical Impedance Spectroscopy (EIS) was performed and data shown in Fig 2B, to investigate the electronic charge properties of the modified electrodes, using the redox couple probe $[Fe(CN)6]^{3-/4}$ in the solution of 5mM $Fe(CN)_6^{3-/4-}$ containing 0.1 M KCL, as shown in the Fig 5. The diameter of semicircle element at higher frequencies corresponded to the electron transfer resistance (R_{ct}) between electrode surface and $[Fe(CN)_6]^{3-/4-}$, while the linear part at lower frequency represents the diffusion driven process. The Nyquist curve of the bare GCE displayed a semicircle in the high-frequency region. After introducing ZIF67, the diameter of the semicircle increased, indicating modification with the initially poorly conductive ZIF67. However, the diameter of the semicircle decreased for ZIF67-800 and ZIF67-900 due to their high electrical conductivity. The semicircle was smallest when ZIF67-800 and ZIF67-900 were used as electrode material, which can be attributed to the graphitization of carbon. This suggests that the poor conductivity of ZIF67 was overcome by carbonization, indicating high interfacial electron transfer for ZIF67-800 and ZIF67-900.

Electrochemical behavior of DP and UA

The electrochemical behaviors of dopamine (DP) and uric acid (UA) for different electrode materials were investigated in phosphate buffer at pH 6 using cyclic voltammetry and differential pulse voltammetry. Fig 3, shows the cyclic voltamtery curve obtained for ZIF67 based materials obtained at the scan rate of 100 mV/s. A small oxidation peak was observed for DP at the bare Glassy Carbon Electrode (GCE). However, when ZIF67 was employed, the current density increased significantly indicating superior electrocatalytic activity and fast electron transfer for DP at 0.01V vs Ag/AgCl. Upon the introduction of carbonized ZIF67, a substantial increase in the oxidation peak current was observed, attributed to the greater surface area and porosity along with high conductivity of ZIF-T. Notably, ZIF67-800 displayed the highest oxidation peak current, suggesting enhanced DP oxidation due to the synergistic effect of ZIF67's porosity and the superior conductivity of graphitic carbon formed after carbonization. Furthermore, ZIF67-800/GCE shifted the oxidation peak potential for DP and UA to less negative values, accompanied by a significant increase in current density. Specifically, for DP, the shift was observed from 0.2V to 0.01V, and for UA, it shifted from 0.31V to 0.18V. Fig 6 also reveals two well-defined oxidation peaks corresponding to DP and UA in mixtures of both compounds. The oxidation peak currents for DP and UA were significantly higher for ZIF67-800 than those obtained with other electrode materials[23]. For ZIF67-800, the peak potential for DP was observed at 0.01V with a current response of 0.28 mA/cm^2, and similarly, for UA, the peak potential was observed at 0.18V with a current response of 0.39mA/cm^2. The distinct electrochemical signals at the ZIF67-800/GCE electrode provide a favorable opportunity for the effective and simultaneous determination of DP and UA in phosphate buffer.

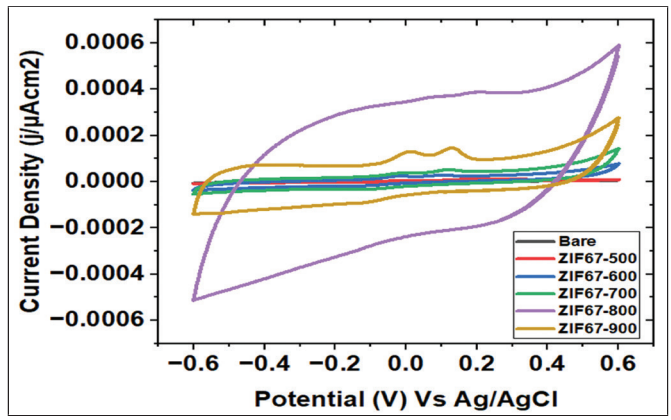

Fig 3 Cyclic Voltammetry results of all materials in presence of 100M concentration of DP and UA with a scan rate of 100mV/s

Simultaneous determination of DP and UA

In order to achieve the optimum electrochemical results using DPV, pH and scan rates were optimized to pH- 6 and scan rate to 10mV.s^{-1}. The simultaneous determination of DP and UA for all the carbonized materials were studied using DPV and shown in Fig 4. DPVs were recorded for various concentrations of DP and UA from 10 to 500µM. Fig 4A, shows DPV curves of DP and UA in mixture solution by simultaneously changing their concentrations. The peak current (I_{pa}) were proportional to their concentration from 10 µM to 500 µM for DP and from 10 µM to 500 µM for UA. The regression equation utilized was I_{pa}(µA.cm^{-2}) = 0.9673C(µM) (R=0.98) for DP and I_{pa}(µA.cm^{-2}) = 0.107C(µM)-(R=0.98) for UA, respectively. The detection limit (LOD) for DP and UA were estimated to be 23.3µM and 17.8µM (S/N=3), respectively. The sensitivity for DP and UA were 1999.3 µA. µM^{-2}cm^{-2} and 1069.3 µA. µM^{-2}cm^{-2}, respectively. Comparing the data for the simultaneous and quantitative determination DP and UA, ZIF67-800/GCE shows best performance as expected sue to its high current sensitivity and good resolution.

Fig 4B, shows DPV data with variation in concentration of DP, where UA was maintained at constant concentration of 100 µM. The peak current of DP was found to be proportional to the concentration, which was varied from 10 µM to 500 µM (R=0.97). The regression equation of I_{pa}(µA.cm^{-2})=0.116C(µM) – (R=0.98) was followed with the sensitivity of 1569 µA.µM^{-2}.cm^{-2}. Similar patterns were observed for UA with respect to DP at a constant concentration of 100 µM as shown in the fig 4C, the peak current of UA was proportional to the concentration from 10 µM–500 µM (R=0.98) with a regression equation of Ipa(µA. cm^{-2})=0.073(µM)–(R=0.98), sensitivity was 1009 µA.µM^{-2}.cm^{-2}, indicating that the oxidation of DP and UA at ZIF67-800 modified electrode took place independently without any mutual interference.

These results indicate that ZIF67-800/GCE can be effectively employed for the simultaneous determination of dopamine (DP) and uric acid (UA) without interference between the two analytes. Table 1 provides a summary comparing ZIF67-800 modified electrodes with other carbonized modified electrodes for the simultaneous detection of DP and UA. The table illustrates that the modified electrode developed in this study exhibits a low detection limit and a wide linear range. The improved electrocatalytic performance of ZIF67-800/GCE can be attributed to its highly porous structures with a high degree of graphitization, improving the electronic conductivity. Graphitic nitrogen doped porous carbon structures are known for their high electrochemical performances.

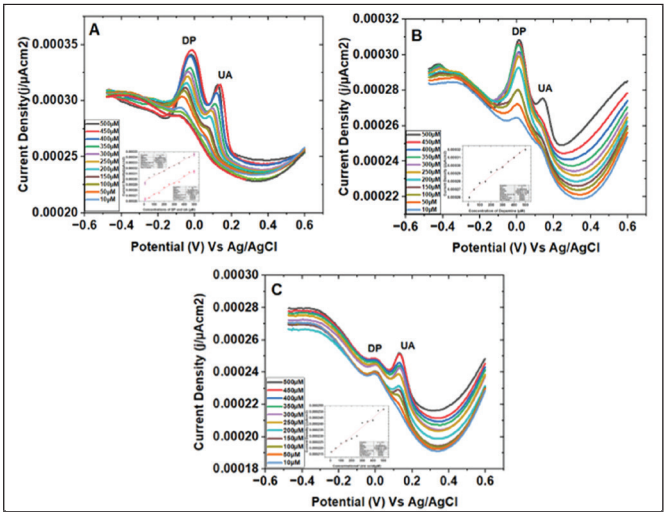

Fig 4A DPV cures for Simultaneous detection of DP and UA at different concentration, B) DPV curves for detection of DP with concentration of UA as constant and C)DPV curves for detection of UA with concentration of DP as constant

Table 1) Comprehensive comparison of developed ZIF67-T materials for the simultaneous detection of DP and UA

Materials	Linear range(µM)		Detection limit (µM)		Sensitivity (µA. µM^{-2}.cm^{-2})	
	DP	UA	DP	UA	DP	UA
ZIF67-500	50-1000	50-1000	49.1	40.3	488.9	217.8
ZIF67-600	50-1000	50-1000	44.9	45.3	699.33	500.3
ZIF67-700	50-1000	30-1000	35.5	25.3	747.4	899.7
ZIF67-800	10-1000	10-1000	23.3	5.3	1999.8	1069.4
ZIF67-900	50-1000	40-1000	49.2	25.9	680.3	789.3

Mechanism

When a sample containing both dopamine and uric acid is introduced to the modified electrode, both analytes can be simultaneously detected through their distinct electrochemical signals. The modified electrode facilitates the oxidation of dopamine, resulting in an oxidation peak in the current-voltage curve at 0.01V. Uric acid also undergoes oxidation, but at a different potential of 0.18V compared to dopamine. This selective detection of uric acid leads to a separate oxidation peak in the current-voltage curve, with its peak potential and current intensity being characteristic of uric acid. Fig 5 illustrates the mechanism of simultaneous detection of dopamine and uric acid on the modified electrode surface. To establish the linear range, a series of standard solutions with known analyte concentrations are prepared. Sensor is then employed to measure the current response at each concentration. By plotting the response against concentration, the linear range is determined by identifying the range of concentrations exhibiting a linear relationship. The Limit of Detection (LOD) can be calculated as the concentration corresponding to a certain multiple of the standard deviation of the blank signal divided by the slope of the calibration curve. Sensitivity is calculated as the slope of the calibration curve, obtained through linear regression fitting of the experimental data points.

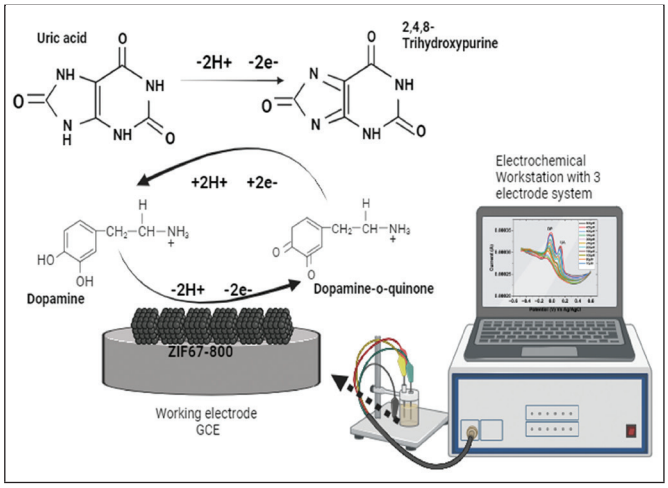

Fig 5 Mechanism of simultaneous detection of dopamine and uric acid on the surface of modified electrode

Selectivity, stability and reproducibility

Resistance to interference is a crucial parameter for an electrochemical sensor. Ascorbic acid (AA), which is a major interfering species affecting the electrochemical detection of dopamine (DP) and uric acid (UA) in the analysis of real samples, was tested at high concentrations. Fig 6A, depicts the interference of DP on the oxidation of AA. It exhibited a poor electrochemical response on ZIF-T and the separation of the oxidation peak potentials of DP and UA was significant enough for clear distinction. This may be attributed to electrostatic repulsion caused by the negatively charged carboxylate groups on the graphitic carbon, which exclude most of the AA anions from the electrode surface. Fig 6B demonstrates the insignificant interferences observed for several compounds, including AA, glucose, urea, hydrogen peroxide, and ethanol. The Differential Pulse Voltammetry (DPV) curve for these interfering species shows no additional peaks. All these results collectively indicate the excellent selectivity of ZIF67-800/GCE.

The stability of ZIF67-800 was assessed (Fig 6C) in a mixed solution containing 100 µM DP and 100 µM UA. The oxidation currents using this method displayed a relative standard deviation (RSD) of 19.0% for DP and 12.2% for UA in seven successive measurements, demonstrating excellent stability. Reproducibility was tested using four different modified electrodes, yielding an RSD of 5.4% for DP and 3.23% for UA. Therefore, ZIF67-800 exhibits good reproducibility along with considerable stability for the simultaneous determination of DP and UA.

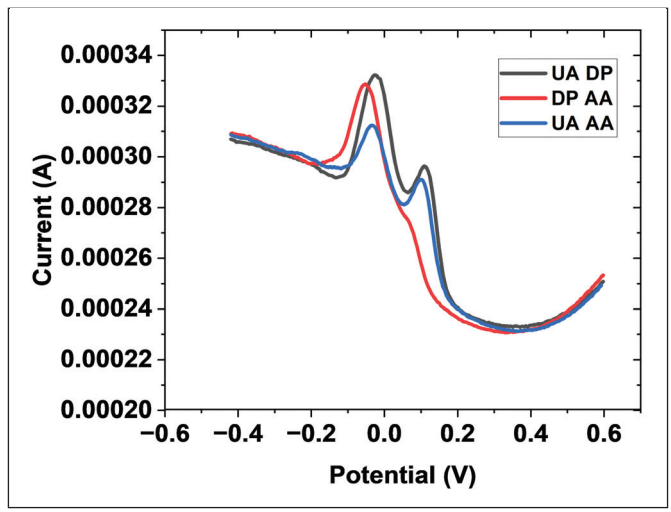

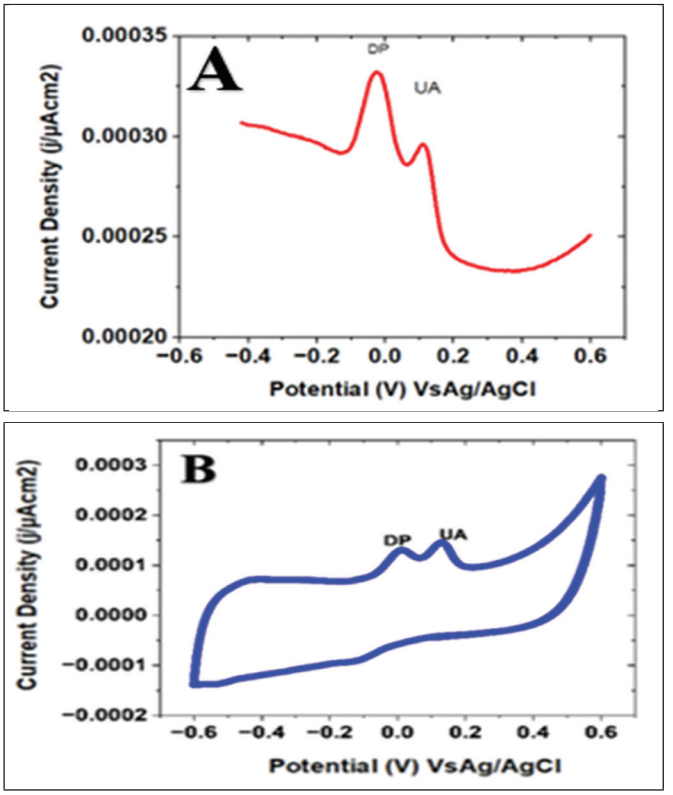

Fige 6A DP interfering for AA oxidation on ZIF67-800 (B)Interference studies in presence of AA, glucose, urea, hydrogen peroxide and ethanol and C Stability of ZIF67-800 after 1000cycles

Analytical application

To assess the materials performance in real samples, ZIF67-800 was employed for the determination of dopamine (DP) and uric acid (UA) in human plasma. Differential Pulse Voltammograms (DPVs) of phosphate buffer (pH=6) in both the absence and presence of a human plasma sample are depicted in Fig 7. A significant increase in peak current was observed at a potential of 2.5V, indicating the presence of UA in the sample.

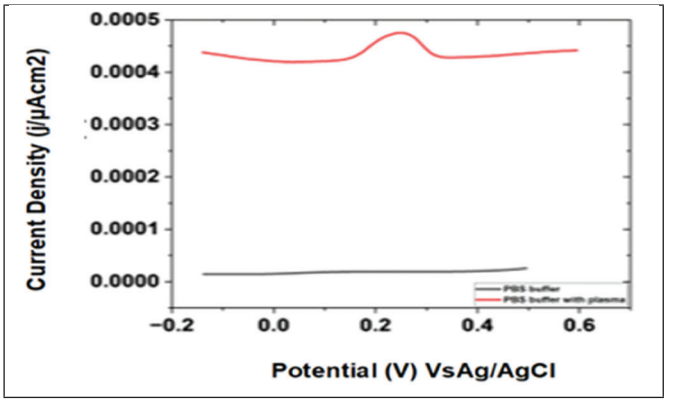

Fig 7 Detection of uric acid in human plasma

Conclusions

In summary, we successfully fabricated a modified glassy carbon electrode by employing a drop-casting technique with ZIF-T. The resulting ZIF67-800-modified electrode exhibited excellent electroactivity for the oxidation of both dopamine (DP) and uric acid (UA). We harnessed this ZIF67-800-modified electrode for the simultaneous determination of DP and UA, and the oxidation peak potentials for these analytes displayed clear distinctions, underscoring its remarkable selectivity and sensitivity. The glassy carbon electrode demonstrated favourable analytical parameters, including a wide linear range and a low detection limit. These attributes can be attributed to the porous structures with a high degree of graphitization, along with the Co nanoparticles acting as catalysts to promote carbon graphitization and facilitate rapid electron transfer. Notably, graphitic carbon structures are known for their higher electrical conductivity compared to amorphous carbon. Furthermore, we successfully applied this glassy carbon electrode to detect DP and UA in human plasma, highlighting its promising potential for real sample analysis.

Acknowledgement

The authors are thankful to the Department of Science and Technology(DST/TMD/HCF/2K18/130) and SERB-Power(SPG/2023/000046) for funding assistance. We would also like to thank SAIF IIT, Bombay for Material Characterization.

References

[1] J. Tang, S. Jiang, Y. Liu, S. Zheng, L. Bai, J. Guo and J. Wang, "Electrochemical determination of dopamine and uric acid using a glassy carbon electrode modified with a composite consisting of a Co(II)-based metalorganic framework (ZIF67) and graphene oxide", Microchimica Acta 185(2018), 486-497, https://doi.org/10.1007/s00604-018-3025-x .

[2] M. U. Anu Prathap and R. Srivastava, "Tailoring properties of polyaniline for simultaneous determination of a quaternary mixture of ascorbic acid, dopamine, uric acid,

and tryptophan," Sensors and Actuators B: Chemical, vol. 177(2013), pp. 239–250, doi: 10.1016/j.snb.2012.10.138.

[3] J. C. Ndamanisha and L. Guo, "Electrochemical determination of uric acid at ordered mesoporous carbon functionalized with ferrocenecarboxylic acid-modified electrode," Biosens Bioelectron, vol. 23(2008), no. 11, pp. 1680–1685, doi: 10.1016/j.bios.2008.01.026.

[4] M. R. Moghadam, S. Dadfarnia, A. M. H. Shabani, and P. Shahbazikhah, "Chemometric-assisted kinetic–spectrophotometric method for simultaneous determination of ascorbic acid, uric acid, and dopamine," *Anal. Biochem.*, vol. 410(2011), no. 2, pp. 289–295, doi: 10.1016/j.ab.2010.11.007.

[5] M. Orts-Arroyo, I. Castro, and J. Martínez-Lillo, "Detection of Hypoxanthine from Inosine and Unusual Hydrolysis of Immunosuppressive Drug Azathioprine through the Formation of a Diruthenium(III) System," *Biosensors*, vol. 11(2021), no. 1, p. 19, doi: 10.3390/bios11010019.

[6] X. Lian and B. Yan, "Phosphonate MOFs Composite as Off–On Fluorescent Sensor for Detecting Purine Metabolite Uric Acid and Diagnosing Hyperuricuria," *Inorg. Chem.*, vol. 56(2017), no. 12, pp. 6802–6808, doi: 10.1021/acs.inorgchem.6b03009.

[7] Y. Tao, Y. Lin, J. Ren, and X. Qu, "A dual fluorometric and colorimetric sensor for dopamine based on BSA-stabilized Aunanoclusters," *Biosens. Bioelectron.*, vol. 42(2013), pp. 41–46, doi: 10.1016/j.bios.2012.10.014.

[8] J. Wang *et al.*, "Dopamine and uric acid electrochemical sensor based on a glassy carbon electrode modified with cubic Pd and reduced graphene oxide nanocomposite," *J. Colloid Interface Sci.*, vol. 497(2017), pp. 172–180, doi: 10.1016/j.jcis.2017.03.011.

[9] G. Wang *et al.*, "Non-enzymatic electrochemical sensing of glucose," *Microchim. Acta*, vol. 180(2013), no. 3–4, pp. 161–186, doi: 10.1007/s00604-012-0923-1.

[10] C. Shan, H. Yang, D. Han, Q. Zhang, A. Ivaska, and L. Niu, "Graphene/AuNPs/chitosan nanocomposites film for glucose biosensing," *Biosens. Bioelectron.*, vol. 25(2010), no. 5, pp. 1070–1074, doi: 10.1016/j.bios.2009.09.024.

[11] L. Zhang, C. Liu, Q. Wang, X. Wang, and S. Wang, "Electrochemical sensor based on an electrode modified with porous graphitic carbon nitride nanosheets (C3N4) embedded in graphene oxide for simultaneous determination of ascorbic acid, dopamine and uric acid," *Microchim. Acta*, vol. 187(2020), no. 2, p. 149, doi: 10.1007/s00604-019-4081-6.

[12] B. Sriram, M. Govindasamy, S.-F. Wang, R. Jothi Ramalingam, H. Al-lohedan, and T. Maiyalagan, "Novel sonochemical synthesis of Fe3O4 nanospheres decorated on highly active reduced graphene oxide nanosheets for sensitive detection of uric acid in biological samples," *Ultrason. Sonochem.*, vol. 58(2019), p. 104618, doi: 10.1016/j.ultsonch.2019.104618.

[13] K. Samoson *et al.*, "Facile fabrication of a flexible laser induced gold nanoparticle/ chitosan/ porous graphene electrode for uric acid detection," *Talanta*, vol. 243(2022), p. 123319, doi: 10.1016/j.talanta.2022.123319.

[14] H. Shu *et al.*, "Single-step electrochemical deposition of high performance Au-graphene nanocomposites for nonenzymatic glucose sensing," *Sens. Actuators B Chem.*, vol. 220(2015), pp. 331–339, doi: 10.1016/j.snb.2015.05.094.

[15] I. Shackery, U. Patil, A. Pezeshki, N. M. Shinde, S. Im, and S. C. Jun, "Enhanced Non-enzymatic amperometric sensing of glucose using Co(OH)2 nanorods deposited on a three dimensional graphene network as an electrode

material," *Microchim. Acta*, vol. 183(2016), no. 8, pp. 2473–2479, doi: 10.1007/s00604-016-1890-8.

[16] N. Kau, G. Jindal, R. Kaur, and S. Rana, "Progress in development of metal organic frameworks for electrochemical sensing of volatile organic compounds," *Results Chem.*, vol. 4(2022), p. 100678, doi: 10.1016/j.rechem.2022.100678.

[17] C. Duan, Y. Yu, and H. Hu, "Recent progress on synthesis of ZIF67-based materials and their application to heterogeneous catalysis," *Green Energy Environ.*, vol. 7(2022), no. 1, pp. 3–15, doi: 10.1016/j.gee.2020.12.023.

[18] R. S. Mane, S. Pradhan, V. Somkuwar, R. Bhattacharyya, P. C. Ghosh, and N. Jha, "An electron 'donor–acceptor–donor' strategy to activate ZIF67 as a cathode material for fuel cells and zinc ion hybrid supercapacitor," *React. Chem. Eng.*, vol. 8(2023), no. 4, pp. 891–907, doi: 10.1039/D2RE00357K.

[19] J. Qian, F. Sun, and L. Qin, "Hydrothermal synthesis of zeolitic imidazolate framework-67 (ZIF67) nanocrystals," *Mater. Lett.*, vol. 82(2012), pp. 220–223, doi: 10.1016/j.matlet.2012.05.077.

[20] J. Tang *et al.*, "Thermal Conversion of Core–Shell Metal–Organic Frameworks: A New Method for Selectively Functionalized Nanoporous Hybrid Carbon," *J. Am. Chem. Soc.*, vol. 137(2015), no. 4, pp. 1572–1580, doi: 10.1021/ja511539a.

[21] A. F. Gross, E. Sherman, and J. J. Vajo, "Aqueous room temperature synthesis of cobalt and zinc sodalite zeolitic imidizolate frameworks," *Dalton Trans.*, vol. 41(2012), no. 18, pp. 5458–5460, doi: 10.1039/C2DT30174A.

[22] Y. Guo *et al.*, "Effect of Various Pyrolysis Temperatures on ZIF67 Derived Nanoporous Carbons," *Bull. Chem. Soc. Jpn.*, vol. 90(2017), no. 8, pp. 939–942, doi: 10.1246/bcsj.20170138.

[23] J. Tang *et al.*, "Electrochemical determination of dopamine and uric acid using a glassy carbon electrode modified with a composite consisting of a Co(II)-based metalorganic framework (ZIF67) and graphene oxide," *Microchim. Acta*, vol. 185(2018), no. 10, p. 486, doi: 10.1007/s00604-018-3025-x.

SUPPLEMENTARY FIGURES

Effect of Pyrolysis temperature on ZIF67 for Simultaneous Electrochemical Detection of Dopamine and Uric acid

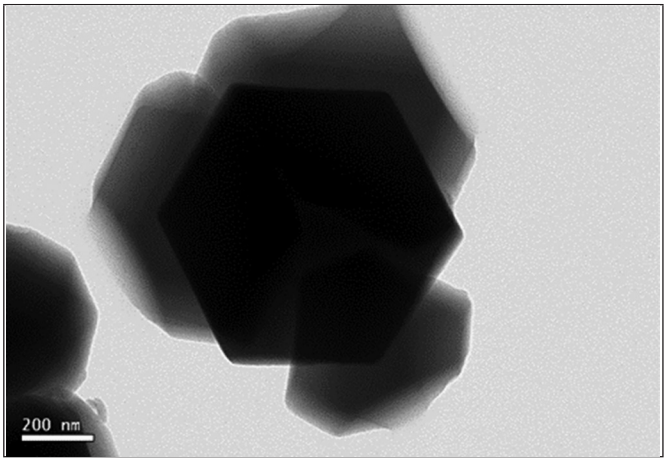

Figure 1 SEM image of ZIF67 before Pyrolysis

Figure 1.The SEM image showed typical uniform morphology of polyhedral crystals.

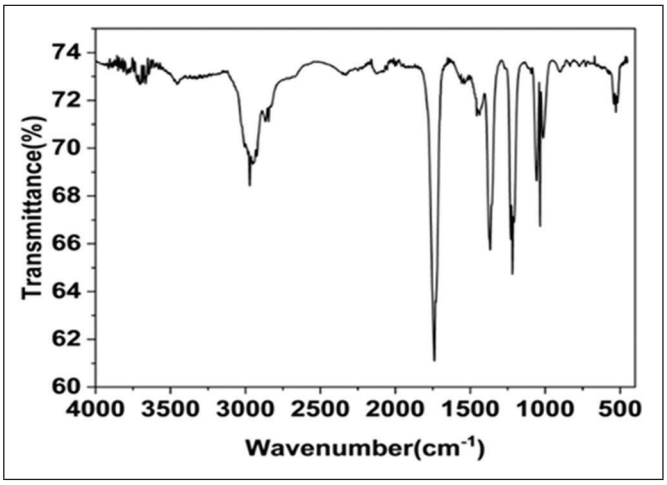

Figure 2 FTIR of ZIF67

FT-IR spectra can give the information on the structural properties and functional groups. For ZIF67, typically the peaks come in the range of 600 to 1500cm-1 from the stretching and bending modes of imidazole ring, the peak at 1584cm-1 can be assigned as C=N stretch mode in 2-methylimidalzole, and the peaks at 2930 and 3145cm-1 attributed to the stretching mode of C-H from the aromatic ring and the aliphatic chain [21]. After pyrolysis at high temperature, the absence of the aforementioned peaks confirms the successful elimination of functional groups during the pyrolysis processing S3 shows the FTIR spectra of ZIF67-800.

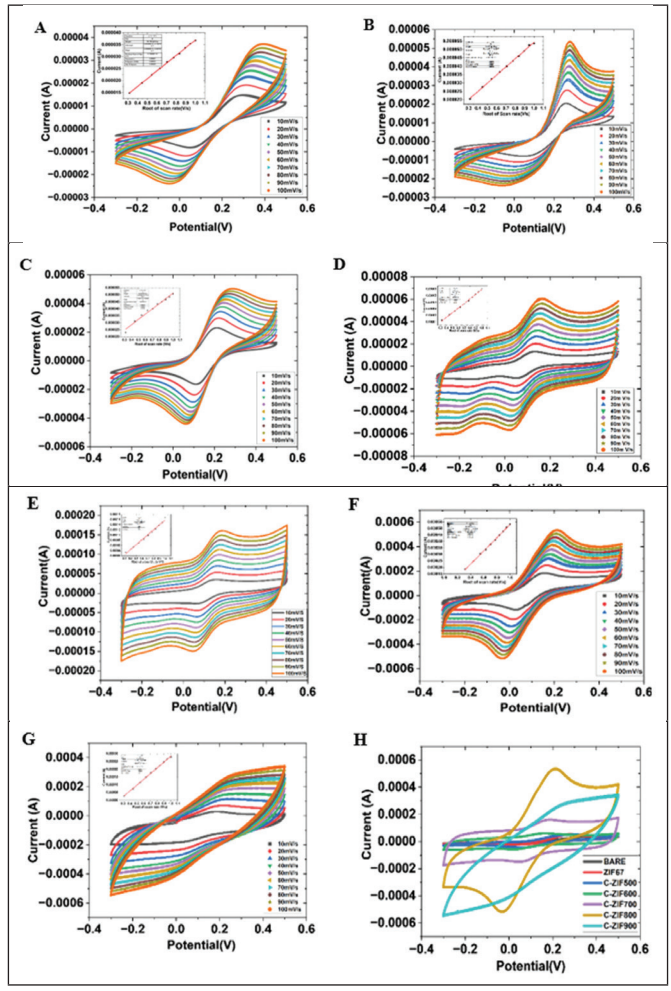

Figure 3 Cyclic voltammograms of bare GCE A), ZIF67 B), ZIF67-500 C), ZIF67-600 D), ZIF67-700 E), ZIF67-800 F) and ZIF67-900 G) in 5.0 mM[Fe(CN)$_6$]$^{3-/4-}$ containing 0.1 M KCl and H) Comparison of all the materials for investigate the effective surface area of the electrode.

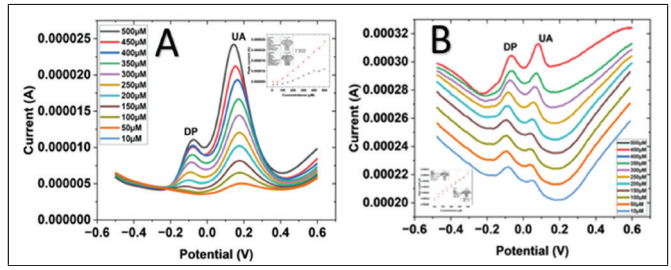

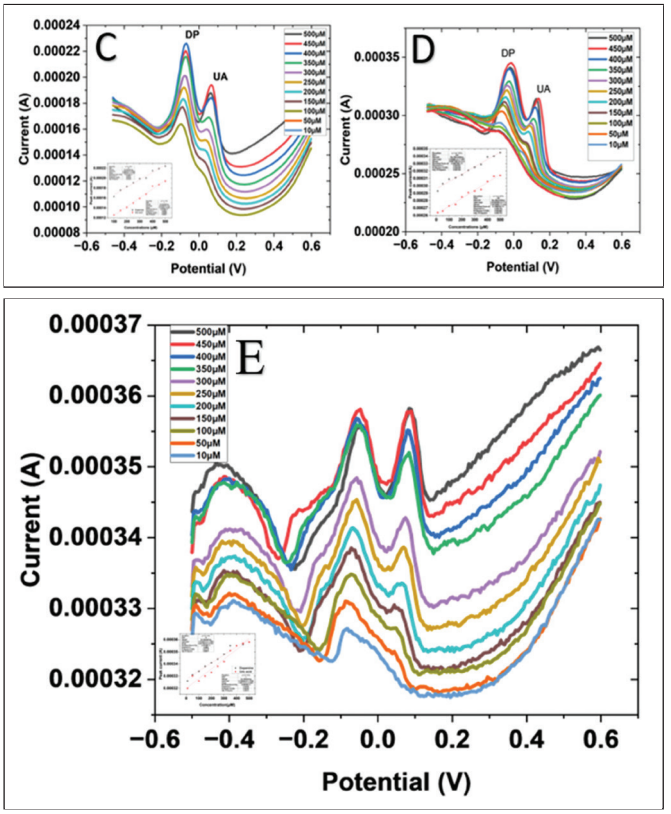

Figure 4 DPV cures for Simultaneous detection of DP and UA at different concentration for different modified electrode A))ZIF67-500, B) ZIF67-600, C) ZIF67-700, D) ZIF67-800 and E) ZIF67-900

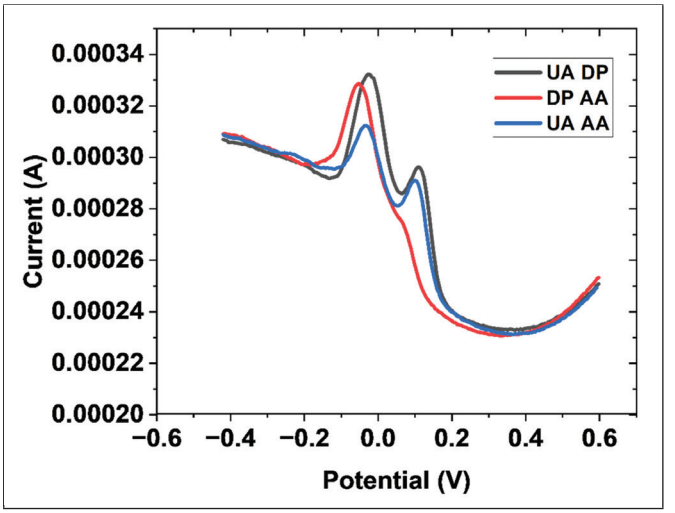

Figure 5 DPV curve shows DP interfering for AA oxidation on ZIF67-800

Carbonaceous Two-Dimensional Electrode Materials for High Performance Electrochemical Double Layer Capacitors

Dhiman Kalita [a, b], B. Sheetal Priyadarshini [a, b], Unnikrishnan Manju [a, b*]

[a] *Materials Chemistry Department, CSIR-Institute of Minerals and Materials Technology, Bhubaneswar, Odisha - 751013, India*

[b] *Academy of Scientific and Innovative Research (AcSIR), Ghaziabad, Uttar Pradesh - 201002, India*

** Corresponding author : manju@immt.res.in*

Abstract

Research dedicated towards improving the efficiency and performance of the Electrochemical Double Layer Supercapacitors (EDLCs) can prove to be pivotal for sustainable energy storage. Selection of proper electrode material is imperative for enhancing the performance as the energy storing mechanism is dependent on the redox reactions occurring on the surface of the electrodes. 2D materials have been extensively studied for fabrication of electrode materials in EDLCs due to their unique layered structure and electrochemical properties. This review offers a holistic overview of the carbon-based 2D electrode materials and also discusses the challenges to be addressed for high performance EDLCs.

Keywords: *Supercapacitors, Energy, 2D materials, Graphene, MXene,*

1.1 Introduction

The depletion of fossil fuel reserves and the increasing energy demand urge us to unplug ourselves from its reliance on fossil fuels and look for development of alternating energy sources from renewable energy, such as solar and wind power. These sources are intermittent in nature and hence require energy storage for the harvested energy, such as batteries and capacitors. Batteries are preferred for applications requiring high energy density but restricted power output; on the other hand, capacitors are favored in those requiring high power. However, for applications requiring high energy as well as power density, neither batteries nor capacitors are sufficient, which prompts to an investigation of new types of energy storage systems known as electrochemical capacitors.

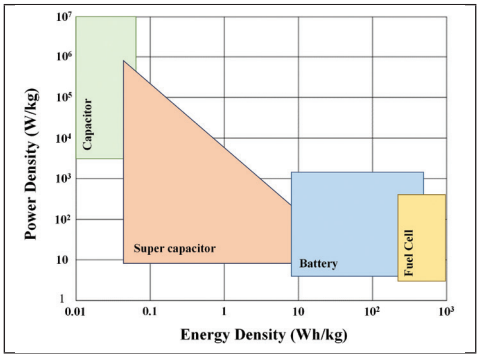

Figure 1: Ragone plot for energy storage devices [1]

Electrochemical capacitors (ECs) are electrical energy storage devices based on the electric double-layer existing at the interface between a solid electrode and an electrolyte. Hermann von Helmholtz proposed the electric double-layer theory that focus on the interfacial electrochemical reactions between a charged electrode and an electrolyte. ECs also known as supercapacitors or ultracapacitors can store larger amounts of energy than that conventional capacitors as depicted in the Ragone plot (Figure 1) [1]. Low capacitance values in the range of microfarad to picofarad of electrostatic capacitors limit their use in low-power applications. Whereas, the need for high-power capabilities due to the rapid growth in mobile electronic gadgets and electrical vehicles led to the development of supercapacitors. Becker at SOHIO in 1957 invented the first supercapacitor with exceptionally high capacitance with carbon material used as electrode [2]. Later, Boos developed the first practical supercapacitor in 1970 [3].

Supercapacitors use electrode materials with a high specific surface area and thinner dielectrics, resulting in very high specific capacitance [4],[5] They are also environment friendly, have a long

service lifetime, can operate in a wide temperature range, and can retain charge even at high applied current; which make them suitable for consumer electronics, transport, and smart meters [4], [5], [6], [7]. Supercapacitors can be divided into three categories on the mechanism on energy storage as shown in Figure 2.

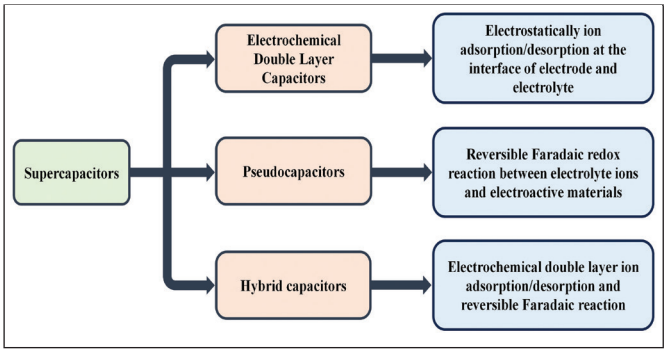

Figure 2: Supercapacitors types based on energy storage mechanism

Mostly, the progress of supercapacitor focuses on the development of electrode materials. Scientist have designed, developed and integrated one-dimensional, two-dimensional and three-dimensional electrode materials into supercapacitors to fabricate high performance electrode materials. In this review we focus on the electric double layer capacitor (EDLC) and concentrate on the electrode materials based on two-dimensional carbon materials.

1.2. Electrochemical Double Layer Capacitors

An electrochemical device comprises two electrodes with an electrolyte sandwiched between them. A typical double-layer capacitor is shown in Figure 3. The positive charges that accumulate on the positive electrode attract an equal number of negative charges due to Coulomb's force. However, they possess a net negative charge near the electrode due to the heat fluctuation in the electrolyte. The balance of charges between the electrode and the electrolyte is a representation of an electric double layer. The same phenomena occur across the negative electrode as well, which forms another electric double layer. Therefore, a complete two electric double layers with the positive electrode-electrolyte interface and the negative electrode-electrolyte interface is formed.

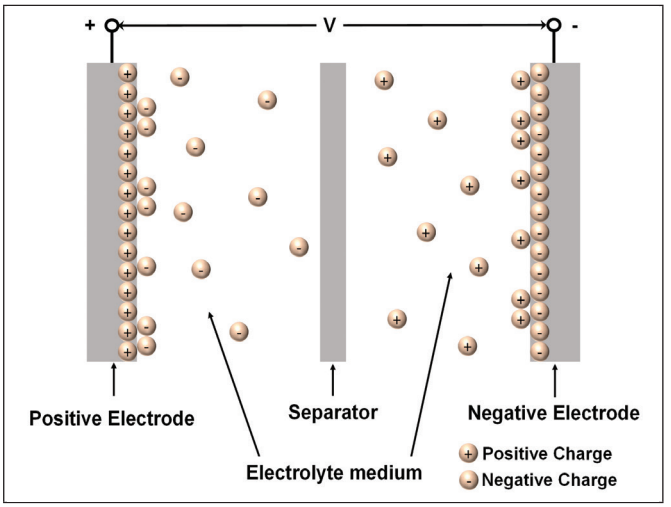

Figure 3: Schematic of electric double-layer capacitor

1.2.1. Working Mechanism

The initial development of the electric double layer model was based on an aqueous electrolyte. Later, non-aqueous as well as ionic liquids electrolytes were also used. The charge generated at the interface between the electrode and the electrolyte solution is balanced by an induced accumulation ions having opposite charges near the electrode surface in the electrolyte through the exertion of Coulomb's force as shown in Figure 4. Heat fluctuation helps scatter net negative charge ions with a higher concentration near the positive electrode surface and vice-versa. This scattered negative charged layer with the electrode positive charge array is termed a "diffuse double-layer" or "diffuse layer". This diffuse layer is also called the "Gouy point charge model" or the "Gouy-Chapman model" (Figure 4a). The diffuse layer thickness is dependent on the temperature, concentration of the electrolyte, number of charges carried by the ions, and the dielectric constant of the electrolyte.

In general, at high temperatures, the diffuse layer thickness increases. Whereas, at higher concentrations, a high number of charges carried by the ions and dielectric constant, the diffuse layer thickness decreases. A model with low temperature

and high electrolytic concentration, charge number carried by the ions, and dielectric constant gives a very thin diffuse layer leading to a compact electric double-layer termed as Helmholtz layer (Figure 4b) [8]. In a working model, these two layers coexist as shown in Figure 4c and it is termed as the Stern-Grahame model.

According to the fundamental relationship of capacitors ($C= (\varepsilon_0 \times \varepsilon_r \times A)/d$), the capacitance of a standard capacitor can be increased by increase in the dielectric constant of the material and surface area and the distance between the interplanar distance. However, such improvement can be achieved by the modification of the materials and the design of the capacitor. The selection of electrode materials and the design of electrodes play an important role in the subsequent electrochemical performance. 2D materials with a larger surface area have been developed as promising materials for electrodes [9],[10] After the discovery of "wonder material" graphene, the development of 2D nanostructured materials drastically increased. In the next section, we have discussed about the various carbon-based materials for the use of electrode material.

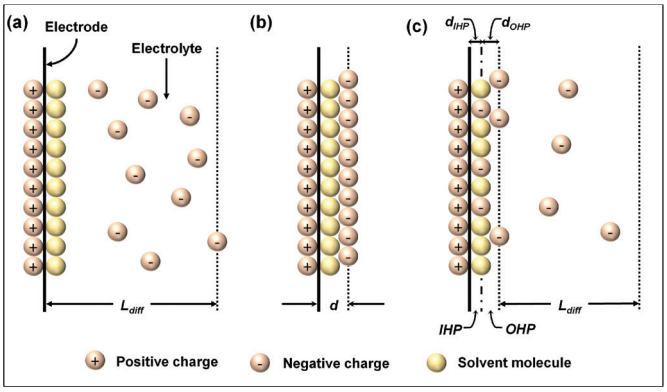

Figure 4: Schematics of the interface of electrode and electrolyte of electric double-layer. (a) Diffuse layer or Gouy-Chapman model, L_{diff} is the length of the diffuse layer. (b) Helmholtz layer, d is the double-layer thickness. (c) Stern-Grahame layer, IHP, and OHP are the inner and outer Helmholtz plane, and d_{IHP} and d_{OHP} are the respective thickness.

1.3. 2D Carbon based Electrode Material

Energy stored in EDLCs is primarily governed by the surface-controlled electrochemical phenomenon occurring on the electrodes. The choice of the electrode material is essential as they provide sites for charge separation at the electrode-electrolyte interface, i.e., Helmholtz double layer. The electric double layers formed at the interface between both the electrodes with the electrolyte influence the differential capacitance which decides the performance of the EDLC. Hence, it is imperative to enlarge the overall surface area of the electrode materials which renders more readily available active sites for energy carriers for efficient energy storage.

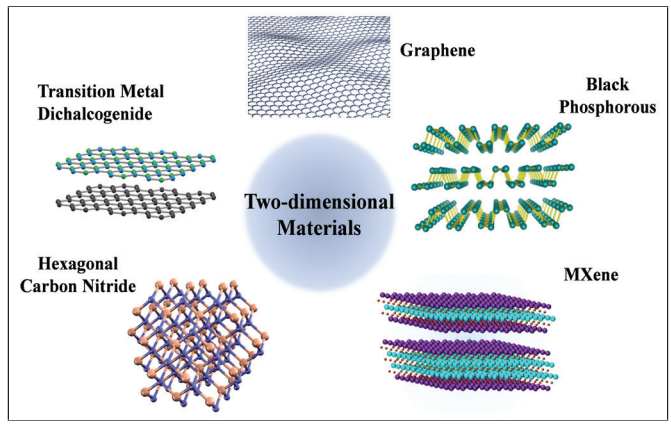

Figure 5: Some commonly explored two-dimensional materials as electrode materials for supercapacitor applications.

Ideally, the electrodes should be characterized by high surface area, good stability, superior mechanical properties, and excellent electrical conductivity [11]. Various nanostructured materials have been investigated for supercapacitor applications as electrode materials owing to the higher surface area than their bulk counterpart. 2D materials, possessing typical ultrathin and nanolayered structures, are considered promising electrode materials in EDLCs due to their large surface area and unique morphology (Figure 5) [12],[13] In recent years, many fabrication methods have been implemented to develop 2D electrode materials. To fabricate high-performance EDLC, both positive and negative electrode plays a critical role. However, very less importance has been given to the negative electrode materials. Different negative electrode materials have diverse operating voltage ranges, which drastically affect their performance. Usually, 2D materials show much better performance as negative electrodes than the positive electrodes [14].

1.4.1 Graphene

Owing to its peculiar two-dimensional honeycomb structure with sp^2 hybridized carbon sheets in hexagonal lattice conformation, graphene has been studied intensely for supercapacitor applications among other carbon-based materials [15]. The exceptionally high specific surface area of about 2630 $m^2 g^{-1}$, coupled with high electrical conductivity of about 10^6 S cm^{-1}, makes them an excellent choice as electrode materials in double-layer capacitors. Further, the added advantages of being corrosion resistant in aqueous electrolytes, superior cycle stability, high optical transmittance (97.7 %), higher Young's modulus (~1TPa), good thermal conductivity (~5000 W m^{-1} K^{-1}), and excellent carrier mobility (2 x 10^5 cm^2 V^{-1} s^{-1}) favor its usage in platforms for energy storage [16]. Commercial synthesis of graphene is also made scalable and economical by its facile and low-cost fabrication process using Hummer's method (Figure 6a).

The high carrier mobility of the graphene sheets enhances charge transfer during the charging and discharging process, however individual nanosheets are aggregated during fabrication due to interplanar π- π interaction and van der Waals forces. This drastically reduces the surface area and inhibits the diffusion of electrolyte ions which affects the performance of the EDLC. This is resolved by heteroatom doping and chemical bonding with highly conductive polymers or metal oxides. The composite of graphene with these materials synergistically enhances the ion transport and reduces sheet aggregation in graphene, thus increasing the overall capacitance of the EDLC.

Liu et al. synthesized a novel graphene-polypyrrole composite by hybridizing polypyrrole nanotubes with chemically reduced graphene sheets that combined the advantage of an electric double layer and pseudocapacitor. At a current density of 0.3 A g^{-1}, the hybrid composite electrode offered a very high specific capacitance of 400 F g^{-1}, which was significantly higher than previously reported values [17]. In another study reported by Tai et al., a unique bi-layered graphene/ shape-memory polyurethane (SMPU) electrode was synthesized via a simple bonding method. A graphene paper was closely bonded with SMPU and owing to the flexibility

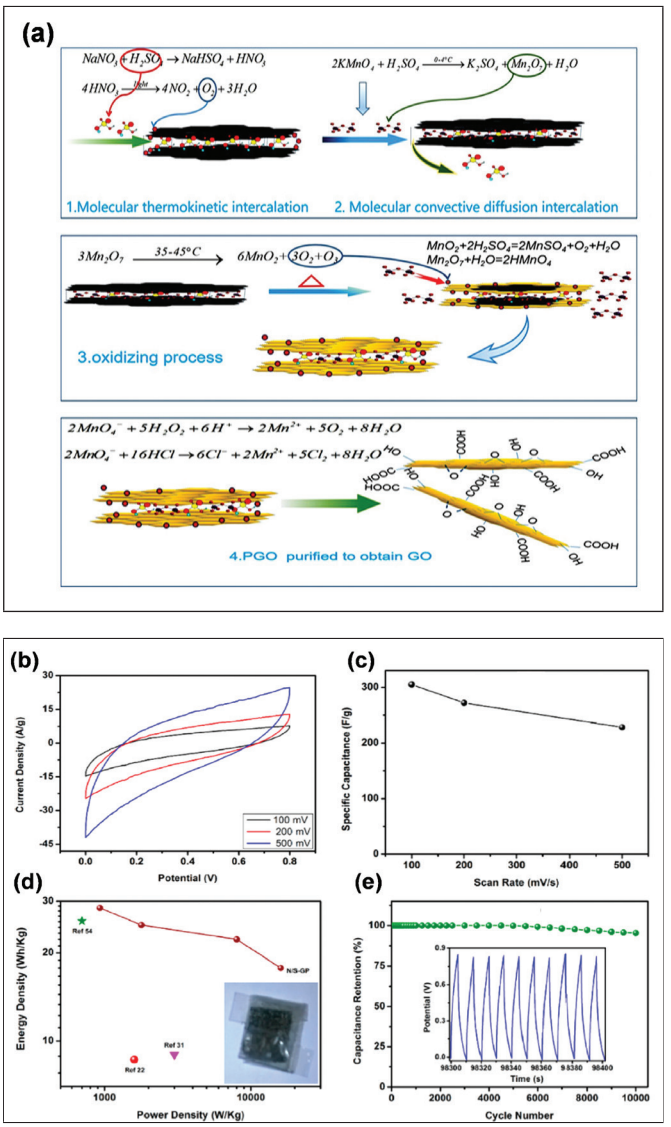

Figure 6: (a)Mechanism of oxidation of flake graphite to graphene oxide (GO) by Hummer's method. The figure encapsulates the oxidative chemical reactions that convert graphene to GO. Reproduced with permission from Ref. [19], Copyright 2022, American Chemical Society. (b) Cyclic voltammograms of supercapacitor device using free-standing dual doped graphene electrode in 6M KOH electrolyte at different scans and (c) the specific capacitance obtained. (d) Ragone plot of the fabricated symmetric supercapacitor as compared with graphene-based supercapacitor devices in ionic and aqueous electrolyte (inset shows the image of the assembled supercapacitor) (e) cyclic stability of the fabricated device at a current density of 5 A g^{-1} (inset shows magnified data of the last 10 cycles) Reproduced with permission from Ref. [20], Copyright 2016, American Chemical Society.

of the graphene paper, the composite film could adapt to different shapes and exhibited exceptional shape-recovering ability. The film shows a superior capacitive performance of 218 F g-1 at a current density of 0.75 A g-1 which is relatively stable up to 2000 charging-discharging cycles [18].

The electrochemical performance of graphene-based electrodes is closely related to the morphology of the material. Akhter et al. developed a flexible 3D architecture of graphene paper doped with nitrogen and sulfur through a one-pot thermal treatment of liquid crystalline graphene oxide and dopant composite followed by a soft assembly approach. This approach ensures layer-by-layer deposition of graphene oxide between which the dopant is trapped resulting in a composite electrode that exhibits a high specific capacitance of 305 F g^{-1} (Figure 6b, c), superior energy density (Figure 6d) and excellent capacitance retention up to 95.4% after 10,000 cycles (Figure 6e). The lightweight framework and binder-free synthesis make it apt for electronics and modern technology due to its economical scalability [20]. Zhang et al. followed a facile one-step synthesis procedure for rGO@NiO composite electrodes for supercapacitor electrode application via the electrode-assisted plasma electrolysis method. The fabrication process is mediated through electrochemical polarization which significantly reduces the deposition time, thus ensuring faster and more efficient synthesis than conventional methods. The hybrid composite delivers a superior specific capacitance of 1093 F g^{-1} at a current density of 1 A g^{-1}. The capacitance retention (87%) and Coulombic efficiency (90.6%) are well maintained over 5000 cycles, thus promising making it a robust electrode material in supercapacitors [21].

The influence of anionic surfactant sodiumlaurylsulphate (SLS) on the electrochemical performance of polyaniline (PANI) wrapped reduced graphene oxide hybrid composites (SPGO) for electrochemical energy storage was explored by Athira et al. The composite was prepared at sub-zero temperatures by oxidative polymerization of PANI on SLS-activated rGO layers that increase the overall surface area and provide ample surface-active sites allowing easy intercalation of electrolyte ions by reducing the diffusion time. The symmetric supercapacitor made up of SPGO electrodes showed a high capacitance of 531 F g^{-1} at a current density of 0.2 A g^{-1}. The prototype device also achieved an excellent working potential of 1.2 V with a specific energy of 26.5 Wh kg^{-1}. Owing to the scaffolding effect of SLS-modified rGO which establishes synergy with PANI and the corresponding Faradaic and double-layer interactions, the SPGO achieved 98% Coulombic efficiency after 5000 cycles which makes it a perfect candidate for electrochemical energy storing applications [22].

Graphene has been combined with a variety of polymers to yield composites with varying morphologies and conformations that have a significant influence on the capacitive properties. The composite of graphene with polypyrrole-based materials is less porous than graphene/PANI due to the larger size of the former. This renders enhanced cyclic stability to the graphene/PANI composites which makes them a better choice for electrode materials. The surfactants are known to improve the porosity of a composite and enhance its surface area. The SLS surfactant is widely used for cleaning and emulsifying purposes by reducing the surface tension of the medium. Its incorporation into GO improved its wettability and contributed to enhancing the specific capacitance of the hybrid composite by decreasing the agglomeration of GO layers which helped in the easy integration of PANI between the rGO layers.

4.2 Carbon-based MXenes

The fascinating structure of MXenes, a new class of 2D materials, has drawn the interest of researchers due to its unique morphology, large interlayer spacing, high electrical conductivity and melting point, exceptional hardness, large surface area, and superior thermal stability and hydrophilic nature. MXenes are transition metal carbides or nitrides having the general formula $M_{n+1}X_nT_x$ where M is a transition metal like Ti, V, Cr, Mo, W and Nb, X is either carbon or nitrogen or both and T is the surface termination groups like -OH, -F or -O. MAX phases, the precursors of MXenes, are a family of layered transition metal carbides or nitrides with the general formula $M_{n+1}AX_n$ where A is a group 13 or 14 element. The selective etching of the highly reactive "A" layers of MAX phases and their replacement with -OH, -F, or -O results in separated 2D-MXene sheets [23].

MXene is characterized by a layered hexagonal structure belonging to the space group $P6_3/mmc$. In addition to the inherent conformation of MXenes that renders more surface-active sites for electrochemical reaction, complete electron transport channels, metallic conductivity and ceramics nature of carbon/nitrogen contribute to enhancing the electrochemical performance that makes them a lucrative electrode material for supercapacitor applications. Further, the tunability of the surface groups endows them with exceptional thermal stability, good mechanical stability, superior optical properties, good hydrophilicity, and corrosion resistance which is an added advantage for usage in supercapacitors [24].

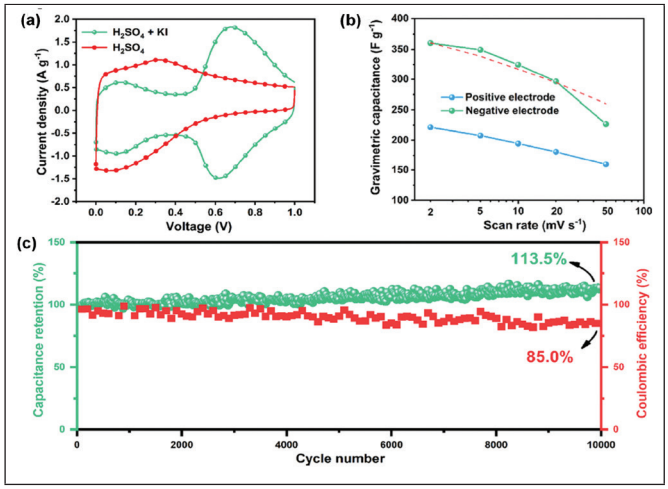

Figure 7: (a) CV curve of the symmetric supercapacitor with MXene electrodes in 3M H_2SO_4 and mixed electrolyte (3M H_2SO_4 and 0.2 M KI) at 5mV/s (b) Gravimetric capacitance of the positive and negative electrode in 3M H_2SO_4 at different scan rates. The difference in capacitances of the electrode occurring due to redox reactions of Ti is evident from the graph. (c) Cyclic stability of the MXene-based electrode in mixed electrolyte over 10,000 cycles at 10 A g^{-1}. Reproduced with permission from Ref. [25], Copyright 2020, American Chemical Society.

Delamination of MXenes involves the exfoliation of the layered MXene by intercalating with organic moieties which increases the interlayer distance, thus reducing the attractive forces between the MXene layers. Studies have shown that the delamination of layered MXenes into flakes enhances the electrochemical energy storing capacity. Dall'Agnese et al. demonstrated that delamination of MXenes resulted in a significant increase in the electrochemical capacitance to 325 F g^{-1} at a current density of 5 A g^{-1} with excellent stability up to 10,000 cycles. The intercalation with dimethyl sulfoxide (DMSO) increased the surface area and modified the surface chemistry which resulted in the enhancement of electrochemical capacitance [26].

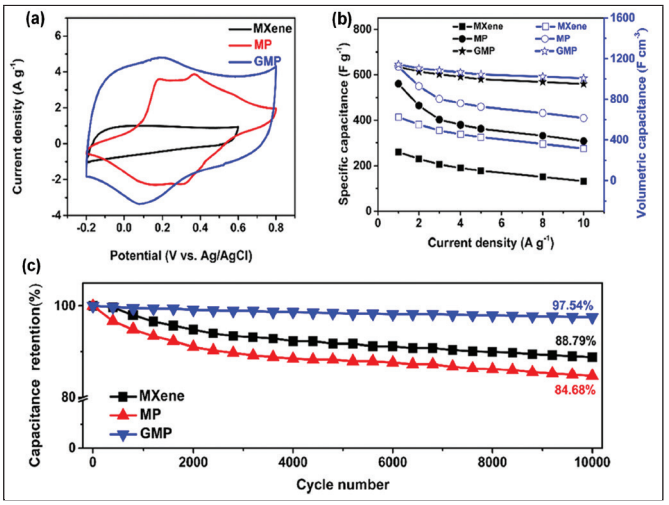

Figure 8: (a) CV curves of MXene, MXene Ti_2CT_x@ polyaniline (MP), and graphene-encapsulated MXene Ti_2CT_x@polyaniline composite (GMP) composite at 5mV s^{-1} showing the highest capacitance of the GMP electrode, indicating fast charge transfer. (b) The specific capacitance of the electrodes at different current densities with GMP showing a maximum specific capacitance of 635 F g^{-1}. (c)Higher stability of capacitance in GMP after 10,000 cycles with a 97.54 % retention at 10 A g^{-1}. Reproduced with permission from Ref. [27], Copyright 2018, American Chemical Society.

In an interesting study, Tian et al. demonstrated that $Ti_3C_2T_x$ based supercapacitors showed an asymmetric voltage splitting between the electrodes in H_2SO_4 electrolyte. They reported that the redox reactions of Ti concerning the bonding/de-bonding of Ti-O with the hydronium ions occur at the negative electrode raising its specific capacitance (361 F g^{-1}) with respect to the positive electrode (221 F g^{-1}) (Figure 7b). They proposed a novel strategy of including a redox electrolyte into the existing H_2SO_4 electrolyte to balance the unequal capacitances. In this study, they used potassium iodide (KI) as the redox electrolyte that is known to take part in reactions taking place at the cathode. They observed that with the addition of the redox

electrolyte the storage mechanism changed from capacitive to battery type (Figure 7a) which ensured higher energy density and displayed excellent cycle stability by retaining ~113% of the capacitance after 10,000 cycles (Figure 7c) [25].

In another study reported by Fu et al., they studied a robust three-component system for supercapacitor applications. The three-component system consisted of accordion-like MXene Ti_3CT_x, ionic-interactive PANI attached to MXene, and a chemically converted graphene sheet (CCG) that encapsulated the whole system into a single composite (GMP). At a pH of 9, the CCG exhibited a negative charge while the MXene-PANI nanocomposite showed a slight positive charge that facilitated the encapsulation of the graphene sheets onto the intercalated MXene system. The conductive PANI was successfully intercalated between MXene sheets, increasing the surface area that resulted in higher current density (Figure 8a) and electrochemical capacitance of 635 F g^{-1} at a current density of 1 A g^{-1} (Figure 8b). Additionally, the GMP electrode also exhibited excellent stability of the capacitance (97.54 %) after 10,000 cycles (Figure 8c). The GMP/graphene pouch-like asymmetric supercapacitor exhibited an exceptional energy density was also 42.3 Wh kg^{-1} at a power density of 950 W kg^{-1} with a cycle stability of up to 94.25 % after 10,000 cycles. This shows that the GMP electrode holds promise in the field of 2D-electrode material for high-performance supercapacitors [27].

MXenes can also be assembled into micro supercapacitors (MSC) that have higher power and energy densities as compared to supercapacitors and can efficiently power up microsensors, micromechanical systems, and smart electronics that require less energy to operate. Peng et al. demonstrated an all-MXene ($Ti_3C_2T_x$) solid-state interdigitated electrodes using spray coating technique as a prospective design for an on-chip energy storage module. The novelty of the MSC lies in the integration of noble-metal-free, all-MXene heterostructures for both electrodes, where the larger MXene flakes constituted the current collector and the smaller flakes formed the active layer. As compared to MSCs with platinum current collectors, the all-MXene MSC displayed excellent stability, lower contact resistance, and higher capacitances. The areal and volumetric capacitances of the all-MXene MSC were found to be ~27 mF cm^{-2} and 357 F cm^{-3}, respectively. The device exhibited a capacitance retention of 100% at a scan rate of 50 mV s^{-1} after 10,000 cycles which vouches for its robust nature. This unique study opens doors for a myriad of designs that can be incorporated into MSC using MXenes to enhance the volumetric and areal capacitances for increasing their electrochemical energy storing abilities [28].

MXenes are attractive candidates for electrode materials owing to their metallic conductivity, low ion diffusion barrier, higher surface area, and tuneable surface properties but pristine MXene possesses the inherent drawbacks of restacking of MXene layers, easy oxidation on coming in contact with water and mechanical flexibility. However, these can be reduced by forming composites of MXenes with organic moieties that act as spacers and increase the interlayer distance between the successive MXene layers, and prevents the restacking of the layers. It also increases the surface area of the MXenes which enhances the overall electrochemical performance.

4.3 Carbon Nitride

Carbon nitride (CN) is a two-dimensional graphene-like structure with high nitrogen content, unique optical properties, attractive electronic structure, and superior chemical and thermal stability. It exists in seven phases namely, α-C_3N_4, β-C_3N_4, cubic-C_3N_4, pseudocubic-C_3N_4, g-h-triazine, g-o-triazine, and g-h-heptazine (Figure 9). However, the graphitic carbon nitride (g-C_3N_4) phase has attracted the attention of researchers due to its inherent stability at ambient conditions. The g-C_3N_4 structure constitutes a nitrogen-substituted graphene network with sp^2 hybridized carbon and nitrogen, forming a π-conjugated structure. The nitrogen-rich structure results in higher electrons in the π-conjugated bond thus improving the electrical conductivity. Further, g-C_3N_4 is stable to harsh chemicals and resists degradation on being exposed to acids, alkalis, or other organic solvents, making them favorable to be used as electrode materials [29].

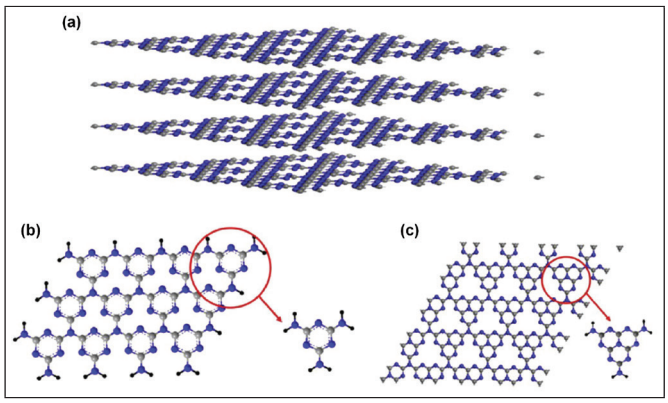

Figure 9: Chemical structure of the widely researched phases of carbon nitride: (a) g-C_3N_4 layered 2D stacked structure, (b) s-triazine and, (c) heptazine structure. Reproduced with permission from Ref. [30], Copyright 2020, American Chemical Society.

Nanostructures of g-C_3N_4 like nanotubes, nanorods, nanosheets, etc, are proven to be more efficient than their bulk counterparts. Tahir et al. explored tubular g-C_3N_4, fabricated using melamine and nitric acid, for supercapacitor applications due to the distinct morphology and high surface area of 182.61 m^2/g. It displayed a good specific capacitance of 233 F g^{-1} at a current density of 0.2 A g^{-1} in a 6 M KOH electrolyte.

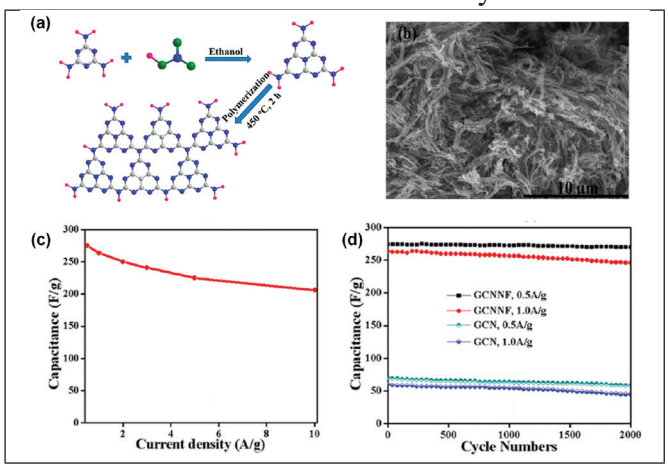

Figure 10: (a) Schematic of the fabrication procedure of GCNNF (b) Scanning electron micrograph of GCNNF (c) Variation of the capacitance of GCNNF with respect to the current density (d) Cyclic stability of GCNNF and graphitic carbon nitride (GCN) at 0.5 and 1 A g^{-1} for over 2000 cycles. Reproduced with permission from Ref. [32], Copyright 2013, American Chemical Society.

The superior performance of the tubular g-C_3N_4 is attributed to the high nitrogen content that renders higher surface area and consequently higher active sites. This novel electrode also shows exceptional cycle stability with about 90% capacitance retention after 1000 cycles. The authors also reported that tubular g-C_3N_4 possesses excellent photocatalytic properties and can prove to be an efficient material for energy storage and photocatalysis [31].

Tahir et al. also studied pure carbon nitride and developed a facile and environment-friendly chemical route to synthesize graphitic carbon nitride nanofibers (GCNNF) (Figure 10a, b). The synthesized GCNNF were investigated for their potential applications as electrode materials in supercapacitors due to high surface area and enhanced nitrogen content as compared to bulk C_3N_4, which improved the electrical conductivity. The GCNNF exhibited superior capacitance of 263.75 F g^{-1} at 1 A g^{-1} in a 0.1 M Na_2SO_4 electrolyte (Figure 10c) and capacitance retention of 96.3% after 2000 cycles (Figure 10d) [32]. Gonçalves et al. studied pristine carbon nitride obtained from pyrolysis of urea followed by exfoliation. The synthesized material exhibited high capacitance of 113.7 F g^{-1} at a current density of 0.2 A g^{-1} which displayed a retention of 89.2 % of its initial value after 5000 cycles [33]. Dong et al. designed an electrode from a sandwich-like composite of g-C_3N_4 with polypyrrole fabricated via a chemical oxidation method. The composite yielded a capacitance of 471 F g^{-1} specific capacitance at a current density of 1 A g^{-1} with about 80% retention ability up to 1000 cycles [34].

Carbon nitride is an attractive choice for electrodes in supercapacitors owing to the higher nitrogen content that enriches them with active sites for reaction. However, g-C_3N_4 is characterized by low electrical conductivity and a smaller surface area that severely affects the electrochemical performance in supercapacitor applications. Additionally, a higher concentration of non-graphitic nitrogen and a large bandgap of ~ 2.7 eV mandates different approaches like altering the morphology and doping with other conductive materials to make it suitable for supercapacitor applications. The interlayer van der

Waals interaction in g-C_3N_4 results in restacking of the single layers that diminish its power and energy density. Strategies like hybridization with materials having higher conductivity and downsizing them to the nanoscale have yielded optimistic results which pave the way for a brighter future of g-C_3N_4 in the field of electrochemical energy storage.

5. Future Challenges

Supercapacitors have acquired a niche position in the field of electrochemical energy harvesting due to the high-power density that gives them an edge over the slow kinetics of secondary batteries. The energy density of the supercapacitors is governed by its electrodes which are the sites of electrochemical reactions. 2D materials have been widely explored for electrode applications in supercapacitors due to the unique morphology that endows them with exceptionally high surface area. However, challenges remain in the practical application of 2D-based hybrid electrode materials. Most of the 2D materials are synthesized through a complex chemical process which is energy and time intensive. One-pot synthesis is a more favorable approach to fabricating 2D materials which does not require an exfoliation process but only a few members of the 2D family can be prepared via a single step. Research should be aimed at designing and developing economically feasible and industrially scalable procedures of 2D materials fabrication. Additionally, surfactant contamination and intercalation residues also result in impurities that affect the electrochemical performances. Further, a hybrid of 2D materials with other conductive materials for asymmetric devices can also boost the device's performance. Cycle stability is an important parameter that gauges the performance of the supercapacitors and about 1000 to 10,000 cycles are carried out at lab-scale to check the device's stability. Rigorous cycling is known to induce corrosion in the supercapacitor components and reduces the capacitance and increases the ESR. Stability data from extensive cycling of the electrodes should be included to test the device's potential for real-life application. A major drawback in the performance of the supercapacitors lies in the self-discharging phenomenon, a thermodynamic instability triggered by the redistribution of ions within the pores. The usage of organic electrolytes has been reported to overcome this difficulty. However. much understanding is yet to be acquired on the performance of supercapacitors in organic electrolytes. There is a scarcity of DFT (density functional theory) studies that can support experimental evidence and further provide innovative designs for enhancing the efficiency of supercapacitors. Structural and electronic parameters like bond length, bond angle, lattice energy, density of states, and charge transfer can be easily predicted by DFT studies that will prove to be helpful for developing efficient models. This can also help in integrating the supercapacitor in electronic devices into a single component that is beneficial while developing efficient models for practical applications.

6. Conclusion

2D materials have the potential to perform adeptly as electrode materials due to high exposed surface area, atomic layer thickness, large surface area to volume ratio, and tunable surface properties. The most commonly used carbon-based electrode materials like graphene, MXene, and carbon nitride towards the electrochemical performances of supercapacitors proves their efficiency over other nanomaterials. However, much research needs to be focused on polishing the shortcomings by developing efficient synthesis procedures, designing newer hybrid structures, and integrating them in electronic devices. This will enable the production of new generation, efficient and high-performance supercapacitors that will be the eco-friendly alternative to existing conventional energy storage devices.

Acknowledgment

D.K. and UM would like to thank the Council of Scientific and Industrial Research (CSIR) for his fellowship and financial support through OLP-102, respectively.

References:

[1] M. Winter, R.J. Brodd, What Are Batteries, Fuel Cells, and Supercapacitors?, Chem. Rev. 104 (2004) 4245–4269. https://doi.org/10.1021/cr020730k.

[2] H.I. Becker, Low voltage electrolytic capacitor, (1957). US2800616A.

[3] D.L. Boos, and G. Heights, Electrolytic capacitor having carbon paste electrodes, (1970). US3536963A.

[4] C. Chen, Y. Zhang, Y. Li, J. Dai, J. Song, Y. Yao, Y. Gong, I. Kierzewski, J. Xie, L. Hu, All-wood, low tortuosity, aqueous, biodegradable supercapacitors with ultra-high capacitance, Energy Environ. Sci. 10 (2017) 538–545. https://doi.org/10.1039/C6EE03716J.

[5] Y.J. Heo, J.H. Lee, S.H. Kim, S.J. Mun, S.Y. Lee, S.J. Park, Paper-Derived Millimeter-Thick Yarn Supercapacitors Enabling High Volumetric Energy Density, ACS Appl. Mater. Interfaces 14 (2022) 42671–42682. https://doi.org/10.1021/acsami.2c10746.

[6] J.H. Lee, G. Yang, C.H. Kim, R.L. Mahajan, S.Y. Lee, S.J. Park, Flexible solid-state hybrid supercapacitors for the internet of everything (IoE), Energy Environ. Sci. 15 (2022) 2233–2258. https://doi.org/10.1039/D1EE03567C.

[7] Y. Shao, M.F. El-Kady, J. Sun, Y. Li, Q. Zhang, M. Zhu, H. Wang, B. Dunn, R.B. Kaner, Design and Mechanisms of Asymmetric Supercapacitors, Chem. Rev. 118 (2018) 9233–9280. https://doi.org/10.1021/acs.chemrev.8b00252.

[8] H.V. Helmholtz, On the conservtion of force : a physcial memoir, in: R Kahl (Ed.), Selected Writing of Hermann Von Helmholtz, Wesleyan University Press., Connecticut, 1971, pp. 3-55.

[9] J.N. Coleman, M. Lotya, A. O'neill, S.D. Bergin, P.J. King, U. Khan, K. Young, A. Gaucher, S. De, R.J. Smith, I. V Shvets, S.K. Arora, G. Stanton, H.-Y. Kim, K. Lee, G.T. Kim, G.S. Duesberg, T. Hallam, J.J. Boland, J.J. Wang, J.F. Donegan, J.C. Grunlan, G. Moriarty, A. Shmeliov, R.J. Nicholls, J.M. Perkins, E.M. Grieveson, K. Theuwissen, D.W. Mccomb, P.D. Nellist, V. Nicolosi, Two-Dimensional Nanosheets Produced by Liquid Exfoliation of Layered Materials, Science 331 (2011) 568–571. https://www.science.org/doi/10.1126/science.1194975.

[10] B. Anasori, M.R. Lukatskaya, Y. Gogotsi, 2D metal carbides and nitrides (MXenes) for energy storage, Nat. Rev. Mater. 2 (2017) 16098. https://doi.org/10.1038/natrevmats.2016.98.

[11] T.-H. Gu, N.H. Kwon, K.-G. Lee, X. Jin, S.-J. Hwang, 2D inorganic nanosheets as versatile building blocks for hybrid electrode materials for supercapacitor, Coord. Chem. Rev. 421 (2020) 213439. https://doi.org/10.1016/j.ccr.2020.213439.

[12] S. Huang, X. Zhu, S. Sarkar, Y. Zhao, Challenges and opportunities for supercapacitors, APL Mater. 7 (2019) 100901. https://doi.org/10.1063/1.5116146..

[13] S. Najib, E. Erdem, Current progress achieved in novel materials for supercapacitor electrodes: mini review Nanoscale Adv. 1 (2019) 2817–2827. https://doi.org/10.1039/C9NA00345B.

[14] M.S. Javed, A. Mateen, I. Hussain, S. Ali, S. Asim, A. Ahmad, E. tag Eldin, M.A. Bajaber, T. Najam, W. Han, The quest for negative electrode materials for Supercapacitors: 2D materials as a promising family, Chem. Eng. J. 452 (2023) 139455. https://doi.org/10.1016/j.cej.2022.13945.

[15] A. Muzaffar, M.B. Ahamed, K. Deshmukh, J. Thirumalai, A review on recent advances in hybrid supercapacitors: Design, fabrication and applications, Renew. Sustain. Energy Rev. 101 (2019) 123–145. https://doi.org/10.1016/j.rser.2018.10.026.

[16] A. Yu, I. Roes, A. Davies, Z. Chen, Ultrathin, transparent, and flexible graphene films for supercapacitor application Appl. Phys. Lett. 96 (2010) 253105. https://doi.org/10.1063/1.3455879.

[17] J. Liu, J. An, Y. Ma, M. Li, R. Ma, Synthesis of a Graphene-Polypyrrole Nanotube Composite and Its Application in Supercapacitor Electrode, J. Electrochem. Soc. 159 (2012) A828–A833. DOI: 10.1149/2.093206jes.

[18] Z. Tai, X. Yan, Q. Xue, Shape-alterable and -recoverable graphene/polyurethane bi-layered composite film for supercapacitor electrode, J. Power Sources 213 (2012) 350–357. https://doi.org/10.1016/j.jpowsour.2012.03.086.

[19] X. Chen, Z. Qu, Z. Liu, G. Ren, X. Chen, Z. Qu, Z. Liu, and G. Ren, ACS Omega 7, 23503–23510 (2022) ACS Omega 7 (2022) 23503–23510. https://doi.org/10.1021/acsomega.2c01963.

[20] T. Akhter, M.M. Islam, S.N. Faisal, E. Haque, A.I. Minett, H.K. Liu, K. Konstantinov, S.X. Dou, Self-Assembled N/S Codoped Flexible Graphene Paper for High Performance Energy Storage and Oxygen Reduction Reaction, ACS Appl. Mater. Interfaces 8 (2016) 2078–2087. https://doi.org/10.1021/acsami.5b10545.

[21] Y. Zhang, Y. Shen, X. Xie, W. Du, L. Kang, Y. Wang, X. Sun, Z. Li, B. Wang, One-step synthesis of the reduced graphene oxide@NiO composites for supercapacitor electrodes by electrode-assisted plasma electrolysis, Mater. Des. 196 (2020) 109111. https://doi.org/10.1016/j.matdes.2020.109111.

[22] A.R. Athira, S. Deepthi, T.S. Xavier, Impact of an anionic surfactant on the enhancement of the capacitance characteristics of polyaniline-wrapped graphene oxide hybrid composite, Bull. Mater. Sci. 44 (2021) 178. https://doi.org/10.1007/s12034-021-02481-8.

[23] S. Venkateshalu, A.N. Grace, MXenes—A new class of 2D layered materials: Synthesis, properties, applications as supercapacitor electrode and beyond, Appl. Mater. Today 18 (2020) 100509. https://doi.org/10.1016/j.apmt.2019.100509.

[24] M. Hu, H. Zhang, T. Hu, B. Fan, X. Wang, Z. Li, Emerging 2D MXenes for supercapacitors: status, challenges and prospects, Chem. Soc. Rev. 49 (2020) 6666–6693. DOI: 10.1039/D0CS00175A.

[25] Y. Tian, C. Yang, Y. Luo, H. Zhao, Y. Du, L.B. Kong, W. Que, Understanding MXene-Based "Symmetric" Supercapacitors and Redox Electrolyte Energy Storage, ACS Appl. Energy Mater. 3 (2020) 5006–5014. https://doi.org/10.1021/acsaem.0c00527.

[26] Y. Dall'Agnese, M.R. Lukatskaya, K.M. Cook, P.-L. Taberna, Y. Gogotsi, P. Simon, High capacitance of surface-modified 2D titanium carbide in acidic electrolyte, Electrochem. Commun. 48 (2014) 118–122. https://doi.org/10.1016/j.elecom.2014.09.002.

[27] J. Fu, J. Yun, S. Wu, L. Li, L. Yu, K.H. Kim, Architecturally Robust Graphene-Encapsulated MXene Ti2CTx@Polyaniline Composite for High-Performance Pouch-Type Asymmetric Supercapacitor, ACS Appl. Mater. Interfaces 10 (2018) 34212–34221. https://doi.org/10.1021/acsami.8b10195.

[28] Y.-Y. Peng, B. Akuzum, N. Kurra, M.-Q. Zhao, M. Alhabeb, B. Anasori, E.C. Kumbur, H.N. Alshareef, M.-D. Ger, Y. Gogotsi, All-MXene (2D titanium carbide) solid-state microsupercapacitors for on-chip energy storage, Energy Environ. Sci. 9 (2016) 2847–2854. DOI: 10.1039/C6EE01717G.

[29] Y. Wang, L. Liu, T. Ma, Y. Zhang, H. Huang, 2D Graphitic Carbon Nitride for Energy Conversion and Storage, Adv. Funct. Mater. 31 (2021) 2102540. https://doi.org/10.1002/adfm.202102540.

[30] M. Majdoub, Z. Anfar, A. Amedlous, Emerging Chemical Functionalization of g-C3N4: Covalent/Noncovalent Modifications and Applications, ACS Nano 14 (2020) 12390–12469. https://doi.org/10.1021/acsnano.0c06116.

[31] M. Tahir, C. Cao, F.K. Butt, F. Idrees, N. Mahmood, Z. Ali, I. Aslam, M. Tanveer, M. Rizwan, T. Mahmood, Tubular graphitic-C3N4: a prospective material for energy storage and green photocatalysis, J. Mater. Chem. A 1 (2013) 13949. DOI: 10.1039/C3TA13291A.

[32] M. Tahir, C. Cao, N. Mahmood, F.K. Butt, A. Mahmood, F. Idrees, S. Hussain, M. Tanveer, Z. Ali, I. Aslam, Multifunctional g-C3N4 Nanofibers: A Template-Free Fabrication and Enhanced Optical, Electrochemical, and Photocatalyst Properties, ACS Appl. Mater. Interfaces 6 (2014) 1258–1265. https://doi.org/10.1021/am405076b.

[33] R. Gonçalves, T.M. Lima, M.W. Paixão, E.C. Pereira, Pristine carbon nitride as active material for high-performance metal-free supercapacitors: simple, easy and cheap, RSC Adv. 8 (2018) 35327–35336. DOI: 10.1039/C8RA06656F.

[34] G. Dong, H. Fan, K. Fu, L. Ma, S. Zhang, M. Zhang, J. Ma, W. Wang, The evaluation of super-capacitive performance of novel g-C3N4/PPy nanocomposite electrode material with sandwich-like structure, Compos. Part B Eng. 162 (2019) 369–377. https://doi.org/10.1016/j.compositesb.2018.12.098.

PROFORMA OF SUBSCRIPTION FORM

I /We wish to subscribe **The Journal of Electrochemical Society of India (JECSI)** for ..... year(s) for which (i) a Demand Draft vide …….....……. dated …….....…… issued from (Name of the bank…….....)favouring **ELECTROCHEMICAL SOCIETY OF INDIA JOURNAL, payable at Bengaluru or (ii) NEFT/IMPS vide UTR no……..dated for Rs/US $…….is enclosed.**

NAME…….

DESIGNATION…….

POSTAL ADDRESS…….

……PIN…….....

E-MAIL…….Phone no.……

Subscriber ID (for renewal only)……

Signature…….

Bank account details	**Subscription details:**
Name: Electrochemical Society of India Journal Account No. 110045333254 Bank Name: Canara Bank Customer ID: 309740255 IFSC Code: CNRB0000683 MICR Code: 560015023 Indian Institute of Science Canara Bank IISc, Bangalore - 560012	**Print only**: For institutions & Individuals: Annual 6 issues: Rs 2000/- (India), Annual 6 issues: USD 250.00 incl. postages (abroad), For students: Annual 6 issues: Rs 1000/- **Print & Online (customer type: institution):** USD 100.00 & INR 5000.00 Please note that institutional prices are available only for libraries of higher education institutions and research organizations.

Journal of the Electrochemical Society of India

Vol. No. 73 (1 & 2), Jan-March 2024

CODEN - JESIA 72 [3&4] 2023 ISSN:0013-466X

Email : ecsiiisc@gmail.com

FROM IV

See Rule VIII

1.	Place of publication	:	Bengaluru
2.	Periodicity of its publication	:	Quarterly
3.	Printer name	:	Poornima Printers
	Whether the Citizen of india	:	YES
	Address of the printer	:	No. 3&4, Sy. No. 51/14, Chowdeshwarinagar, Pipeline Road, Laggere, Bengaluru - 560058
4.	Publishers Name	:	**The Electrochemical Society of India**
5.	Editor's Name	:	Dr. U. Kamachi Mudali
	Whether Citizen of India	:	Yes
	Address	:	**The Electrochemical Society of India** Indian Institute of Science Campus, Bangalore - 560 012
6.	Name and Address of Individuals who own the newspaper/holders and partners and shareholders	:	**The Electrochemical Society of India** Indian Institute of Science Campus, Bangalore - 560 012. holding more than 1% of the total capital.

I, Dr. U. Kamachi Mudali hereby declare that the particulars given above are true to the best of my knowledge and belief.

Sd/-

Dr. U. Kamachi Mudali

Chief Editor, JECSI

(Publisher)

THE ELECTROCHEMICAL SOCIETY OF INDIA

Indian Institute of Science Campus, Bengaluru - 560 012, India
Phone : +91-80-22932613
E-mail : ecsiiisc@gmial.com | www.ecsi.in

CALL FOR NOMINATIONS FOR ECSI AWARDS- 2024

Shri S.K. Seshadri Memorial Mascot National Award
(Instituted in the year 1980)

With a view to stimulate interest among Scientists and Technologists in the field of corrosion, the Electrochemical Society of India has instituted the prestigious "**Shri S. K. Seshadri Memorial Mascot National Award"** for notable and outstanding contributions in the field of Industrial Corrosion. The award is sponsored by Director, M/s. Biosafe Solutions.

1. The research work considered for this award should be in the field of Corrosion Science and Technology, Corrosion Prevention and Allied aspects. Industrial Significance to be highlighted and Industrial applicability is desired.
2. The work should have been carried out to bring it to the point of application. The process of development and test schedules may have been carried out during the preceding couple of years, but should have culminated in a fruitful result. The work need not necessarily have been published.

THE N. M. SAMPAT AWARD - 2024
(Instituted in the year 1986)

With a view to recognize outstanding services rendered to the Electroplating industry andTechnology, the Governing Council of the ECSI has with great pleasure has instituted "**The N. M. Sampat Award".** This award is sponsored by M/S Canning Mitra Phoenix Limited, Mumbai. Research work considered for this award should be in the field of Metal Finishing, Electroplating, Surface Coating and Modification, and allied fields. Work carried out in these areas with possible industrial applicability or academic excellence would be considered. The work need not have been published but industrial applications should have been established.

ECSI- METROHM National Award - 2023
(Instituted in the year 2021)

With a view to recognize the contributions made by individuals in the field of basic electrochemistry, electrochemical instrumentation and devices, theoretical and; experimental electrochemistry, the Electrochemical Society of India has instituted this prestigious award **"ECSI- METROHM National Award for Electrochemical Science".** The award is sponsored by M/s Metrohm India Ltd. Chennai. Meritorious work in any field of Electrochemical Science would qualify for this award.

ECSI- AMARA RAJA National Award- 2023
(Instituted in the year 2021)

With a view to stimulate interest among Scientists and Technologists in the field of Batteries, Fuel Cells and Sensors, the Electrochemical Society of India has instituted the prestigious award **"ECSI- AMARA RAJA National Award for Advanced Electrochemical Technology".** The award is sponsored by M/s. Amara Raja Batteries Ltd. Tirupathi. Meritorious work in the field of Batteries, Fuel Cells and Sensors would qualify for this award.

ECSI-Dr. K. Elayaperumal National Award- 2023
(Instituted in the year 2022)

With a view to recognize the outstanding contributions of individuals made in the area of Corrosion Mitigation in Industries, The Electrochemical Society of India has instituted the prestigious award "ECSI- Dr. K. Elayaperumal National Award for Excellence in Industrial **Electrochemical Science and Technology"** from this year. The award is sponsored by Dr. K. Elayaperumal and his family. Meritorious work in the area of corrosion mitigation in industries would qualify for this award.

GUIDELINES FOR NOMINATION

1. Nominations may be made by Research Organizations/Institution/ Industries/Individuals.
2. The nomination should be accompanied by the complete bio-data and important contributions for which the nomination is being made.
3. The work should have been carried out to bring it to the point of application. The process of development and test schedules may have been carried out during the preceding couple of years, but should have culminated into a fruitful result at least during the year of application.

Each of the above awards carries a Scroll of Honor and cash prize.

Awardees are required to present their work in the form of an **Award Lecture** and also submit a written manuscript for publication in the Journal of Electrochemical Society of India. Complete Nominations in all respects for the above awards should reach The Secretary, The Electrochemical Society of India, Indian Institute of Science Campus, Bengaluru - 560 012.

Nominations complete in all respects for the above awards should reach
Hon President or General Secretary,
The Electrochemical Society of India, Indian Institute of Science Campus,
Bengaluru - 560 012,
E-Mail: ecsiiisc@gmail.com

on or before 31st of July 2024
The Awards will be presented during the annual
ICONEST-2024 Conference

Dr. S. T. Aruna
Hon. President, ECSI

Dr. Ajay Krishnan
Hon. Gen. Secretary, ECSI

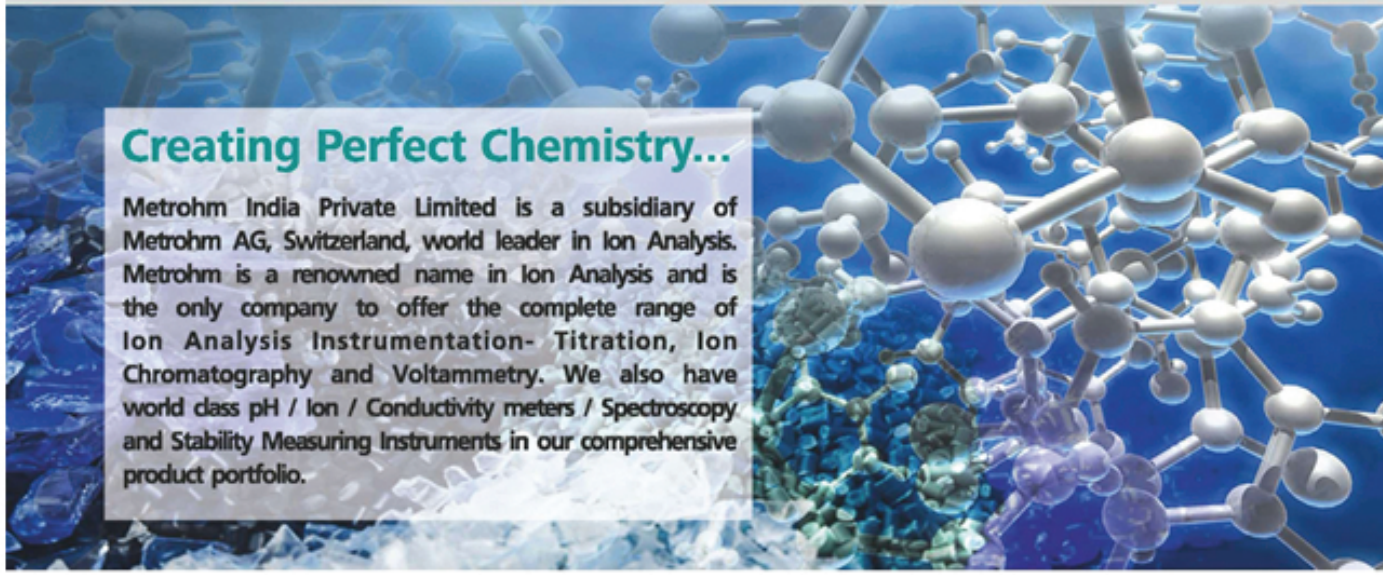

Creating Perfect Chemistry...

Metrohm India Private Limited is a subsidiary of Metrohm AG, Switzerland, world leader in Ion Analysis. Metrohm is a renowned name in Ion Analysis and is the only company to offer the complete range of Ion Analysis Instrumentation- Titration, Ion Chromatography and Voltammetry. We also have world class pH / Ion / Conductivity meters / Spectroscopy and Stability Measuring Instruments in our comprehensive product portfolio.

Titrator

Ion Chromatography

Voltammetry

Electrochemical station

NIRS Analyzer

Raman Spectroscopy

Labwater Purification

Surface Area Analyzer

We also have:

- Electrochemical research instrumentation from Metrohm Autolab
- On-line and at-line process analyzers for process monitoring from Metrohm Process Analytics
- NIR and Raman Spectroscopy solutions from Metrohm and B&W Tek
- Innovative technology for electrochemistry research from Dropsens
- BET surface area, pore size distribution from MicrotracBEL Corp., Japan
- Testing instrumentation for the energy storage device and energy conversion device markets from Arbin instruments
- Lab water solutions from Elga
- Pipetting and dispensing solutions from Socorex

PARTICIPATE IN WATER SURVEY

SCAN ME

GET YOUR FREE GIFT!

Metrohm India Private Limited
Metrohm-SIRI Towers, 3&4, Fourrts Avenue, Annai Indira Nagar
Okkiyam, Thoraipakkam, Chennai - 600097, India.
Ph: +91 44 40440440 | Customer support: +91 44 40440444

For details, e-mail us at **info@metrohm.in** or visit us at **www.metrohm.in**

Metrohm
India Private Ltd.